

UC San Diego

UC San Diego Electronic Theses and Dissertations

Title

Continental margin architecture : sea level and climate

Permalink

<https://escholarship.org/uc/item/5385g992>

Author

Hill, Jenna Catherine

Publication Date

2007

Peer reviewed|Thesis/dissertation

UNIVERSITY OF CALIFORNIA, SAN DIEGO

Continental Margin Architecture:
Sea Level and Climate

A dissertation submitted in partial satisfaction of the
requirements for the degree Doctor of Philosophy
in
Earth Sciences

by

Jenna Catherine Hill

Committee in charge:

Professor Neal Driscoll, Chair
Professor Scott Ashford
Professor Kevin Brown
Professor Chris Charles
Professor Graham Kent

2007

The dissertation of Jenna Catherine Hill is approved, and it is
acceptable in quality and form for publication on microfilm:

Chair

University of California, San Diego

2007

To my family

TABLE OF CONTENTS

Signature Page.....	iii
Dedication.....	iv
Table of Contents.....	v
List of Figures.....	x
List of Tables.....	xiii
Acknowledgements.....	xiv
Vita.....	xix
Abstract.....	xxi
Chapter 1: Introduction.....	1
References.....	6
Chapter 2: Large-scale elongated gas blowouts along the U.S. Atlantic margin.....	7
2.1 Abstract.....	8
2.2 Introduction.....	9
2.3 Data acquisition.....	11
2.4 Results.....	12
2.4.1 Morphology of shelf edge depressions.....	12
2.4.2 Stratal geometry of shelf-edge deposit.....	14
2.4.3 Seismic signature of gas-charged sediments.....	14
2.4.2 Spatial relation between trapped gas and the shelf-edge delta...	15
2.5 Discussion.....	16
2.5.1 Origin of shelf-edge depressions, or “gas blowout” features.....	16

2.5.2 Morphology of gas blowouts.....	17
2.5.3 Downslope creep and gas migration.....	18
2.5.4 Gas distribution.....	20
2.5.5 Origin of the gas.....	21
2.5.6 Relationship between gas and slope instability.....	24
2.5.7 Implications for stability of the U.S. east coast margin.....	26
2.6 Conclusions.....	27
2.7 Acknowledgements.....	28
2.8 Chapter acknowledgement.....	28
Figures.....	29
References.....	37
Chapter 3: New evidence for high discharge to the Chukchi shelf since the Last Glacial Maximum.....	41
3.1 Abstract.....	42
3.2 Introduction.....	42
3.3 Results.....	43
3.4 Discussion.....	45
3.5 Conclusions.....	53
3.6 Acknowledgements.....	53
3.7 Chapter acknowledgment.....	54
Figures.....	55
References.....	62
Chapter 4: Evidence for iceberg armadas on the Chukchi shelf during the Younger Dryas.....	65

4.1 Abstract.....	66
4.2 Results and discussion.....	66
4.3 Chapter acknowledgment.....	74
Figures.....	75
References.....	78
Chapter 5: Paleodrainage on the Chukchi shelf reveals sea level history and meltwater discharge.....	81
5.1 Abstract.....	82
5.2 Introduction.....	82
5.2 Regional setting.....	84
5.2.1 Tectonics.....	84
5.2.2 Drainage patterns.....	85
5.2.3 Recent glaciations.....	86
5.3 Data Acquisition.....	87
5.4 Results.....	88
5.4.1 Acoustic facies.....	88
5.4.2 Sediment facies.....	93
5.4.3 Onshore drainage.....	97
5.5 Discussion.....	97
5.5.1 Multiple sea level cycles.....	97
5.5.2 Meltwater discharge.....	102
5.5.3 Onshore and offshore drainage patterns.....	105
5.5.4 Climate.....	108

5.5.6 Sea level and Holocene sedimentation.....	110
5.6 Conclusions.....	113
5.7 Chapter acknowledgement.....	114
Figures.....	115
References.....	137
Chapter 6: Conclusions.....	143
6.1 U.S. Atlantic margin: Slope stability.....	144
6.2 Chukchi margin of Alaska: Drainage and sedimentation history.....	146
References.....	150
Appendix: Active methane venting observed at giant seafloor pockmarks along the mid-Atlantic shelf break with the Autonomous Underwater Vehicle SeaBED.....	151
A.1 Abstract.....	152
A.2 Introduction.....	152
A.3 Data acquisition.....	155
A.3.1 SeaBED AUV missions.....	155
A.3.2 Water and sediment sampling program.....	157
A.3.3 Multibeam bathymetric survey.....	158
A.4 Results.....	159
A.4.1 New multibeam map.....	159
A.4.2 AUV along track data.....	159
A.4.3 Spatial distribution of methane anomalies.....	161
A.4.4 Dissolved hydrocarbons in water column samples.....	162
A.4.5 Pore water geochemistry.....	163

A.5 Discussion.....	164
A.5.1 Temporal variations in methane venting.....	164
A.5.2 Methane source.....	165
A.5.3 Methane venting at the pockmarks.....	166
A.5.4 Diffuse vs. focused venting.....	167
A.5.5 Evolution of elongate pockmarks.....	169
A.6 Conclusions.....	171
A.7 Acknowledgments.....	172
A.8 Chapter acknowledgement.....	172
A.9 Appendix: Response and correction of the METS Sensor.....	172
Tables.....	176
Figures.....	178
References.....	187

LIST OF FIGURES

Figure 2.1	En echelon, large-scale, elongate gas blowout features offshore of Virginia and North Carolina.....	29
Figure 2.2	Survey ship track coverage superposed on NOAA 3’’ gridded bathymetry in 3-dimensional perspective view.....	30
Figure 2.3	Chirp subbottom profiles across the blowout features.....	31
Figure 2.4	Chirp subbottom profiles showing shelf-edge delta, gas at inner wall and deformed strata.....	32
Figure 2.5	Backscatter images from the side-scan mosaics.....	33
Figure 2.6	Chirp subbottom profiles co-registered with bathymetry and displayed in a 3-dimensional perspective view.....	34
Figure 2.7	Strike and dip chirp subbottom profiles from the Albemarle-Currituck slide area.....	35
Figure 2.8	Schematic outlining the proposed gas blowout process.....	36
Figure 3.1	Location map.....	55
Figure 3.2	CHIRP subbottom profile across the incised valley (Line 2).....	57
Figure 3.3	CHIRP subbottom profile across the incised valley (Line 3).....	59
Figure 3.4	Profiles across the I-3 and I-4 reflectors compared with floodplain profiles across the three dominant northwestern rivers.....	60
Figure 4.1	Map of the eastern Chukchi margin showing CHIRP profiles across the ice scour surface and sediment core locations.....	75
Figure 4.2	3-dimensional perspective view of CHIRP profiles across the ice scour region.....	76
Figure 4.3	Sediment core locations projected onto the CHIRP profiles, along with sediment analyses.....	77
Figure 5.1	Location map of northern Alaska and the adjacent Chukchi margin showing SIO CHIRP and USGS Boomer subbottom tracks.....	115

Figure 5.2 Simplified tectonic map of northern Alaska and adjacent Chukchi margin.....	116
Figure 5.3 CHIRP subbottom profile showing northward dipping Cretaceous strata.....	117
Figure 5.4 Interpreted channel map showing profiles crossing the southern incised valley (VI-0, VI-1, VI-2), meltwater drainage (I-3, I-4), CM feature and northern valley.....	118
Figure 5.5 CHIRP subbottom profile across the incised valley (line 1).....	119
Figure 5.6 CHIRP subbottom profile across the incised valley (line 2).....	120
Figure 5.7 CHIRP subbottom profile across the incised valley (line 3).....	122
Figure 5.8 3-dimensional perspective view of CHIRP and boomer subbottom profiles across the incised valley region, looking offshore.....	124
Figure 5.9 3-dimensional perspective view of CHIRP and boomer subbottom profiles across the northern valley region, looking onshore.....	126
Figure 5.10 Plot showing the base of paleochannel (or valley) thalwegs relative to modern sea level versus distance from the coastline.....	127
Figure 5.11 Sedimentary facies of vibracores in southern incised valley coregistered with CHIRP subbottom data.....	128
Figure 5.12 Sedimentary facies of piston cores in southern incised valley coregistered with CHIRP subbottom data.....	129
Figure 5.13 Sedimentary facies of piston core JPC02 in Hope Valley, coregistered with CHIRP subbottom data (line 10).....	131
Figure 5.14 Sedimentary facies of mid/outer shelf vibracores.....	132
Figure 5.15 Profiles across the I-3 and I-4 reflectors compared with floodplain profiles across the three dominant northwestern Alaskan rivers inferred to connect with the midshelf valley.....	133
Figure 5.16 Eustatic sea level curve and associated Marine Isotope Stages (MIS)...	134
Figure 5.17 Map of western Brooks Range showing the mapped extent of Glacial Lake Noatak deposits from the LGM.....	136

Figure A.1 Bathymetric map of the survey area produced with the ELAC-1180 multibeam sonar during the July 2004 survey.....	178
Figure A.2 CHIRP seismic profile across a shelf edge pockmark.....	179
Figure A.3 The SeaBED AUV.....	180
Figure A.4 Near bottom currents measured by the ship's ADCP in the survey area.....	181
Figure A.5 Near-bottom water properties collected by the SeaBED AUV during dive 16.....	182
Figure A.6 Along track data from dive 16.....	183
Figure A.7 Bathymetry maps of the pockmarks showing the spatial distribution of the methane anomaly.....	184
Figure A.8 CTD and dissolved methane concentration profile from hydrocast 5 compared with CTD profile from AUV dive 9 ascent.....	185
Figure A.9 Proposed methane venting scenario.....	186

LIST OF TABLES

Table 3.1 Options for explaining observed stratigraphy.....	61
Table A.1 Hydrocarbon concentrations in hydrocast samples.....	176
Table A.2 Pore water geochemistry data.....	177

ACKNOWLEDGEMENTS

I have had so many wonderful experiences during my time at SIO, yet only a small fraction could be crammed into my dissertation. First and foremost, I would like to thank my advisor, Neal Driscoll, who has been (and will continue to be) an enormous inspiration through the years, an excellent mentor and generous friend. I have also had the pleasure of a great many adventures, discussions and long laughs with the entire Driscoll lab group, which includes Danny Brothers, Jeff Dingler, Rebecca Fenwick, Jen Haas, Alex Hangsterfer, Leah Hogarth, Liz Johnstone, Nico LeDantec, Christie Lindemann, Justin McCullough, Jessica Raymond, Kurt Schwehr and J.P. Walsh. I have also enjoyed the considerable support of the geologic community at SIO, among whom I would especially like to thank Lihini Aluwihare, Jeff Babcock, Chris Charles, Dru Clark, Graham Kent, Dick Norris and Warren Smith.

I may have chosen a path other than SIO were it not for the encouragement and support of the folks in the Seafloor Mapping Group at the U.S. Geological Survey, including Bill Schwab, Dave Foster and Bill Danforth, among many others. I am also grateful for the support and inspiration I derived from the excellent geology faculty at Oberlin College, and I can only hope that one day I will live up to their standards in my own teaching career.

Much of my time at SIO was actually spent in a great many places around the globe besides San Diego. Numerous trips to Woods Hole to work on my Chukchi cores were aided by Jim Broda, Jeff Donnelly, Lloyd Keigwin, Ellen Roosen, Jess Tierney, Chris Reddy and everyone at the USGS Woods Hole Field Center. With a

total of ~10 months at sea during my graduate career, I must thank the ship's crews of the USCGC Healy, R/V Melville, R/V Cape Hatteras, R/V Sproul, R/V Thompson, R/V Saemundsson, R/V LeConte, NOAA Ship Nancy Foster, and M/V Moonlighting. With so much ship time and data, I would like to highlight the role of my many collaborators, including Julie Brigham-Grette, Rich Camilli, Milene Cormier, Jeff Donnelly, Ryan Eustice, Paul Gayes, Neal Gielstra, John Goff, Miriam Kastner, Lloyd Keigwin, Kori Newman, Gretchen Robertson, Hanu Singh, Evan Solomon, Jamie Phillips, Larry Phillips, and Jeff Weissel.

I would like to thank the Los Angeles Chapter of the ARCS Foundation for their generous financial support; and I would like to extend a special thanks to Mr. and Mrs. Edward Carson who have underwritten my scholarship for the last several years. My research has been funded by the National Science Foundation Office of Polar Programs and Division of Ocean Sciences.

As for my family, I can not begin to thank them enough. I have wanted to become a geologist for as long as I can remember and they have stood behind my increasing fascination with all things earth and rock related from the very first inkling. It is only with their enduring love, unfaltering support and amazing inspiration that I have been able to make this journey and for that I am eternally grateful.

Chapter 2, in full, is a reprint of the material as it appears in *Journal of Geophysical Research*: Hill, J.C., Driscoll, N.W., Weissel, J.K. and Goff, J.A., 2004. Large scale elongated gas blowouts along the U.S. Atlantic margin. *Journal of Geophysical Research* 109, doi: 10.1029/2004JB002969.

The CHIRP subbottom and side-scan sonar data were collected aboard the R/V Cape Hatteras in 2000, prior to my arrival; however, I was responsible for all the data processing and visualization. The data interpretation and text editing was done in conjunction with Neal Driscoll, Jeffrey Weissel and John Goff.

Chapter 3, in full, is the material as submitted to *Quaternary Research*: Hill, J.C., Driscoll, N.W., Brigham-Grette, J., Donnelly, J.P., Gayes, P.T., and Keigwin, L.D., 2007. New evidence for high discharge to the Chukchi shelf since the Last Glacial Maximum. *Quaternary Research*, in press.

The CHIRP subbottom data and sediment cores were collected aboard the USCGC Healy in 2002. I was involved in the instrument deployment, data acquisition, and sediment coring, as well as responsible for the post-cruise data processing and sediment analyses. Paul Gayes was in charge of the shipboard vibracoring operations. Jeff Donnelly and Lloyd Keigwin provided laboratory support for the sediment analyses. The data interpretation and text editing was done in conjunction with Neal Driscoll, Julie Brigham-Grette, Jeff Donnelly, Paul Gayes, Lloyd Keigwin and Larry Phillips.

Chapter 4, in full, is the material as submitted to Science: Hill, J.C. and Driscoll, N.W., 2007. Evidence for iceberg armadas on the Chukchi shelf during the Younger Dryas. *Science, submitted.*

The CHIRP subbottom data and sediment cores were collected aboard the USCGC Healy in 2002. I was involved in the instrument deployment, data acquisition, and sediment coring, as well as responsible for the post-cruise data processing and sediment analyses. Jeff Donnelly and Lloyd Keigwin provided laboratory support for the sediment analyses. The data interpretation and text editing was done in conjunction with Neal Driscoll.

Chapter 5, in full, is the material as submitted to Marine Geology: Hill, J.C. and Driscoll, N.W., 2007. Paleodrainage on the Chukchi shelf reveals sea level history and meltwater discharge. *Marine Geology, submitted.*

The CHIRP subbottom data and sediment cores were collected aboard the USCGC Healy in 2002. I was involved in the instrument deployment, data acquisition, and sediment coring, as well as responsible for the post-cruise data processing and sediment analyses. Jeff Donnelly and Lloyd Keigwin provided laboratory support for the sediment analyses. Larry Phillips provided valuable additional data collected by the U.S. Geological Survey. The data interpretation and text editing was done in conjunction with Neal Driscoll.

The appendix, in full, is the material as submitted to Earth and Planetary Science Letters: Newman, K.R., Cormier, M., Weissel, J.K., Driscoll, N.W., Kastner, M., Solomon, E.A., Robinson, G., Hill, J.C., Singh, H., Camilli, R., and Eustice, R., 2007. Active methane venting observed at giant seafloor pockmarks along the mid-Atlantic shelf break with the Autonomous Underwater Vehicle SeaBED. *EPSL, submitted.*

The multibeam bathymetry data and sediment samples were collected aboard the R/V Cape Hatteras in 2004. I was involved in the sediment coring and data collection. Geochemical analyses were completed by Miriam Kastner, Evan Solomon and Gretchen Robertson. AUV deployment and operations were conducted by Hanumant Singh, Richard Camilli and Ryan Eustice. Data interpretation and text editing were done in conjunction with Kori Newman, Milène Cormier, Jeff Weissel, Neal Driscoll, Miriam Kastner, Evan Solomon, Hanumant Singh and Richard Camilli.

VITA

1999	B.A. Geology, Environmental Studies, Oberlin College
1999 – 2001	Seafloor Mapping Intern, U.S. Geological Survey, Woods Hole Field Center
2001 – 2007	Ph.D. student, University of California, San Diego
2007	Ph.D., Earth Sciences, University of California, San Diego

PUBLICATIONS

Hill, J.C. and Driscoll, N.W., Paleodrainage on the Chukchi shelf reveals sea level history and meltwater discharge, *Marine Geology*, *submitted*.

Hill, J.C. and Driscoll, N.W., Evidence for iceberg armadas on the Chukchi shelf during the Younger Dryas, *Science*, *submitted*.

Hill, J.C., Driscoll, N.W., Brigham-Grette, J., Donnelly, J.P., Gayes, P.T. and Keigwin, L.D., New evidence for high discharge to the Chukchi shelf since the Last Glacial Maximum, *Quaternary Research*, *in press*.

Hill, J.C., Driscoll, N.W., Weissel, J.K., and Goff, J.A., 2004, Large scale elongated gas blowouts along the U.S. Atlantic margin, *Journal of Geophysical Research*, 109:B9, doi: 10.1029/2004JB002969

Hill, J.C., Driscoll, N.W., Phillips, R.L., Donnelly, J.P., Brigham-Grette, J., Gayes, P.T. and Keigwin, L.D., 2006, A large incised valley on the Chukchi shelf: Implications for high discharge, sea level fluctuations and climatic variations since the LGM, *Eos Trans. AGU*, 87(36), Ocean Sci. Meet. Suppl., Abstract OS16A-15

Hill, J.C., Driscoll, N.W., Donnelly, J.P., 2005, Holocene record of deglaciation on the Chukchi shelf, offshore NW Alaska, *Eos Trans. AGU*, 86(52), Fall Meet. Suppl., Abstract OS51B-0567

Hill, J.C., Driscoll, N.W., Weissel, J.K., Kaster, M., Singh, H., Cormier, M., Camilli, R., Eustice, R., Lipscomb, R., McPhee, N., Newman, K., Robertson, G., Solomon, E., and Tomanka, K., 2004, A Potential Link between Fluid Expulsion and Slope Stability: Geochemical Anomalies Measured in the Gas Blowouts along the U.S. Atlantic Margin Provide New Constraints on their Formation, *Eos Trans. AGU*, 85(47), Fall Meet. Suppl., Abstract OS23B-1307

Hill, J.C., Driscoll, N.W., Brigham-Grette, J., Lundeen, Z., 2003, Large incised channels on the Chukchi Shelf provide new constraints on onshore drainage: Implications for tectonic and climatic evolution of NW Alaska, Eos Trans. AGU, 84(46), Fall Meet. Suppl., Abstract OS52B-0911

Hill, J.C., Driscoll, N.W., Weissel, J.K., and Goff, J.A., 2002, Large-Scale Elongated Gas Blowouts, Offshore Virginia/North Carolina: Process and Product, Eos Trans. AGU, 83(47), Fall Meet. Suppl., Abstract OS71C-0305

ABSTRACT OF THE DISSERTATION

Continental Margin Architecture:
Sea Level and Climate

by

Jenna Catherine Hill

Doctor of Philosophy in Earth Sciences

University of California, San Diego, 2007

Professor Neal Driscoll, Chair

The stratigraphy and morphology of continental margins provide important insights into the evolution, history and paleoenvironments of these important regions that define the transition between continent and ocean. Research presented here illustrates how sea level fluctuations and climatic variability shape continental margin stratigraphy and morphology.

Using CHIRP subbottom and side-scan sonar we imaged a series of large scale, elongated gas blowout features located on the outermost shelf-edge of the U.S. Atlantic margin. The stratal geometry suggests a composite formation, combining gas accumulation beneath a shelf-edge delta, down-slope creep of the deltaic strata

and fluid expulsion. The abundance of gas on the margin may be related to hydrate dissociation from bottom water warming during interglacial periods and subsequent trapping by lowstand delta deposits. The location of the blowouts near the shelf break, as well as the proximity to other large slides on the slope indicates that these features may represent incipient large-scale failure of the outer shelf/upper slope.

On the Chukchi shelf, offshore northwestern Alaska, CHIRP subbottom data imaged an extensive network of paleochannels infilled by a complex stratigraphy that records multiple sea level cycles as well as massive glacial discharge. Typically channels are incised as a result of base level lowering; however, the two most recent incisions on the shelf appear to have been downcut during the period of rapid sea level rise following the LGM; the downcutting triggered instead by climatic variations during deglaciation (i.e., catastrophic meltwater drainage). CHIRP subbottom data also imaged a regionally extensive heavily ice scoured surface on the outer Chukchi shelf. The stratigraphy is suggestive of discharge of a large number of icebergs in a single event, followed by largely iceberg free conditions. Both the iceberg scours and meltwater drainage appear to be sourced from the northwestern Alaskan margin during the most recent deglaciation and suggest a greater extent of continental glaciation than previously recognized. The drainage and ice discharge history across the shelf highlights the role of climatic variability and sea level change in shaping the Chukchi margin.

Chapter 1

Introduction

Understanding continental margin formation and evolution is of fundamental importance from a scientific perspective as well as from a societal perspective. Continental margin architecture is in large part shaped by three major processes, tectonic deformation, eustatic sea level fluctuations, and climate. The overarching goal of this thesis is to determine how these fundamental processes shape continental margins architecture and stratigraphy. If we knew the relationship between process and product, then we could interpret better the history of relative sea level, sediment flux, and processes as recorded by continental margin stratigraphy.

Sequence stratigraphic models of shelf morphology define a chronostratigraphic framework of depositional patterns in terms of eustatic sea level change, sediment supply and subsidence/uplift (*Vail 1987; Van Wagoner et al., 1990; Christie-Blick and Driscoll; 1995*). In general, sediment preservation on continental shelves is a balance between rate of sediment supply and the rate of accommodation addition or destruction. Climate largely controls sediment supply and sediment dispersion, while eustatic sea level fluctuations and tectonic uplift or subsidence determine the availability of accommodation. Continental margin architecture results from the complex interplay of all of these processes.

The research presented in this dissertation primarily focuses on the effects of sea level and climate variability on margin morphology and stratigraphy, employing a suite of geophysical and sampling tools (e.g., CHIRP subbottom data, Boomer subbottom data, side-scan sonar data, multibeam bathymetry, sediment coring and analysis).

The second chapter investigates the role that sea level and climate fluctuations can play on slope stability. Numerous processes can trigger slope failure, such as earthquakes, rapid sediment deposition and oversteepening, increased pore pressure (e.g., hydrate dissociation and gas migration), and sea level fluctuations. Understanding the processes that contribute to slope instability is important both in terms of geological processes that shape margin morphology, (e.g., canyon cutting and mass wasting), and also from a societal perspective as submarine landslides have the potential for tsunami generation. Along the U.S. Atlantic margin there are a number of lowstand deltas that serve as somewhat impermeable capping sediments for free gas trapped beneath. On the outershell, offshore of Virginia/North Carolina, there are a series of large gas blowout features, where the pressure from gas buildup below a shelf-edge delta has exceeded the overburden. The abundant gas in the region may be related to melting of gas hydrates at depth on the slope. This may result from the introduction of warmer waters following the reorganization of ocean circulation patterns during the most recent deglaciation. Situated on the shelf edge, these gas blowout features appear to represent an incipient submarine landslide and provide ideal circumstances where we may be able to investigate the causes of slope failure prior to the slumping event. We hypothesize that cracks observed on many continental margins may evolve into the headwalls of future submarine landslides (e.g., Goleta [*Greene, et al., 2006; Zumberge, et al., 2006*], U.S. East Coast [*Driscoll et al., 2000; Hill, et al., 2004; Newman, et al., in prep*], Storegga Slide [*Bryn, et al., 2003*]).

Several mechanisms have been proposed to trigger submarine failures, nevertheless, how these processes act alone or in concert to trigger slope failure remain poorly understood. One main reason is that many slope failures are examined after the fact and then by examining the slide scar and consequent slide deposit researchers attempt to reconstruct the sequence of events that led to the observed failure. There is much conjecture about when slope failure occurs during a sea-level cycle. Recent work on slope failure in the Atlantic and on the Storegga Slide complex show that slope failure is complex and is not simply related to eustatic sea level regressions. In fact, these studies indicate the greatest amount of failures along continental margins may occur during the transgression. The research presented here reveals a relationship between downslope creep, permeability pathways and potential slope failure.

The remaining chapters focus on the Chukchi margin of Arctic Alaska, examining drainage patterns and climatic variability across the region. The broad, shallow Chukchi shelf is an ideal location for sea level studies since vertical sea level fluctuations on the order of several meters can translate laterally into kilometers of shelf exposure. Channel sequences preserved on shelves provide insight into past base level change, paleodischarge, and climate fluctuations. Additionally, determining the extent of glaciation here has important implications for the development of global climate models, the understanding of freshwater balances in the Arctic and the degree of climate variability across the region. Numerous paleochannels are observed across the Chukchi shelf, both individually and within incised valleys. Many of these paleochannel and valleys appear to have been

downcut and incised as a result of base level lowering during the multiple sea level cycles. The most recent incisions, however, appear to have been downcut during the most recent deglaciation, a period of rapid sea level rise. In the absence of base level lowering, the simplest explanation for the incisions appears to be elevated discharge as a result of glacial meltwater input. Additional evidence of ice on the margin at this time is found on the outershelf where CHIRP subbottom data imaged a regionally extensive ice scour surface that dates to the most recent deglaciation. This study area has provided a valuable opportunity to examine not only shelf morphology, but also onshore-offshore interactions. This research has yielded new insights into the deglacial history of the northwestern Alaskan margin and Chukchi shelf. Specifically, we have documented an iceberg scour event that correlates with the Younger Dryas. The mineralogy of the associated sediments suggests a northwest Alaskan source. Increased discharge during the relative sea level rise following the LGM is also indicative of meltwater drainage from the northwest Alaskan margin. Together this evidence suggests a greater extent of continental glaciation in northwestern Alaska that previously recognized.

The appendix provides a follow-up to Chapter 2, including the results of geochemical analyses and AUV surveys that indicate there is indeed methane along the inner walls of the gas blowout features. This geochemical data corroborates our predictions based on the geophysical data presented in Chapter 2.

References

- Bryn, P., Berg, K., Forsberg, C.F., Solheim, A., and Kvalstad, T.J., 2005. Explaining the Storegga Slide. *Marine and Petroleum Geology*, 22:11-19.
- Christie-Blick, N. and Driscoll, N. W., 1995. Sequence Stratigraphy. *Annual Review of Earth and Planetary Sciences*, 25: 451-478.
- Driscoll, N. W., Weissel, J. K. and Goff, J. A., 2000. Potential for large-scale slope failure and tsunami generation along the U.S. mid-Atlantic coast. *Geology*, 28: 407-410.
- Greene, H.G., Murai, L.Y., Watts, P., Maher, N.A., Fisher, M.A., Paull, C.E., and Eichhubl, 2006. Submarine landslides in the Santa Barbara Channel as potential tsunami sources. *Natural Hazards and Earth System Sciences*, 6: 63-88.
- Hill, J. C., Driscoll, N. W., Brigham-Grette, J., Donnelly, J. P., Gayes, P. T. and Keigwin, L. D., 2007. New evidence for high discharge to the Chukchi shelf during the Last Glacial Maximum. *Quaternary Research*, in press.
- Newman, K.R., Cormier, M., Weissel, J.K., Driscoll, N.W., Kastner, M., Solomon, E.A., Robinson, G., Hill, J.C., Singh, H., and Camilli, R., 2007. Active methane venting observed at giant seafloor pockmarks along the mid-Atlantic shelf break with the Autonomous Underwater Vehicle SeaBED, *EPSL*, submitted.
- Vail, P. R., 1987. Seismic stratigraphy interpretation utilizing sequence stratigraphy, In: Bally, A. W. (Ed.), *Atlas of seismic stratigraphy*, Tulsa: American Association of Petroleum Geologists, pp. 1-10.
- Van Wagoner, J. C., Mitchum, R. M., Campion, K. C. and Rahmanian, V. D., 1990. *Siliciclastic sequence stratigraphy in well logs, cores and outcrops: Concepts for high-resolution correlation of time and facies*, Tulsa: American Association of Petroleum Geologists, 55 p.
- Zumberge, M., et al., 2006. Studies of the Gaviota Slide offshore southern California, In: *Geohazards*, ECI Symposium Series, Volume P7.

Chapter 2

Large-scale elongated gas blowouts along the U.S. Atlantic margin

2.1 Abstract

In May 2000, we surveyed a series of en echelon, asymmetric depressions along the outer shelf off Virginia and North Carolina using high resolution chirp and side-scan sonar. The features, which are elongated parallel to the shelf-edge and have steep landward walls, are approximately 4 km long, 1 km wide and up to 50 m deep. Based on internal stratal geometry interpreted from chirp profiles, the depressions do not appear to result from simple, down-to-the-east, normal displacement along deep-seated faults or structure. Rather, the depressions appear to have been excavated primarily by gas expulsion, creating large scale asymmetric gas escape structures that have been termed “gas blowouts.” Gas appears to have been trapped beneath a shelf-edge delta a few tens of meters thick exhibiting internal soft sediment deformation suggestive of progressive downslope (seaward) creep. These new data suggest the blowouts occurred when thin-skinned deformation and creep of the surficial deltaic sediment layers, together with updip/upslope gas migration, led ultimately to gas pressure in excess of the overburden. The location of the expulsion craters along the shelf edge and their elongated, asymmetric shapes strongly suggests a causal relation between the downslope creep of the delta and the expulsion event. We suggest a positive feedback between upward migration of gas-rich fluids through the low-stand delta and the downslope creep processes, which play an important role in controlling slope stability.

2.2 Introduction

Seafloor pockmarks and trapped gas have been observed along many continental margins (*Josenhans et al.*, 1978; *Hovland et al.*, 1984; *Hovland and Judd*, 1988; *Yun et al.*, 1997; *Vogt et al.*, 1999). These features are indicators of past or present fluid migration. Pockmarks are usually circular depressions ranging in size from meters to hundreds of meters with depths on the order of centimeters to tens of meters (*Hovland et al.*, 2002). However, seafloor pockmarks exhibit marked variability in size and shape as a result of different excavation histories (*Hovland et al.*, 2002). For example, elongated pockmarks or depressions, where one axis is much greater than the other, occur along slopes or in areas where the seafloor is affected by strong currents (*Hovland et al.*, 2002). In addition to asymmetry, areas exhibiting linear trends of pockmarks are commonly associated with a structural control on their formation.

Shallow gas associated with pockmarks along continental margins can be either thermogenic or biogenic in origin (*Hovland and Judd*, 1988; *Kvenvolden*, 1993). If the source is thermogenic, deep-seated faults are required to allow upward migration of the gas to charge shallow regions. If the gas is biogenic, it can be produced in situ by methanogenesis of organic material, or derived from gas hydrate dissociation at greater water depths (>500 m), with subsequent upslope migration. Until recently, most of the discussion on hydrate dissociation was focused on depressurization by sea-level falls during glacial periods, and the effect of the resulting release of overpressured gas-charged fluids on slope stability. Consequently, gas hydrate dissociation on passive margins was thought to occur

during the Last Glacial Maximum (LGM) (*Paull et al.*, 1996). While methane release by depressurizing gas hydrate could occur during sea-level falls, hydrate dissociation might also occur during interglacials/interstadials due to secular warming of bottom waters (*Bratton*, 1999; *Driscoll et al.*, 2000; *Kennett et al.*, 2000; *Mienert et al.*, 2002; *Vogt and Jung*, 2002). Thus, while there is general agreement that dissociation of gas hydrates can provide overpressured, gas-charged pore fluids that would promote slope instability on continental margins, there is no consensus on whether the mechanism happens preferentially during glacial or interglacial intervals.

Side-scan and subbottom data acquired during the May 2000 CH1000 survey aboard the *R/V Cape Hatteras* imaged a series of large asymmetric depressions along the U.S. mid-Atlantic margin (Figs. 1, 2). The en echelon depressions, located at ~100m water depth, are approximately 4 km long, 1 km wide and up to 50 m deep. The location of these features near the shelf break, their elongation parallel to the shelf edge and their steeper inner or landward walls, as well as the proximity of the large, late Pleistocene Albemarle-Currituck slide to the south lead *Driscoll et al.* (2000) to suggest these features might represent incipient large-scale failure of the outer shelf/upper slope. The asymmetric cross-sectional morphology of the depressions identified from the NOAA 3'' bathymetry suggested an origin through a small amount of down-to-the-east normal slip (*Driscoll et al.*, 2000). The data presented here indicate the origin of the depressions is more complex and suggest the features are gas expulsion craters, or “blowouts” along the shelf edge.

Here we describe the nature of the gas blowout features in detail, presenting the formation of these features in light of their morphology, stratal geometry, and location on the shelf. This study area (Fig. 2.1) provides an ideal opportunity to examine the interplay between downslope creep, differential slope permeability, and the upslope migration of gas-charged pore-water. We seek to determine if the blowouts represent an early phase of slope instability, and to examine whether their composite formation, involving several simultaneous factors (e.g., gas accumulation, deformation of undercompacted sediment and fluid flow), might provide new insights to the triggering mechanisms of slope failure.

2.3 Data Acquisition

The CH1000 side-scan and chirp sonar survey covered the outer shelf region from Cape Hatteras to the Norfolk Canyon (Fig. 2.2). Sonar data were acquired using the Scripps Institution of Oceanography (SIO) SUBSCAN system, which is based on components manufactured by EdgeTech. The system includes: (1) a DF1000 dual-frequency (100 and 500 kHz) side-scan instrument and (2) an X-Star chirp subbottom reflection sonar with sub-meter vertical resolution. The two sonar instruments were towed in tandem arrangement at depths from several to a few tens of meters above the seafloor. Data were acquired at a ship speed of ~4-5 knots. Towfish navigation was obtained by monitoring fish depth and the winch cable payout in relation to topside DGPS receivers. The CH1000 cruise track (Fig. 2.2) was designed to provide (a) detailed dip-line coverage (200 m line spacing) from the outer shelf to the upper slope across the northern blowouts B and C, (b) detailed strike line coverage (200 m line

spacing) of the blowouts, and (c) regional reconnaissance dip lines at 2 km spacing from the Norfolk Canyon to the Albemarle-Currituck slide. Subbottom reflection profiles were acquired using a 1-5.5 kHz chirp signal with a 50 ms sweep. Side-scan data were obtained on swaths extending out ~200 m either side of the towfish, providing ~100% overlap on dip and strike lines over the northern blowouts (Fig. 2.2, inset).

The chirp subbottom data were processed using the *SIOSEIS* (Henkart, 2003) and *Seismic Unix* (Cohen and Stockwell, 1999) seismic processing software packages. The side-scan data were processed using *Xsonar* (Danforth *et al.*, 1997). We constructed three mosaics of the 100 kHz side-scan data using: (1) all the dip lines, (2) the west-looking portions of the strike line data, and (3) the east-looking portions of the strike line data.

2.4 Results

2.4.1 Morphology of shelf edge depressions

The shelf edge depressions are located on the outermost shelf, in approximately 100 m of water, between the Norfolk Canyon to the north, and the Albemarle-Currituck submarine slide to the south (Figs. 1, 2). Both the bathymetry and the subbottom data show a varying cross-sectional asymmetry across the depressions (Figs. 1, 3). The slope of the landward walls is generally very steep, while the seaward walls show a more irregular morphology, ranging from gentle and relatively flat to somewhat steep (Figs. 3, 4). North and south of the main area of large, elongated depressions are several smaller, more circular craters (Fig. 2.1c).

Throughout most of the region the depressions are a sufficient distance landward from the shelf edge that there is a distinctive seaward wall. However, in regions where the depression is very close to the shelf edge, the seaward wall appears as more of a collapse structure, where the outermost portion of the shelf has moved a short distance downslope, creating an open-sided feature (e.g., Fig.3a, line 67). As expected, the relief of the seaward wall systematically diminishes toward the northern and southern termination of the elongated depressions.

Many of the chirp profiles show evidence of thinly laminated, recent sediment several meters thick that onlaps to the underlying depression surface (Fig. 2.3). Sediment deposited within the depressions and on the sloping walls modifies the overall morphology of the features, such that the greater the sediment infill, the smoother the features appear. Both the chirp and side-scan sonar data show evidence of southerly transport of the recent sediment (Figs. 3b, 5b). The strike lines shown in Figure 3b (e.g., line 285/286) display small prograding clinoforms along the northern flank of the depressions, with minimal recent sediment build up on the southern end. The side-scan data have regions of high backscatter on the shelf directly landward of the shelf-edge depressions (Fig. 2.5b) that appear to be mobile sediment bedforms. The linear features or ridges are asymmetric, with a sharp northern boundary and diffuse southern face of the bedform (Fig. 2.5b). In addition, long tails of high backscatter are observed on the southern side of the features (Fig. 2.5b).

2.4.2 Stratal geometry of shelf-edge deposit

The outer several kilometers of the margin in the shelf-edge depression region is covered by a well-stratified wedge of sediment that appears to be a shelf-edge delta (e.g., Fig. 2.4a, inset). The strata imaged in the dip profiles show evidence of an offlapping sequence perched on the edge of the margin (Fig. 2.3a, e.g. line161/162). Several, short gravity cores (<15 cm long) taken during the CH1000 survey revealed that the surface sediment is poorly sorted, consisting of gravels and silty clays. The stiff, cohesive nature of the sediments prevented the acquisition of longer cores. Thus, the deeper sediments were not sampled, and therefore their age remains unconstrained.

Strata in the offlapping wedge are not continuous and are disrupted at several length scales. The strata have small-scale “apparent folds,” or undulations, with highly variable layer thicknesses (e.g., Fig. 2.4c, inset). These features are short-wavelength and difficult to correlate laterally across adjacent profiles 200 m apart (Fig. 2.6). There is no systematic relationship between the apparent folds and the walls of the shelf-edge depressions.

2.4.3 Seismic signature of gas-charged sediments

Trapped gas is recognized in seismic data as bright, high-amplitude reflections that obscure deeper returns (*Hovland and Judd, 1988*). This reflection character of gas is observed in the shelf-edge deposit (Figs. 3, 4, 6). In addition to this particular reflection signature commonly associated with gas, acoustically transparent “wipe-out” zones that disrupt the stratigraphy are observed (e.g., Fig. 2.3a). Such features

have been identified in other gas-prone regions and are termed “columnar disturbances” (*Hovland and Judd, 1988*). The columnar disturbances or acoustic wipe-out zones occur in the landward walls, seaward walls, and beneath the shelf-edge craters (Figs. 3 and 4). Inboard of the laminated strata, a blotchy, unstratified acoustic character is observed in the surface sediments, and appears to be a large, composite acoustic wipe-out zone.

Bright reflections associated with trapped gas in the chirp data are often observed immediately below the steep, landward sides of depressions B and C (e.g., Figs. 3a, line 161/162, line 31; Fig. 2.4b, inset). The strike-line side-scan data show lineated zones of very high backscatter a few hundred meters long, parallel or subparallel to outcropping shelf-edge strata along the inner crater walls (e.g., Fig. 2.5a, inset) that correlate spatially with bright reflections seen in the chirp profiles. These same zones can be identified in both the east- and west-looking swaths (Fig. 2.5a, inset), indicating that these patches are reflectivity changes resulting from seabed roughness rather than large-scale seafloor slope variations.

2.4.4 Spatial relation between trapped gas and the shelf-edge delta

The sonar data shows evidence for extensive amounts of gas at shallow depths along the outer shelf, between Cape Hatteras and the Norfolk Canyon. There is a strong spatial correlation between trapped gas on the outer shelf, the shelf-edge depressions, and finely laminated deltaic strata. Landward of this deposit, gas appears to be freely venting and no large depressions are observed. This same spatial correlation is observed in the Albemarle-Currituck slide region, where numerous gas

pockets are observed, both trapped and freely venting. The chirp profiles across the upper slide region have evidence of internal deformation in layered strata along the shelf-edge, and are associated with bright reflections attributed to trapped gas (Fig. 2.7a). Additionally, there is a prominent dome shaped feature in the topography (Fig. 2.7b). The center of the dome is characterized by high backscatter and generally mottled acoustic signature, however there are some steeply dipping reflections beneath the middle of the dome.

2.5. Discussion

2.5.1 *Origin of shelf-edge depressions, or “gas blowout” features*

Prior to surveying the region, it seemed plausible that the shelf-edge depressions might have been controlled by normal faulting with collapse and rollover of the hanging wall into the fault trace (*Driscoll et al.*, 2000). However, the chirp reflection profiles show no evidence of large normal faults. The highly layered stratigraphy of the outer shelf provides clear marker horizons from which we can discern the lack of offset. Downslope creep along bedding planes is the only type of mass movement that can be identified from the chirp reflection data.

Trapped gas is evident in chirp reflection profiles across our study area, and appears to have a strong spatial correlation with a thin (few tens of meters) wedge of stratified sediment draped across the outermost shelf/upper slope. Gas also appears to be present (possibly venting) along the landward walls of the shelf-edge depressions. The lack of large normal faults, along with observations of soft sediment deformation

of the layered strata and the abundant presence of gas led us to conclude that these are gas escape features, or gas blowouts, created during expulsion episodes.

2.5.2 Morphology of gas blowouts

Strings of pockmarks are expected to nucleate along zones of weakness in the upper sediments (Hovland et al, 2002). In the blowout region, it appears gravitational forces have created a tensional stress on the shelf-edge delta sediments, as evidenced in the downslope creep of these strata. The en echelon arrangement of the blowout features also points to a tensional stress regime within the upper sediments and fluid flow focusing along weaknesses in the deltaic strata. While this might seem to indicate that the shelf-edge region would be dominated by extensional faulting, many of the dip seismic crossings of depressions (Fig. 2.3, line 161/162, line 157; Fig. 2.4, line 168/169) show no evidence for large down-to-the-east normal offset.

The morphology of the seaward wall changes with proximity to the shelf/slope break. Where the blowout is coincident with the shelf/slope break, the seaward wall appears to have collapsed. The morphology here is different than the seaward walls where the blowouts are set slightly inboard of the shelf/slope break, in that the collapsed walls are less steep, with minimal to no landward dip (e.g., Fig. 2.3a, line 67).

Variability in size and shape is observed along the series of blowouts, with a number of small more circular depressions superposed on the larger depressions (Fig. 2.1c). It is unclear whether the smaller (up to ~1 km in diameter), more circular

blowouts broaden and link together to form elongate features through time or are formed subsequently as a result of continued fluid venting.

The chirp subbottom data shows evidence of recent sediment infill in the blowout depressions in the form of southward prograding clinoforms, with thicknesses reaching up to ~5 m (Fig. 2.3b, line 285/286). The southern transport direction is consistent with the current flow direction inferred from the asymmetric bedforms observed in the side-scan data (Fig. 2.5b). Reworking and erosion of the shelf-edge delta and transgressive deposits by Gulf Stream outer shelf return flow currents might be the source of the mobile sediment. Given the patchiness of the sediment deposits, it is difficult to infer an accumulation rate for the region. Based on the locations of the gas blowouts and the overlying sediment infill, the best available age estimate for the blowouts is that they postdate the last major period of lower sea level, i.e. the LGM, and that they predate the southward prograding clinoforms in the craters. The lack of channels developed in the offlapping wedge suggests it must have been deposited subsequent to the LGM, when the shelf edge was most recently exposed.

2.5.3 Downslope creep and gas migration

The location of the blowout depressions along the shelf edge and their highly elongated, asymmetric shapes suggests a causal link between the downslope creep of the deltaic sediments and fluid expulsion. The strata imaged by the chirp profiles display several criteria diagnostic of soft sediment deformation and creep features (e.g., Fig. 2.4c): thickening and thinning of chaotic or transparent layers;

segmentation and rotation of superjacent sections; and homoclinal contacts that emphasize contrasts between transparent and reflective intervals (*O'Leary and Laine, 1996*).

We believe these deltaic stratal patterns do not result from primary depositional processes, such as sediment waves (*Schwehr et al., 2002*). Rather, we suggest the apparent fold patterns have formed by downslope creep processes that have progressively deformed the shelf-edge/upper slope sediments since their deposition. Such sedimentary deformation would have been facilitated by: (1) deposition of the low-stand delta across the outermost shelf and upper slope, providing a clear downslope gradient; (2) likely relatively rapid deposition (compared to interglacial/interstadial sedimentation at the same location), perhaps leading to undercompaction within the wedge; and (3) presence of clay layers within the sequence or at the base, which would provide possible decollement surfaces, facilitating downslope sliding.

We surmise that downslope creep within the low-stand wedge is linked to gas release through the shelf-edge seafloor in the following way: clay-rich layers in the low-stand delta and underlying highstand deposits are an effective seal to the vertical movement of gas. However, sand-prone layers within the delta and below the delta would allow gas-charged fluids to migrate upsection and updip along bedding planes. At some point, the buoyancy of the gas-charged fluids would exceed the confining pressure of the overburden, resulting in expulsion of gas-charged fluid and sediment to form the observed excavations. This scenario is illustrated schematically in Figure 8.

2.5.4 Gas distribution

Chirp and side-scan data suggest that gas-rich fluids have continued to accumulate and discharge through the floors of the excavations, particularly along the landward walls and beneath the blowouts, after the primary gas expulsion episode (Fig. 2.3a, line 161/162, line 31; Fig. 2.4c). Authigenic carbonate precipitation occurs in areas where gas charged fluid venting is active, or has been recently active (e.g., *Hovland and Judd*, 1988). Such seepage sites have been found on almost all active margins and on many passive margins (cited in *Naehr et al.*, 2000). We suggest the high amplitude backscatter observed along the bedding plane outcrop in the inner wall of blowout C represents authigenic carbonate precipitation on the seafloor (Fig. 2.5a, inset), which is consistent with observations from Hydrate Ridge (*Johnson et al.*, 2003). They observed similar high backscatter returns in side-scan data from Hydrate Ridge and correlated the high backscatter to the occurrence of authigenic carbonates using manned submersibles, ROVs, camera tows, and cores.

Although the shelf-edge delta appears to provide a relatively impermeable capping layer for gas, allowing gas to buildup below this layer, there exists large lateral variability, and the seal is not entirely impermeable. Throughout the mid-shelf region where the delta is absent the gas appears to be discharging freely through the seafloor, creating a mottled seismic character in the surface sediments (Figs. 4b). There are numerous acoustic wipe-out zones (columnar disturbances) throughout the delta section, indicating gas discharge in some places (e.g., Figs. 3, line 31, line 67; 4a; 7). It is difficult to infer the timing of the smaller wipe-out zones, which might be

coincident with the formation of the blowouts, or could post-date or predate blowout formation.

In addition to spatial variability in gas distribution, differences in acoustic character of gas-charged sediments are observed in the shelf-edge delta. For example, when the gas is concentrated beneath an impermeable layer it results in a high-amplitude reflector with acoustic blanking below. Sound velocity in gas-charged sediments is much lower than in non-gassy sediments, creating a large acoustic impedance change that reflects a high proportion of incident acoustic energy (*Hovland and Judd, 1988*). When gas has risen through the overlying sediments, a very different, more transparent, acoustic character results (*Hovland and Judd, 1988; O'Leary and Laine, 1996; Hill et al., 2002*). Previous researchers noticed this acoustic character could be confused with erosional channels (*Hovland and Judd, 1988*). However there is no stratigraphic expression of sediment infill and the acoustically transparent zones are very difficult to trace laterally over any appreciable distance, implying these features are not part of a drainage network (Fig. 2.6). Our preferred interpretation is that gas expulsion has physically disturbed the internal stratigraphic layering of the sediments, and therefore the impedance contrast, resulting in a zone with reduced acoustic reflectivity (*Hovland and Judd, 1988; O'Leary and Laine, 1996; Hill et al., 2002*).

2.5.5 Origin of the gas

Thermogenic gas in Upper Jurassic-Lower Cretaceous rocks was discovered in exploratory drilling of the Baltimore Canyon Trough at ~3700-4700m depth

(Mattick and Libby-French, 1988). However, we surmise that it would be difficult for the thermogenic gas to migrate upsection through various permeability barriers to the shallow depths observed in the chirp profiles, unless there were permeable pathways created by tectonic activity (faults and fractures) extending from deep gas reservoirs to the near-surface. The chirp reflection data suggests such fracture pathways are not present.

We therefore assume that the gas is biogenic in origin, produced either *in situ* by bacterial decay of organic carbon in marine sediments, or by decomposition of gas hydrate deeper on the margin and subsequent updip/upslope migration of the released gas to the blowout sites on the outer shelf. It is difficult to distinguish between these two possible origins. A biological origin of the gas would involve local methanogenesis by microbial reduction of CO₂ or acetate derived from organic carbon in the sediments (Wellsbury and Parkes, 2000). A supply of organic C (> ~0.5 wgt. % of the sediment; e.g., Kennicutt *et al.*, 1993) would be needed, plus burial rapid enough to prevent oxidation of the organic matter in the sulphate reduction zone of the shallow subseafloor environment. Ocean Drilling Program work off New Jersey encountered abundant gas in the undercompacted/ overpressured Pleistocene section of the upper slope (Shipboard Scientific Party, 1998). The Plio-Pleistocene shelf-edge succession there appears to be composed of stacked marine deltaic wedges deposited rapidly during glacials, with intervening thin, hemipelagic muds deposited during sea level transgressions and highstands (Dugan and Flemings, 2000), indicating that favorable conditions are present for biogenic methane production.

Our preferred hypothesis, however, is that gas in this region is related to the dissociation of gas hydrates during the late Pleistocene/Holocene. According to the P-T stability field for methane hydrate and modern bottom water temperatures (e.g., *Kvenvolden*, 1993), the base of the hydrate stability zone would intersect the seafloor at ~650m on the upper continental slope of the mid-Atlantic margin (*Dillon and Max*, 2000). Thus, there should be no gas hydrate present in the sediments directly underlying the shelf-edge blowouts. Gas hydrate might have extended to shallower depths along the margin earlier during glacial cycles depending on the relationship between sea level and bottom water temperature, but the stability zone would still have been much deeper on the slope than the blowout region (c.f. *Vogt and Jung*, 2002).

The stratigraphic relationship of the blowouts with the shelf-edge delta deposits indicates the blowout features occurred since the LGM. We propose that secular warming of bottom waters, caused by the reorganization of water masses during climate fluctuations, may be an important mechanism to dissociate gas hydrates at depth (e.g., *Bratton*, 1999; *Driscoll et al.*, 2000; *Kennett et al.*, 2000; *Mienert et al.*, 2002; *Vogt and Jung*, 2002). *Vogt and Jung* (2002) showed that thermal conduction could melt 10 – 100 m of hydrate in the hydrate stability zone of the upper continental slope within a few thousand years after a rise in bottom water temperatures. Temperature fluctuations on the order of 2.5°C have been documented in the western North Atlantic since the last glaciation (*Dwyer et al.*, 2000). For the U.S. mid-Atlantic margin, post-glacial introduction of warm Gulf Stream waters might have released gas trapped in hydrates along the upper slope, allowing free gas

to migrate upward to the outer shelf region. Gas then either would be trapped by the deltaic strata or escape in other areas of more permeable shelf sediments.

2.5.6 Relationship between gas and slope instability

Both free and hydrate-trapped gas have been recognized previously along the southern North Carolina margin, in association with the Blake Ridge region, as well implicated in triggering the Cape Fear and Cape Lookout landslides (*Popenoe and Dillon, 1996*). Though our study area is to the north of these known gas-prone regions, the seismic reflection profiles provide evidence for an extensive amount of gas along the outer shelf from Cape Hatteras to the Norfolk Canyon, including the Albemarle-Currituck Slide area. Throughout the shelf-edge region, gas appears to be both trapped beneath the finely laminated, clay-rich, capping layer and freely venting in areas where this layer appears to be absent. We suggest that the distribution of slides along the US Atlantic margin may coincide with the distribution of lowstand deltaic sediments; a correlation commonly explained by rapid sedimentation, undercompaction and oversteepening of the shelf edge (e.g., *Embley and Jacobi, 1977*). However, there is also a spatial correlation between shelf-edge delta deposits and trapped gas. The composite formation of the blowout features described here indicates that gas may play a more important role in controlling slope stability in this region than previously recognized. Additionally, similar evidence of shallow gas accumulation is identified in the large, late-Pleistocene Albemarle-Currituck slide region ($\sim 100 \text{ km}^3$ in area; *Prior et al., 1986; Driscoll et al., 2000*), indicating that gas may also have played a role in this slide (Fig. 2.7, line 309/310).

While the origin of gas in the blowout region remains unknown, we propose a two-phase shelf/slope destabilization model, based on the assumption that the gas is related to the dissociation of hydrates at depth. The conceptual model builds on previous understanding regarding slope failure and feedbacks on hydrate stability (Paull *et al.*, 1996; Paull *et al.*, 2000b). In the Paull *et al.* model, lowered sea-level (e.g., during glacial periods) triggers hydrate dissociation and subsequent slope failure. Unloading due to slope failure lowers the overburden and thus causes further hydrate dissociation, which, in turn, may lead to additional slope failure. In this scenario, because of the positive feedback between unloading and hydrate dissociation, small failures could evolve into larger failures (Paull *et al.*, 1996; Paull *et al.*, 2000b). The model presented here is an example of how the interplay of hydrate melting and climate fluctuations can lead to slope instability during interglacial periods.

In our model for this region, the first stage is temperature dependent and the second stage is pressure dependent. Following the LGM, a series of events brought relatively warmer Gulf Stream waters into the region along the lower slope of the western Atlantic margin (Boyle and Keigwin, 1987; Dwyer *et al.*, 2000). The introduction of warmer bottom water is expected to facilitate the initial gas release by shifting the top of the gas hydrate stability zone deeper and melting any hydrates above the new threshold. The free gas should migrate upslope and build up significant overpressure where it is trapped by shelf-edge delta sediments. Downslope creep of the deltaic strata in response to gravitational forces and continued updip/upslope fluid migration could account for gas blowouts similar to the

ones described in detail here. These features may represent the initiation of slope failure in the upper few tens of meters of sediment. Removal of the upper strata might cause further hydrate destabilization downslope through the effects of depressurization.

2.5.7 Implications for stability of the U.S. east coast margin

The association of shallow, trapped gas with shelf-edge delta deposits appears to be the key link in forming the blowout features observed in our study area. However, the question remains as to whether this scenario has occurred or will occur along other parts of the margin. Our side-scan and chirp sonar data indicates an extensive amount of shallow gas present along a large section of the margin, much of which coincides with shelf-edge delta deposits. The region encompassing the Albemarle-Currituck slide received sediment from the Albemarle River during the Pleistocene (*Bunn and McGregor, 1980*) and displays several intriguing features that indicate this area may represent the precondition for a gas blowout. In the case of existing gas blowouts to the north, we have found evidence that well-laminated, internally deformed strata may provide a sufficient trapping mechanism for shallow gas, such that gas pressure can accumulate and eventually exceed the overburden. Similar evidence of shallow, trapped gas in association with layered strata above is also found in the Albemarle-Currituck slide region. While gas blowouts are not found here, there is a prominent topographic dome on the shelf-edge, which suggests that trapped gas may be exerting pressure on the overlying sediments and causing the doming. The evidence is not conclusive, yet it raises the possibility that a gas

blowout scenario might have been the triggering mechanism for the Albemarle-Currituck slide.

2.6 Conclusions

The outermost shelf offshore of Virginia/North Carolina displays a series of en echelon, asymmetric gas blowouts, i.e. elongated pockmarks (e.g., *Hovland and Judd*, 1988). Sonar data have delineated a wedge of stratified sediment draped across the shelf-edge. This sediment wedge appears to be a lowstand delta deposit that was most likely deposited since the LGM. The deltaic strata show evidence of internal deformation that is indicative of downslope creep. There is no evidence of large normal faulting, or other structural control on the stratal geometry. There appears to be a strong spatial correlation between trapped, shallow gas and the shelf-edge delta deposit. Gravitational forces have created a tensional stress on the shelf-edge delta sediments, as evidenced by creep soft sediment deformation. The en echelon arrangement of the blowout features also points to a tensional stress regime within the surficial sediments. Updip/upslope fluid migration most likely occurs in sand-prone layers beneath or within the shelf-edge delta. The buoyancy of the gas-charged fluids eventually should exceed the confining pressure of the overburden, resulting in expulsion of gas-charged fluid and sediment to form the observed excavations. The precise age of the blowouts remains unknown, although they post-date the formation of the shelf edge delta, which is presumably after the LGM. The origin of the gas remains unknown; however, post-LGM formation of the blowout features suggests secular warming of bottom waters and methane hydrate dissociation. The processes

described here indicated that gas may play a more important role in shelf/slope stability than previously recognized.

2.8 Acknowledgements

This research was funded by the National Science Foundation, with grants OCE-9907254 and OCE-9809612. We thank associate editor, W. Waite, and reviewer, W. Dillon for very helpful reviews that have greatly benefited this manuscript.

2.9 Chapter Acknowledgement

Chapter 2, in full, is a reprint of the material as it appears in Journal of Geophysical Research: Hill, J.C., Driscoll, N.W., Weissel, J.K. and Goff, J.A., 2004. Large scale elongated gas blowouts along the U.S. Atlantic margin. Journal of Geophysical Research 109, doi: 10.1029/2004JB002969.

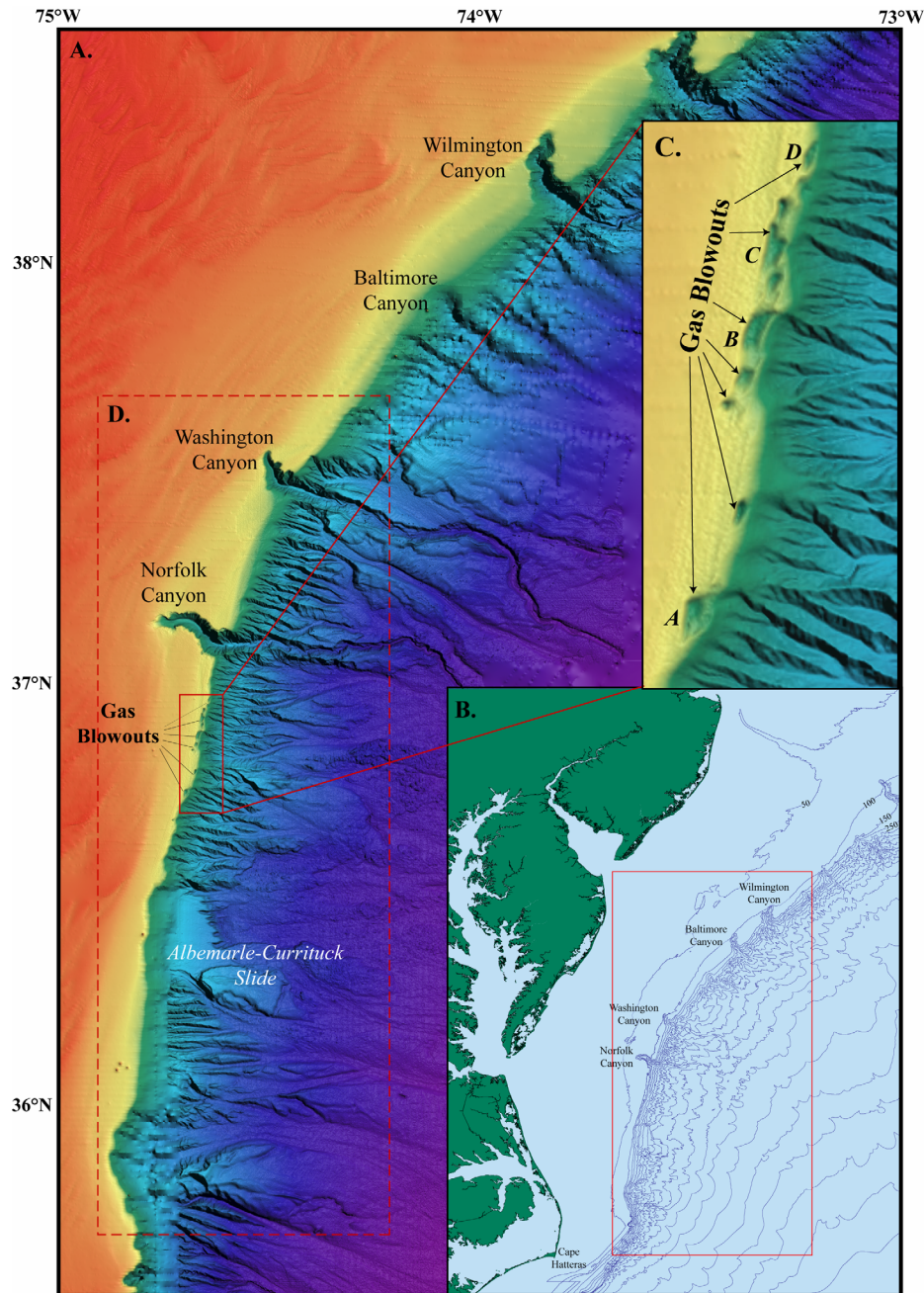


Figure 2.1 *a.* En echelon, large-scale, elongate gas blowout features offshore of Virginia and North Carolina, between the Norfolk Canyon and the Albemarle-Currituck Slide. Bathymetry is from the NOAA 3'' grid. *b.* Location map. *c.* Enlargement of gas blowout features. Individual blowouts are labeled A through D. Red arrows indicate the smaller, more circular blowout features. *d.* Location of Figure 2.

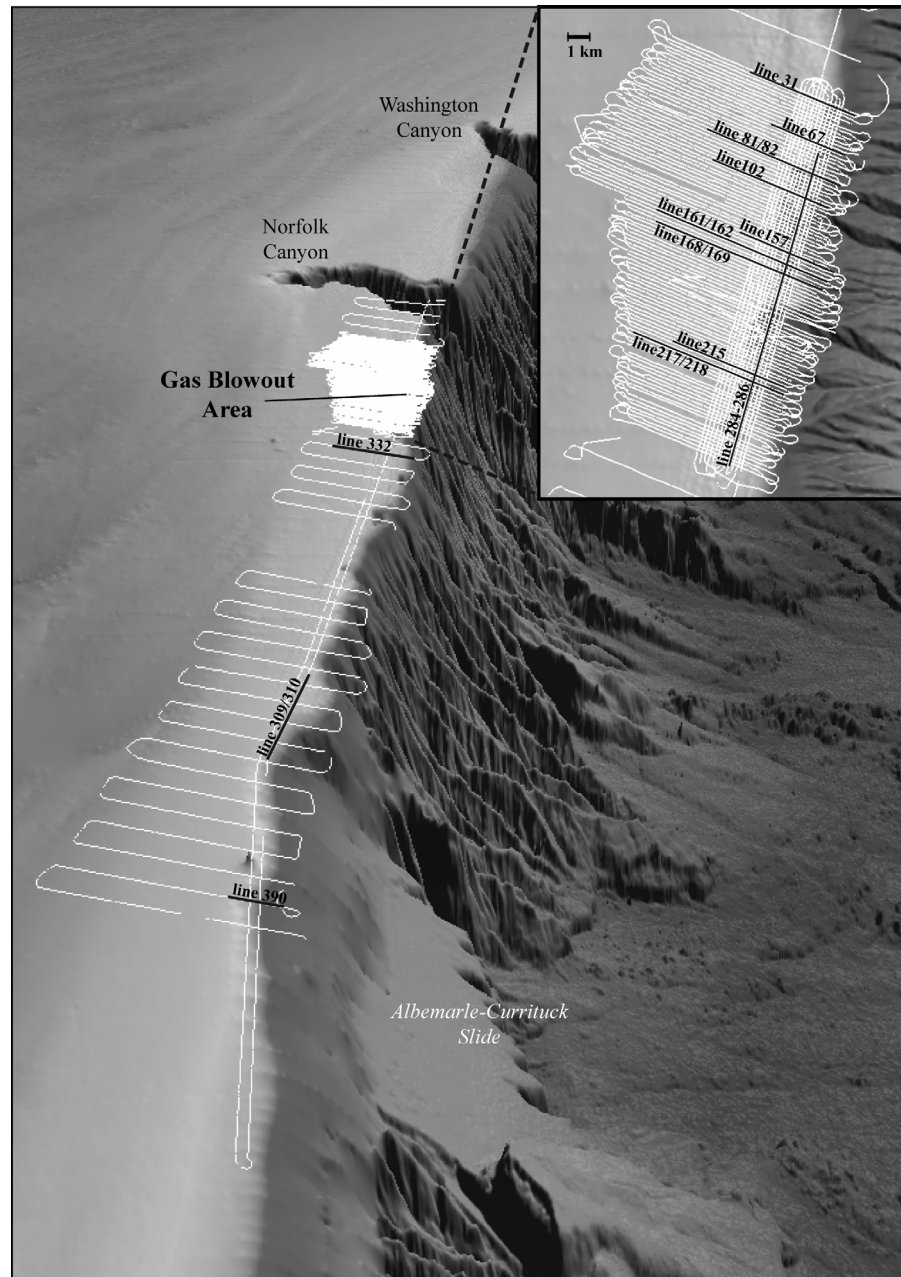
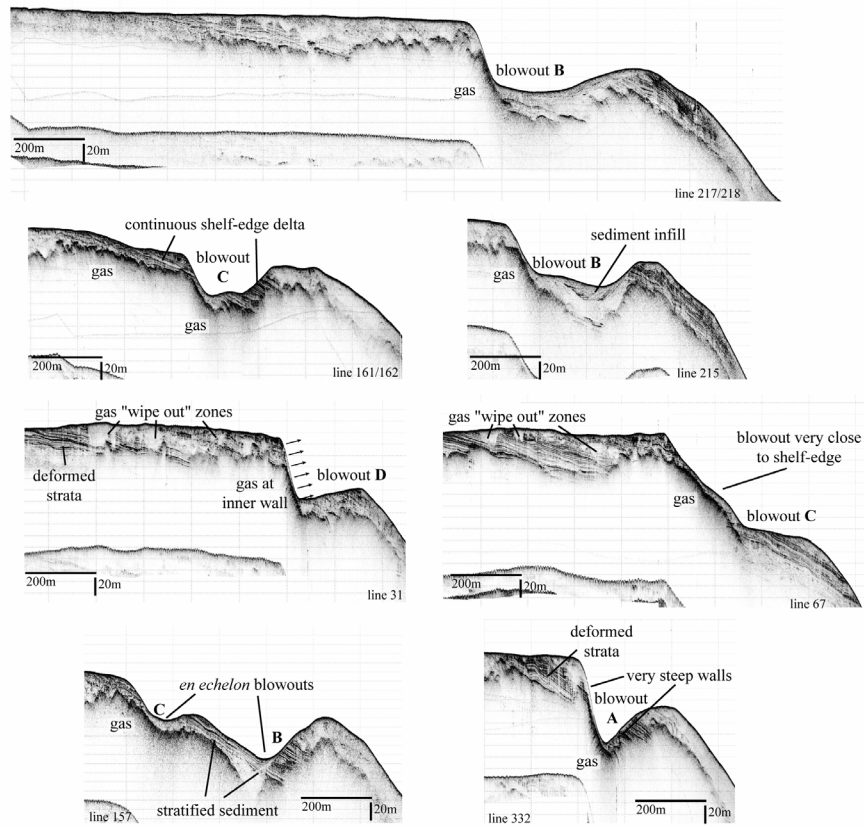


Figure 2.2 Survey ship track coverage superposed on NOAA 3'' gridded bathymetry in 3-dimensional perspective view. Profile line numbers shown in Figures 3, 4, and 7 are labeled. See Figure 1 for location.

A. Chirp dip line profiles



B. Chirp strike line profiles

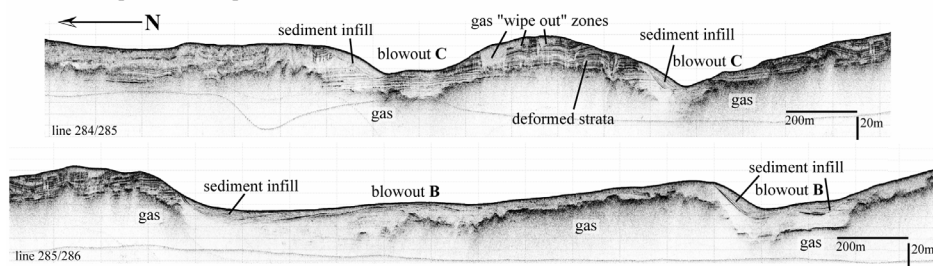
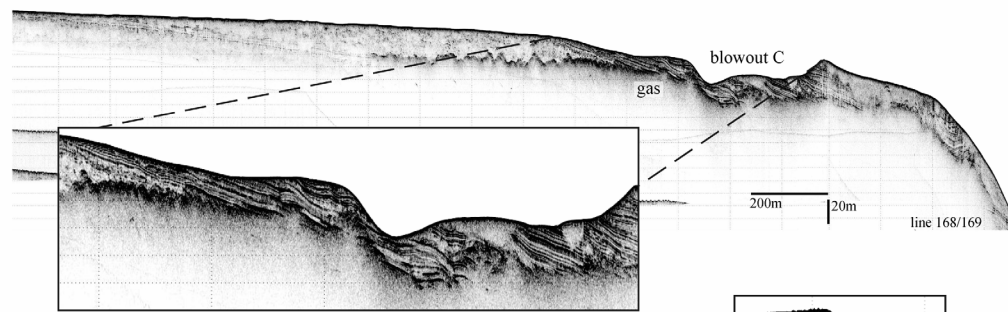
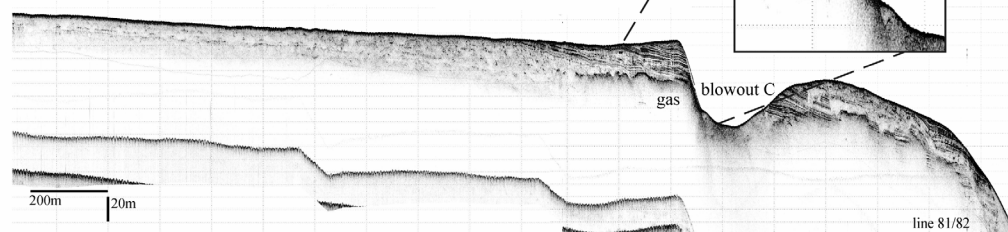


Figure 2.3 a. Dip chirp subbottom profiles (see Figure 2 for location). Gas blowout features have steep landward walls with high backscatter gas prominent at the face of this wall. The internally deformed wedge of stratified sediment perched at the shelf-edge has been locally removed by the gas blowout processes. Stratified sediment is also locally disturbed by gas “wipe-out” zones. b. Strike chirp subbottom profile (see Figure 2 for location). Strike line profiles show similar characteristics to the dip line profiles, including high backscatter gas, internally deformed, stratified sediment, and gas “wipe-out” zones. Additionally, small prograding clinoforms are shown in the sediment infill along the northern walls of the blowout depressions.

A. Shelf-edge delta



B. Gas at inner wall



C. Deformed strata

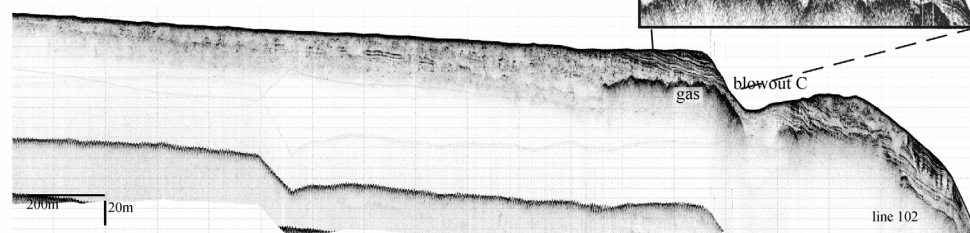


Figure 2.4 *a.* The stratified sediment wedge interpreted as a shelf-edge delta is continuous across the blowout area. *b.* High backscatter gas at the steep, landward wall of the blowout, showing possible evidence of continued gas-charged fluid seepage. *c.* Internal deformation of the stratified sediment as a result of downslope creep.

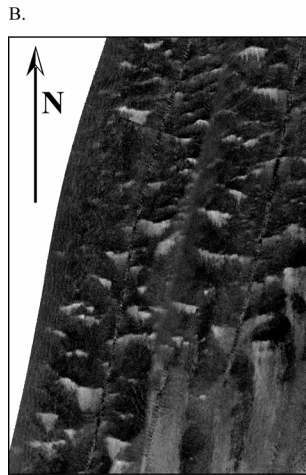
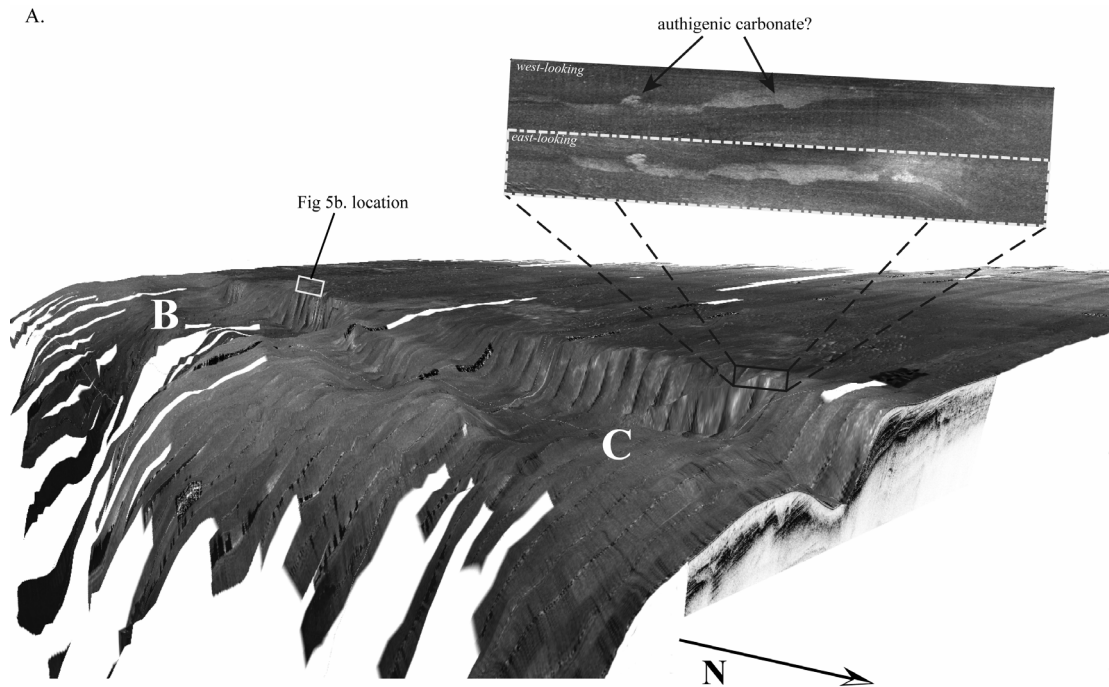


Figure 2.5 *a.* (TOP): Backscatter images from the strike line mosaics: west looking (upper), east looking (lower) from the inner wall of blowout 'C' in the vicinity of chirp profile 81/82 (Fig. 2.4b). West (shallower water) is at the top. Lighter shades correspond to higher backscatter. Low-stand delta bedding outcrop along the blowout inner wall is clearly imaged. The slightly lobate high backscatter zone appears to obscure the outcropping bedding on the downslope side. This relation is consistent with precipitation of carbonate crusts from continued gas-rich discharge after formation of the blowouts. (BOTTOM): Dip line side-scan mosaic draped over the NOAA 3'' bathymetric grid, showing location of the strike images above. The chirp subbottom profile on the right has been co-registered with the dip line mosaic. Blowouts 'B' and 'C' are labeled (c.f. Figure 1). *b.* Portion of strike side-scan mosaic. "Asymmetric bedforms" discussed in the text are labeled. These are interpreted as sand ridges, and the asymmetric nature of the bedform appears to indicate southward sediment transport in the blowout region.

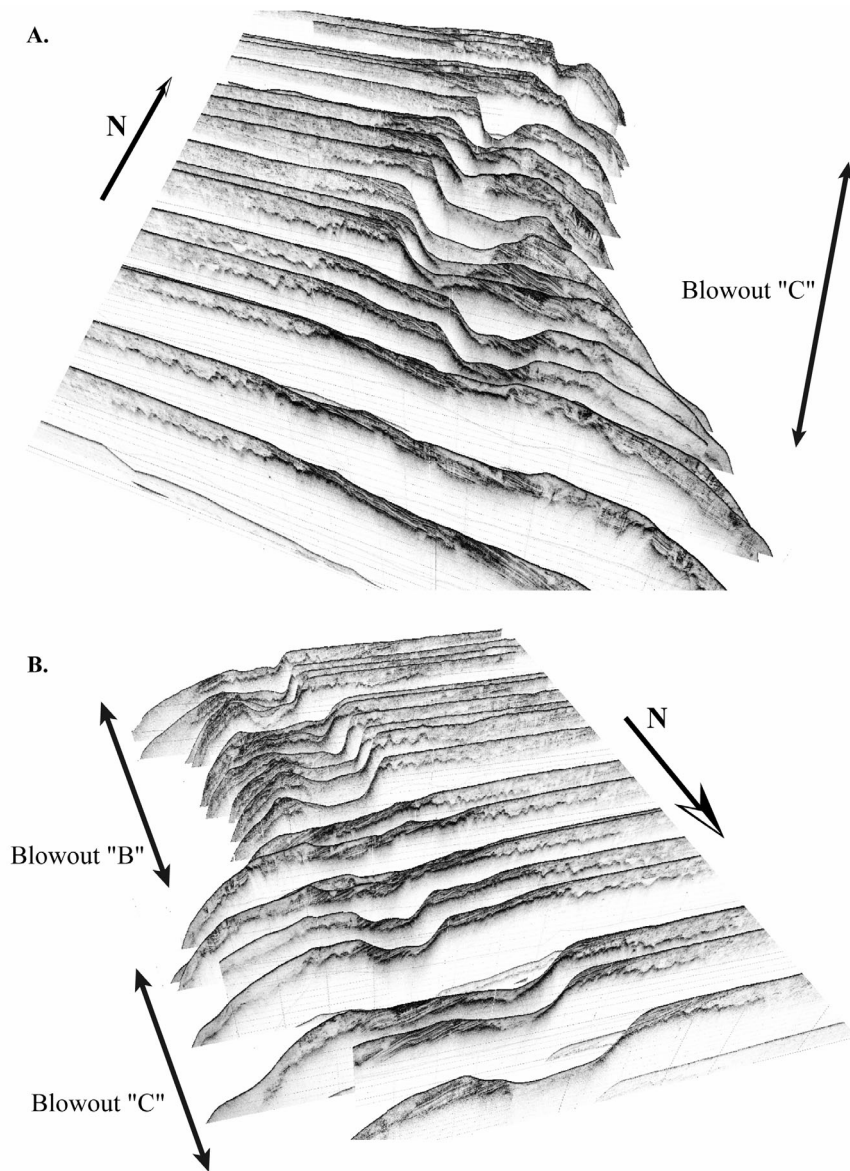
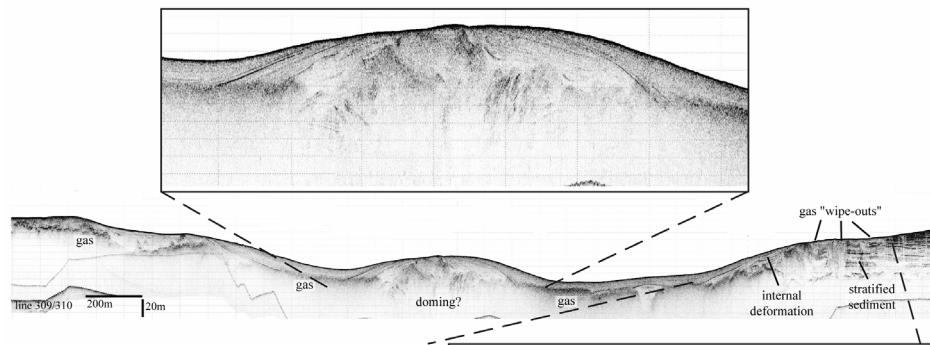


Figure 2.6 *a., b.* Chirp subbottom profiles co-registered with bathymetry and displayed in a 3-D perspective. The blowout features display a distinct en echelon arrangement. A strong correlation between trapped gas and the shelf-edge delta is apparent throughout the region. The deformed strata are difficult to trace laterally between profiles and the deformation and gas make it difficult to observe the character of the deeper stratigraphy along the margin.

A. Chirp dip line profile



B. Chirp strike line profile

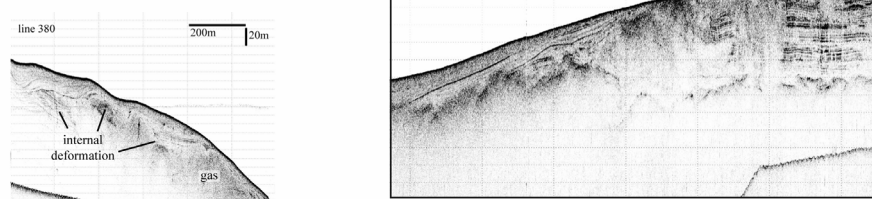


Figure 2.7 Strike (a) and dip (b) chirp subbottom profiles from the Albemarle-Currituck slide area. Similar to the gas blowouts region, this area shows internally deformed, stratified sediments, high-backscatter trapped gas and gas “wipe-out” zones. Additionally, there is a large dome-like feature showing possible evidence of uplift by gas charged fluids.

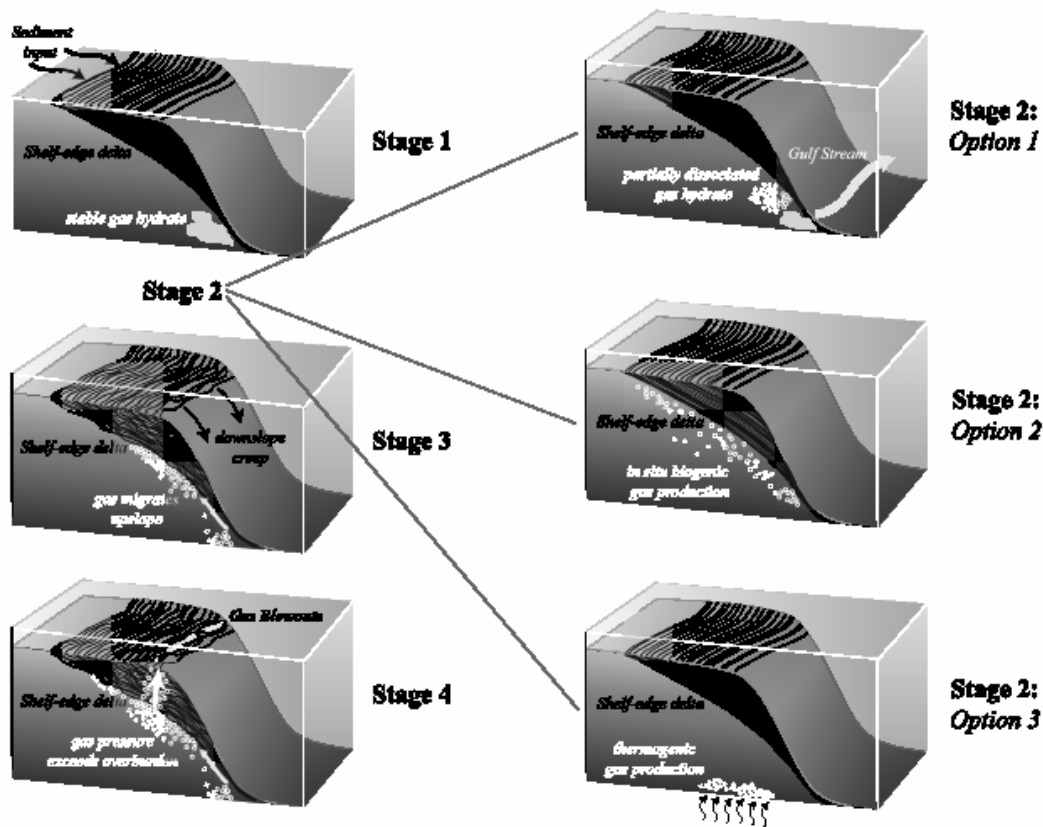


Figure 2.8 Schematic outlining the proposed gas blowout process. **Stage 1:** Build up of shelf-edge delta during period of lowered sea-level, presumably glacial-interglacial transition; stable gas hydrate is present at depth on the upper slope. **Stage 2:** Gas accumulation on the shelf/slope—three possible origins. *Option 1:* Gas is produced from hydrate dissociation. Post-glacial introduction of warm Gulf Stream bottom water top of the gas hydrate stability zone lower on the slope, dissociates hydrates at ~650m water depth. *Option 2:* Biogenic gas is produced in situ from organic Carbon in the sediments. *Option 3:* Thermogenic gas is produced at depth on the lower slope. **Stage 3:** The shelf-edge strata creep downslope, creating permeable pathways for gas to migrate upslope. Biogenic gas, however, may be produced at multiple depths along the slope, including directly beneath the shelf-edge delta and would not require upslope migration. **Stage 4:** Gas accumulates sufficient pressure to exceed the overburden and is expelled through the overlying sediments, creating the gas blowout craters.

References

- Boyle, E. and Keigwin, L. D., 1987. North Atlantic thermohaline circulation during the past 20,000 years linked to high latitude surface temperature. *Nature*, 330: 35-40.
- Bratton, J. F., 1999. Clathrate eustasy: Methan hydrate melting as a mechanism for geologically rapid sea-level fall. *Geology*, 27: 915-918.
- Bugge, T., Belderson, R. H. and Kenyon, N. H., 1988. The Storegga Slide. *Philosophical Transactions of the Royal Society of London, A*, 325: 357-388.
- Bunn, A. R. and McGregor, B. A., 1980. Morphology of the North Carolina continental slope, western north Atlantic, shaped by deltaic sedimentation and slumping. *Marine Geology*, 37: 253-266.
- Cohen, J. K. and Stockwell Jr., J. W., 1999. CWP/SU: Seismic Unix Release 33: a free package for seismic research and processing. Center for Wave Phenomena, Colorado School of Mines.
- Danforth, W. W., 1997. Xsonar/ShowImage; a complete system for rapid sidescan sonar processing and display. U.S. Geological Survey Open File Report 97-0686.
- Dillon, W. P. and Max, M. D., 2000. U.S. Atlantic continental margin: The best known gas hydrate locality, *In* Max, M. D. (Ed.), *Natural gas hydrate in oceanic and permafrost environments*, Dordrecht, Netherlands: Kluwer Academic Press, pp. 157-170.
- Driscoll, N. W., Weissel, J. K. and Goff, J. A., 2000. Potential for large-scale slope failure and tsunami generation along the U.S. mid-Atlantic coast. *Geology*, 28: 407-410.
- Dugan, B. and Flemmings, P. B., 2000. Overpressure and fluid flow in the New Jersey continental slope: Implications for slope failure and cold seeps. *Science*, 289: 288-291.
- Dwyer, G. S., Cronin, T. M., Baker, P. A. and Rodriguez-Lazaro, J., 2000. Changes in North Atlantic deep-sea temperature during climatic fluctuations of the last 25,000 years based on ostracode Mg/Ca ratios. *Geochemistry, Geophysics, Geosystems*, doi: 2000GC000046.
- Embley, R. W. and Jacobi, R. D., 1977. Distribution and morphology of large submarine sediment slides and slumps on Atlantic continental margins. *Marine Geotechnology*, 2: 205-228.

- Evans, D., King, E. L., Kenyon, N. H., Brett, C. and Wallis, D., 1996. Evidence for long-term instability in the Storegga Slide region off western Norway. *Marine Geology*, 130: 281-292.
- Henkart, P., 2003. SIOSEIS. <http://sioseis.ucsd.edu>
- Hill, J. C., Driscoll, N. W., Weissel, J. K. and Goff, J. A., 2002. Large-scale elongated blowouts, offshore Virginia/North Carolina: Process and product. *Eos Trans. AGU*, 83(47), Fall Meet. Suppl.: Abstract OS71C-0305.
- Hovland, M., Judd, A. G. and King, L. H., 1984. Characteristic features of pockmarks on the North Sea Floor and Scotian Shelf. *Sedimentology*, 31: 471-480.
- Hovland, M. and Judd, A. G., 1988. *Seabed pockmarks and seepages*, London: Graham and Trotman, 293 p.
- Hovland, M., Gardner, J. V. and Judd, A. G., 2002. The significance of pockmarks to understanding fluid flow processes and geohazards. *Geofluids*, 2: 127-136.
- Johnson, J. E., Goldfinger, C. and Suess, E., 2003. Geophysical constraints on the surface distribution of authigenic carbonates across the Hydrate Ridge region, Cascadia margin. *Marine Geology*, 202: 79-120.
- Josenhans, H. W., King, L. H. and Fader, G. B. J., 1978. A side-scan sonar mosaic of pockmarks on the Scotian Shelf. *Canadian Journal of Earth Sciences*, 15: 831-840.
- Kennett, J. P., Cannariato, K. G., Hendy, I. L. and Behl, R. J., 2000. Carbon isotopic evidence for methane hydrate instability during Quaternary interstadials. *Science*, 288: 128-133.
- Kennicutt III, M. C., Brooks, J. M. and Cox, H. B., 1993. The origin and distribution of gas hydrates in marine sediments, In Engel, M. H. and S. A. Macko (Eds.), *Organic Geochemistry*, New York: Plenum Press, pp. 535-544.
- Klitgord, K. A., Hutchinson, D. R. and Schouten, H., 1988. U.S. Atlantic continental margin: Structural and tectonic framework, In Sheridan, R. E. and J. A. Grow (Eds.), *The Atlantic Continental Margin of the U.S.*, *The Geology of North America*, Boulder: Geological Society of America, pp. 10-55.
- Kvenvolden, K. A., 1993. Gas hydrates-geological perspective and global change. *Reviews of Geophysics*, 31: 173-187.

- Laberg, J. S. and Vorren, T. O., 2000. The Traenadjupet Slide, offshore Norway--morphology, evacuation and triggering mechanisms. *Marine Geology*, 11: 95-114.
- Mattick, R. E. and Libby-French, J., 1988. Petroleum geology of the United States Atlantic continental margin, In Sheridan, R. E. and J. A. Grow (Eds.), *The Atlantic Continental Margin U.S., The Geology of North America*, Boulder: Geological Society of America, pp. 445-462.
- Mienert, J., Vanneste, M., Berndt, C. and Bunz, S., 2002. Gas hydrate dissociation as a result of Holocene warming influences on slope stability: the Storegga Slide. EGS XXVII General Assembly.
- Mountain, G. S. and Tucholke, B. E., 1985. Mesozoic and Cenozoic geology of the U.S. Atlantic continental slope and rise, In Poag, C. W. (Ed.), *Geologic evolution of United States Atlantic margin*, New York: Van Nostrand, Reinhold Co., pp. 293-341.
- Naehr, T. H., Rodriguez, N. M., Bohrman, G., Paull, C. K. and Botz, R., 2000. Methane-derived authigenic carbonates associated with gas hydrate decomposition and fluid venting above the Blake Ridge diapir, In Paull, C. K., Matsumoto, R., Wallace, P.J., Dillon, W.P. (Eds.), *Proceedings of the Ocean Drilling Program, Scientific Results*, pp. 285-300.
- O'Leary, D. W. and Laine, E., 1996. Proposed criteria for recognizing intrastratal deformation features in marine high resolution seismic reflection profiles. *Geo-Marine Letters*, 16: 305-312.
- Paull, C. K., Ussler III, W., Borowski, W. S. and Spiess, F. N., 1995. Methane-rich plumes on the Carolina continental rise: Associations with gas hydrates. *Geology*, 23: 89-92.
- Paull, C. K., Beulow, W. J., Ussler III, W. and Borowski, W. S., 1996. Increased continental-margin slumping frequency during sea-level lowstands above gas hydrate-bearing sediments. *Geology*, 24: 143-146.
- Paull, C. K., Matsumoto, R., Wallace, P. J. and Dillon, W. P., 2000. *Proceedings of Ocean Drilling Program, Scientific Results*, College Station: Ocean Drilling Program, 459 p.
- Popenoe, P., Schmuck, E. A. and Dillon, W. P., 1993. The Cape Fear Landslide: Slope failure associated with salt diapirism and gas hydrate decomposition, In Schwab, W. C., H. J. Lee and D. C. Twichell (Eds.), *Submarine Landslides: Selected studies from the U.S. Exclusive Economic Zone*, U.S. Geological Survey Bulletin 2002B.

- Prior, D. B., Doyle, K. H. and Neurater, T., 1986. The Currituck Slide, mid Atlantic continental slope--revisited. *Marine Geology*, 73: 25-45.
- Schwehr, K. D., Driscoll, N. W. and Tauxe, L., 2002. Deciphering the origin of the Humboldt Slide using anisotropy of magnetic susceptibility. *EGS-AGU-EUG Joint Assembly*: Abstract EAE03-A-12756.
- Shipboard Scientific Party, 1998. Site 1073, In Austin, J. A., Christie-Blick, N., and Malone, M.J., et al. (Eds.), *Proceedings of the Ocean Drilling Program, Initial Reports*, College Station: Ocean Drilling Program, pp. 153-190.
- Ussler III, W. and Paull, C. K., 2001. Ion exclusion associated with marine gas hydrate deposits, In Paull, C. K. and W. P. Dillon (Eds.), *Natural gas hydrates: Occurrence, distribution, and detection*, American Geophysical Union, pp. 41-52.
- Vogt, P. R., Gardner, J. and Crane, K., 1999. The Norwegian-Barents-Svalbard (NBS) continental margin: Introducing a natural laboratory of mass wasting, hydrates and ascent of sediment, pore water, and methane. *Geo-Marine Letters*, 19: 2-21.
- Vogt, P. R. and Jung, W. Y., 2002. Holocene mass wasting on upper non-Polar continental slopes--due to post-Glacial ocean warming and hydrate dissociation? *Geophysical Research Letters*, doi: 10.1029/2001GL013488.
- Wellsbury, P. and Parkes, R. J., 2000. Deep biosphere: Sources of methane for oceanic hydrates, In Max, M. D. (Ed.), *Natural gas hydrate in oceanic and permafrost environments*, Dordrecht, Netherlands: Kluwer Academic Press, pp. 91-104.
- Yun, J. W., Orange, D. L. and Field, M. E., 1997. Subsurface gas offshore of northern California and its link to submarine geomorphology. *Marine Geology*, 154: 357-368.

Chapter 3

New evidence for high discharge to the Chukchi shelf since the Last Glacial Maximum

3.1 Abstract

Using CHIRP subbottom profiling across the Chukchi shelf, offshore NW Alaska, we observed a large incised valley that measures tens of kilometers in width. The valley appears to have been repeatedly excavated during sea level lowering; however, the two most recent incisions appear to have been downcut during the last sea level rise, suggesting an increase in the volume of discharge. Modern drainage from the northwestern Alaskan margin is dominated by small, low discharge rivers that do not appear to be large enough to have carved the offshore drainage. The renewed downcutting and incision during the deglaciation and consequent base level rise implies there must have been an additional source of discharge. Paleoprecipitation during deglaciation is predicted to be at least 10% less than modern precipitation and thus cannot account for the higher discharge to the shelf. Glacial meltwater is the most likely source for the increased discharge.

3.2 Introduction

Channel sequences preserved on continental shelves provide important information about past base level change and paleodischarge. In most coastal fluvial valleys downcutting results from a base level lowering, such as relative sea level fall, while deposition and infilling of the valley occurs during sea level rise as the system regrades (*Dalrymple et al.*, 1994; *Posamentier and Vail*, 1988). Alternatively, climate change may result in increased discharge or reduced sediment load, creating incision in the absence of base level change (*Schumm et al.*, 1987). CHIRP subbottom data collected on the Chukchi shelf off NW Alaska reveal a large buried

channel system within an incised valley, which is at least 24 km wide and 50 m deep. Below we discuss the valley stratigraphy in terms of multiple incisions, some of which appear to require increased discharge during deglaciation. If correct, this research has important implications for the paleoclimate during deglaciation (wetter) or requires more continental glaciation than previously proposed.

3.3 Results

The incised valley is located in a bathymetric low between the Herald and Hanna Banks, (~50 m water depth), and extends for at least 90 km across the shelf (Fig. 1). Regionally, the valley cuts across steeply dipping, folded and faulted reflectors interpreted to be Cretaceous strata, tilted as a result of thrusting along the Herald Bank (see Fig. 19 of *Phillips, et al.*, 1988). Six distinct and regionally extensive erosional surfaces that separate depositional sequences are identified within the incised valley.

The oldest incision, termed Valley Incision 0 (VI-0), truncates the underlying Cretaceous strata on the northeastern side of the incised valley, downcutting at least 50 m (Figs. 2, 3). A second incision surface, Valley Incision I (VI-1) downcuts acoustically transparent sediment above VI-0 (Unit 0) and coalesces with VI-0 to the southeast (Figs. 2, 3). Together these two incision surfaces define the extent of the incised valley. The sediment in Unit 1, overlying reflector VI-1, is acoustically laminated, continuous over long distances, and locally drapes the underlying topography (Figs. 2, 3). Unit 1 is in turn, truncated and downcut by another incision surface, Valley Incision II (VI-2) (Figs. 2, 3). Infill above VI-2, termed Unit 2, shows

complex stratal geometry characteristic of fluvial cut and fill structures (e.g., cutbanks, and lateral accreting sets; Figs. 2e, 3).

Incision I-3 delineates a channel or valley that is ~4.5 km wide with 45 m of relief (Fig. 2). Reflectors in Unit 3 overlying I-3 are much higher amplitude and more laminated than adjacent Units 1 and 2. Unit 3 strata also exhibit slight thickening toward the basin depocenter. VBC03 (8.66 m) sampled Unit 3 strata overlying I-3 and recovered blocky sands and interbedded sands and silty-clay containing marine shells and foraminifera (Fig. 1). An articulated bivalve mollusk from the base of Unit 3 yielded a radiocarbon age of $12,300 \pm 65$ ^{14}C yrs BP (calendar age ~13,500 yrs BP). Reflector I-4 represents a subsequent episode of erosional truncation that also results in large relief (~20 m) on the unconformity (Fig. 2). Unit 4 fill is locally truncated near the valley walls by reflector FS, a flooding surface observed only in the I-4 channel. Note infill Units 3, 4 and 5 exhibit a similar acoustic character.

A feature approximately 2 km wide and at least 15 m high (Constructional Mound; Fig. 2), adjacent to I-3/I-4, exhibits downlap to the southwest along two different surfaces and is elevated above Unit 2. The uppermost reflectors within CM show minor truncation on the NE side. The CM feature is present in multiple subbottom profiles across the incised valley (Fig. 1b), and shows a three-dimensional morphology in orthogonal Boomer subbottom profiles that intersect at CM. Reflector TS truncates strata across nearly the entire length of the valley, (Transgressive Surface; Fig. 2). TS is interrupted by small, discrete, v-shaped downcutting events,

labeled IS, in the NE. Unit 6 fill above TS appears to drape the underlying strata across the length of the acquired profiles (Fig. 2).

Two piston cores, JPC 09 (8.81 m) and JPC10 (8.13 m) acquired in the incised valley, recovered Units 4 and 6 above I-4 and the NE edge of the CM feature below I-4 (Figs. 1, 2d). Both cores show similar facies, with ~4 m of silty clay at the top (Unit 6), grading into interbedded silty clay and sand (Unit 4), overlying 2-3 m of well sorted, fine sand and fine sand with silty clay rip up clasts at the base of the core on the boundary between the CM feature and Unit 2 (JPC09) and within CM (JPC10; Fig. 2d). JPC 09 recovered an additional layer of small rip up clasts near the base of Unit 4. In both cores, marine shells and foraminifera were observed only in Unit 6. Radiocarbon dating on paired bivalves in JPC10 yielded an average sedimentation rate of ~1.45 m/kyr prior to ~8ka, with a very low sedimentation rate after ~8ka. The oldest date in JPC10 is 10,200 ^{14}C yrs BP (calendar age ~10,770 yrs BP), near the base of Unit 6.

3.4 Discussion

Several interpretations may explain the stratal geometry observed in our CHIRP subbottom data, four of which are outlined in Table 1; however these interpretations are speculative due to the limited core sample information. All scenarios propose similar explanations for the formation of VI-0, VI-1 and VI-2, but we explore alternative scenarios for the formation of I-3 and I-4. Options 1 and 2 predict stratal geometries and chronologies inconsistent with the observations, thus are discarded. In Option 1, I-4 would correspond to Marine Isotope Stage (MIS) 2, I-

3 to MIS 6, and VI-2, VI-1 and VI-0 to successively older glacial periods. This scenario fails to account for the much narrower widths of I-3 and I-4 compared with VI-0, VI-1 or VI-2 and markedly different infill character of Unit 3 and 4 relative to Unit 0, 1, and 2. Given the MIS 2 glaciation is believed to have been limited, restricted primarily to alpine regions, and MIS 6 glaciation was far more regionally extensive, it is difficult to explain why the channel dimensions and relief are similar for I-3 and I-4, yet appear markedly different from the older incisions (e.g., VI-0, VI-1, VI-2). Finally, radiocarbon dating of a marine shell in VBC03 indicate that the basal section of Unit 3 was deposited during the Allerød warm period (~13,500 yrs BP), which postdates the LGM (MIS 2; ~21,000 yrs BP). In Option 2, I-3 and I-4 represent the last phase of localized channel incision within VI-1 and VI-2 valleys, respectively; however erosion associated with I-3 downcuts and truncates Unit 2 sediment, suggesting formation of I-3 must be younger than VI-2. Therefore I-3 cannot be an open channel associated with valley VI-1. While controversy exists regarding the extent and volume of Arctic continental glaciation during the Last Glacial Maximum (LGM) (e.g., *Brigham-Grette, et al.*, 2004; *Grosswald and Hughes*, 2004 and references therein), both Options 3 and 4 require a greater extent of glaciation in NW Alaska than previously recognized. Our preferred scenario, Option 4, as described below, requires the least amount of ice buildup, making it simpler to reconcile the new evidence with existing Arctic studies.

Three regional valley incisions, reflectors VI-0, VI-1 and VI-2 (Figs. 2, 3), are observed in the CHIRP subbottom data, which suggest three events of lowered sea level and valley excavation. Reflector VI-0 appears to represent the oldest valley

incision. The transparent acoustic character of Unit 0 fill makes it difficult to interpret the depositional environment, yet the lack of characteristic fluvial structure suggests this may be a marine or estuarine deposit. Downcutting associated with the formation of VI-1 appears to have removed most of Unit 0 infill. Unit 1 infill shows some geometric evidence of fluvial cross cutting at the base of the deposit (Fig. 2E), but mantles the underlying topography across most of the valley (Figs. 2, 3). The parallel, draping reflectors in the upper part of the package are suggestive of hemipelagic deposition, typical in estuarine or marine environments. Downcutting and truncation of Unit 1 across the width of the valley by reflector VI-2 is consistent with a third sea level fall and fluvial incision reexcavating Unit 1 valley fill. Unit 2 represents fluvial-dominated sedimentation as indicated by internal channel geometry interpreted to record cut and fill structures (Figs. 2e, 3) as the channel migrates within the valley, the details of which are beyond the scope of this paper. A fourth regional reflector (TS), interpreted as the most recent transgressive surface, is observed across the entire valley. TS locally truncates the upper sediments, and is mantled by marine deposits of Unit 6 (Figs. 2, 3).

The ages of the proposed sea level cycles remain uncertain. Without deep core information, the simplest explanation appears to be that the sea level cycles represented by VI-1 and VI-2 correlate to the Illinoian (MIS 6) and Wisconsin (MIS 2) glaciations, respectively. VI-0 would then correspond to an older glaciation, perhaps MIS 12. This interpretation is consistent with the 6 m of negative relief observed at the seafloor above the incised valley, as well as the relatively thin sediment cover in Unit 6 above the most recent transgressive surface, TS (Fig. 2).

Reflectors I-3 and I-4 exhibit large downcutting relief with highly reflective sediment fill (Units 3, 4, 5) that appears to be deposited in an estuarine or marine environment (Fig. 3). Blocky sands and interbedded sands and silty-clays with marine assemblages recovered from Unit 3 (VBC03; Fig. 1) are consistent with the observed stratal geometry. Reflectors I-3 and I-4 coalesce to the NE and Unit 4 onlaps Unit 2 (Fig. 2), indicating the incisions must be younger than VI-2. I-3 and I-4 may have been incised by fluvial processes; however the lack of lateral accreting sets and concomitant fluvial deposition in Units 3, 4, and 5 indicates this segment of the channel was predominantly undergoing erosion and sediment bypass. Note the different acoustic character of Units 1 and 2 versus Units 3, 4, and 5. I-3 and I-4 appear to be younger than VI-2; if the proposed timing of VI-2 (MIS 2) is correct, this suggests I-3 and I-4 occurred during a period of sea level rise following the LGM. This interpretation is consistent with the age determination for the base of Unit 3 (~13,500 yrs BP). Sequence stratigraphic models commonly dictate that fluvial erosion and downcutting will develop during base level lowering as a result of relative sea level fall, while sediment infill accumulates as fluvial systems regrade with the base level rise (*Christie-Blick and Driscoll, 1995*). In the absence of base level lowering, channel incision may result from increase in discharge, a decrease in sediment supply, or a combination of both. Sedimentation rates in both the incised valley (JPC10) and Hope Valley (JPC02; *Keigwin et al., 2006*) appear to have been relatively high during the most recent transgression and dropped dramatically ~7,000 yrs BP. Given these constraints, our preferred interpretation is that the incision

resulted from increased discharge in response to meltwater runoff during deglaciation. High discharge events would scour the upper reaches of the channel, transporting the sediment farther offshore, hence the lack of fluvial fill observed in the subbottom data (Fig.2).

The marine shell dated at 13,500 yrs BP in Unit 3 is 1.24 m above I-3. Using the sedimentation rate determined from JPC10 implies I-3 was formed 14,300 yrs BP, which coincides with Meltwater Pulse 1A (*Fairbanks, 1989*). Thus we speculate I-3 was incised by meltwater discharge during post-LGM warming, with the open channel subsequently infilled by estuarine to marine sediment (Unit 3; Fig. 2). I-4 may represent a second phase of meltwater discharge (e.g., MWP1B; *Fairbanks, 1989*) following a climatic cooling (e.g., Younger Dryas). Unit 4 and 5 infills are interpreted to be of marine origin and reflector FS may represent a period of rapid sea level rise. This explanation is consistent with Unit 5 sediment collected in JPC09/JPC10, which shows interbedded silty clay and fine sand, grading into silty marine clay of Unit 6. While possible that the formation of I-3 and I-4 represent individual bankfull channels, it is more likely that these two erosional surfaces represent valleys carved by high discharge, incising channels.

The depositional structure (CM; Figs. 2, 3) exhibits downlap along multiple surfaces, suggesting a constructional feature rather than an erosional remnant. Note the geometry of CM is different from Unit 2 fluvial fill (e.g., lateral accreting sets). While it is difficult to trace the basal sequences of Unit 4 across the fault on the eastern edge of the channel and determine the relative age of CM, our preferred hypothesis is that the feature was formed after the I-3 incision since there is only

minor truncation of CM. The three-dimensional stratal geometry and sediment facies (i.e., well sorted, fine sand with no marine shells or microfossils) of CM is consistent with a fluvial origin (e.g., bar or braided island; Fig. 3). The large size (2 km wide, 15 m high) implies a high volume discharge. Similar fluvial bars with large dimensions scaled to the magnitude of discharge have been observed in glacial outburst floods (*Marren, 2005*). This scenario is also consistent with the presence of silty clay rip-up clasts on the upper downlap surface of the CM feature (JPC 10; Fig. 2). The presence of CM in several subbottom profiles across the shelf (Fig. 1b), suggests multiple bars or braided islands along the length of the incised valley.

Previous researchers have suggested primary drainage across the Chukchi shelf may have been derived from the Hope Valley to the south (*McManus, et al., 1983*); however, truncation of dipping Cretaceous strata indicates the uplift of Herald Bank, a structural drainage divide, predated channel formation (*Phillips, et al., 1988*). While United States Geological Survey Boomer subbottom data collected in the region (Fig. 1) also provide evidence of numerous small paleochannels between the NW Alaskan margin and our study area, there is no evidence of paleochannels between the Herald Bank and Lisburne Peninsula (*Phillips, et al., 1988*). This evidence precludes flow around Herald Bank from either Hope Valley or other rivers to the south and west as the potential source of the discharge and implies the drainage must be from the northwest Alaskan margin (Figs. 1, 2).

Currently, only small, low discharge rivers drain the western portion of Alaska's North Slope (Fig. 1); however, these rivers have steep banks and incised channel morphologies cut into the Brooks Range foothills, suggesting they may have

been carved by much stronger flows in the past. Profiles across portions of the Kokolik, Kukpowruk and Utukokok Rivers on the coastal plain show broad floodplain valleys (Fig. 4). The active flow occupies a small channel surrounded by meander cutoffs and oxbow lakes while the remaining floodplain is heavily sedimented with fluvial deposits. Note the valley dimensions of these northwestern rivers are less than half the size of the valleys defined by I-3 and I-4 on the midshelf (Fig. 4) and a key point is that the I-3/I-4 valleys do not contain any fluvial sediment unlike their onshore counterparts. Infilling of the onshore channels may have occurred after the maximum flooding, when the rate of sea level rise diminished. Note for comparison, the individual paleochannels preserved in the fluvial sediments of Unit 2 are greater than 500 m across and 8-9 m deep (Fig. 2e), about twice the size of the bankfull channel dimensions observed along the northwestern rivers (*Childers, et al., 1979*).

The formation of I-3 and I-4 during the last sea level rise suggest there must have been an additional source of flow, either in the form of more pluvial conditions immediately following peak glaciation or glacial meltwater. Pollen records indicate higher moisture levels after 10,000 ^{14}C yrs BP with a Holocene peak around 6000 ^{14}C yrs BP (*Edwards, et al., 2001; Mann, et al., 2002*). Paleoprecipitation for this period, however, is estimated to be at least 10% less than the modern (*Edwards, et al., 2001*). Given modern discharge observed across the North Slope of Alaska is insufficient to carve the I-3/I-4 valleys, these observations require another source for the increased discharge. We propose that the increased discharge resulted from meltwater runoff during deglaciation. Meltwater would have originated from the Alaskan margin,

implying a greater extent of continental glaciation than previously recognized (Fig. 1). Pluvial conditions during deglaciation may have increased glacial water storage and perhaps glacial readvances, as well as augmented glacial meltwater discharge. This explanation is consistent with evidence from piston cores JPC10 and JPC02 (Hope Valley), which indicates a dramatic decrease in sedimentation in the last ~7 kyr (*Keigwin, et al.*, 2006.).

Much of the argument for limited glaciation in northern Alaska during the LGM has been centered on evidence for relatively arid conditions, which would limit moisture required for significant ice buildup (e.g. *Brigham-Grette*, 2001 and references within). These conclusions are commonly based on paleoclimate proxies from the eastern and central Brooks Range; however some studies suggest that spatial climatic variability in the region may be significant (*Mock and Anderson*, 1997; *Edwards, et al.*, 2001). LGM ice buildup in the southwestern Brooks Range dammed montane rivers, resulting in Glacial Lake Noatak that eventually drained to the south during deglaciation (*Hamilton*, 2001). It appears plausible that similar glacial conditions may have also existed 15-20 km to the north across the northwestern river headwaters. Our offshore data provides evidences for increased drainage during deglaciation that appears to have drained from the northwestern Alaskan margin. Nevertheless, in the absence of onshore field-based studies in this region, it is difficult to make any definitive assertions about the implied ice extent and source of the increased discharge. We are not arguing for a large ice sheet across the region, but rather suggesting there may have been more extensive alpine glaciation during the LGM than previously recognized.

3.5 Conclusions

The large, northwest trending valley on the Chukchi shelf shows evidence of fluvial downcutting during multiple periods of lowered sea level. The stratal geometry, absence of fluvial fill following the two most recent incisions (I-3/I-4), and age constraints indicate these incisions may have been formed by episodes of high discharge. The modern flow from northwestern Alaskan rivers does not appear to be sufficient to carve these offshore valleys and paleoprecipitation is predicted to be at least 10% less than modern during deglaciation. Therefore the inferred magnitude of discharge needed to carve the I-3/I-4 valleys requires an additional input, most likely from glacial meltwater since the Last Glacial Maximum. The proposed timing of I-3 and I-4, carved by a high volume of discharge during a period of sea level rise, suggests that in glacially dominated landscapes, major incision on the shelf may be unrelated to base level changes, (i.e., are out of phase with sea level cycles). Additionally, our results suggest more climate variability and a greater extent of continental glaciation during the LGM than previously proposed.

3.6 Acknowledgements

This research was supported by grants from the NSF Office of Polar Programs and the Oak Foundation. We would like to thank R. Lawrence Phillips of the U.S. Geological Survey for his contributions, which include participating in the research cruise, providing additional data, thoughtful discussions and insightful reviews of the paper. W. Schwab, J. Anderson, J. Knox and R. Powell provided valuable comments that improved the manuscript.

3.7 Chapter acknowledgement

Chapter 3, in full, is the material as submitted to *Quaternary Research*: Hill, J.C., Driscoll, N.W., Brigham-Grette, J., Donnelly, J.P., Gayes, P.T., and Keigwin, L.D., 2007. New evidence for high discharge to the Chukchi shelf since the Last Glacial Maximum. *Quaternary Research*, *in press*.

Figure 3.1 *a.* Location map showing SIO SUBSCAN CHIRP subbottom data (1-6 kHz signal, 50 ms sweep) acquired on the Chukchi margin aboard the USCGC Healy in 2002 as well USGS Boomer subbottom data collected by *Phillips, et al.* (1984). The locations of the Figure 2 and 3 subbottom profiles and piston cores discussed in the text are labeled. Abbreviations: Ku-Kukpowruk River, Ko-Kokolik River, Ut-Utukok River, Co: Colville River. The primary modern drainage in northern Alaska flows NNE through the Colville River, while the southern Brooks Range drains through Hope Valley, as denoted by the purple arrows. The smaller rivers on the NW margin discussed in the text are highlighted and the proposed paleodrainage direction is shown by the yellow arrow. Also shown is the previously interpreted maximum ice extent for the Pleistocene and Late Wisconsin (LGM) glaciations (*Manley and Kaufman, 2002*). High certainty boundaries have well-defined chronologies, while low certainty boundaries may encompass areas lacking significant field or remotely sensed studies. Note that ice extent is uncertain along the NW Brooks Range foothills that comprise the headwaters of the Kukpowruk, Kokolik, and Utukok Rivers. *b.* Interpreted channel map showing CHIRP and Boomer subbottom crossings of the incised valley (VI-0, VI-1, VI-2), meltwater drainage (I-3, I-4), and the constructional mound (CM) feature. Note the meltwater drainage appears to reexcavate portions of VI-0, VI-1 and VI-2. Relatively small northwest trending channels were also observed in the region between the incised valley and the northwestern Alaskan margin. No channels were observed between the Lisburne Peninsula and Herald Bank. Correlation of channels across the innershelf is difficult because of the poor data quality and azimuth of the Boomer profiles being parallel to the channel trend. The location of floodplain profiles across the northwestern rivers shown in Figure 4 are also highlighted and labeled.

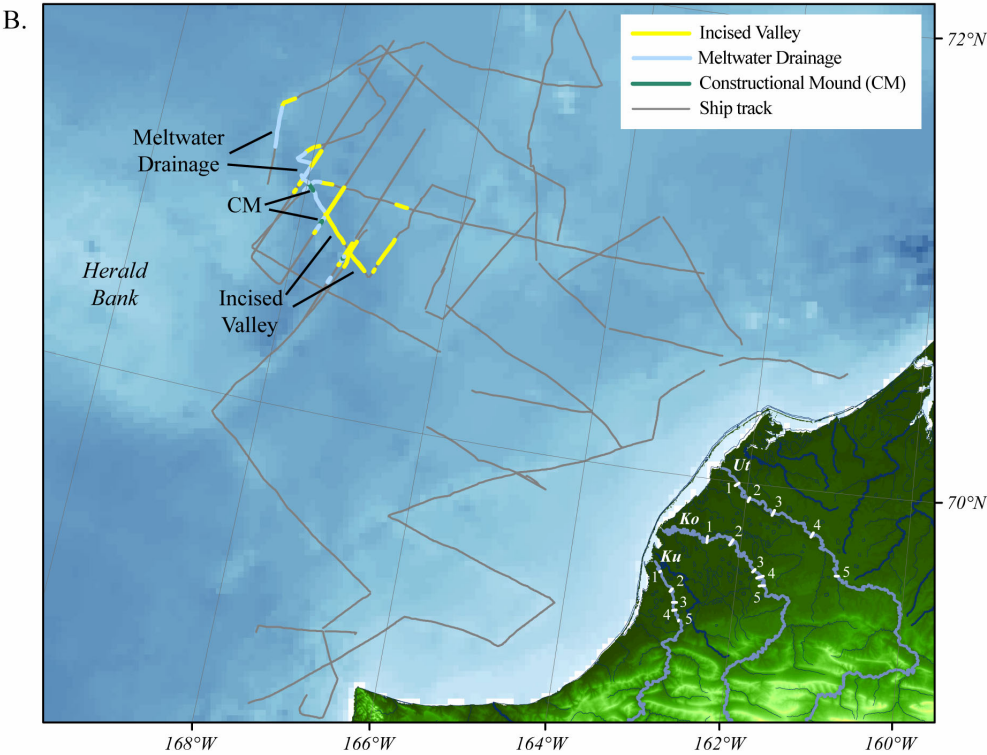
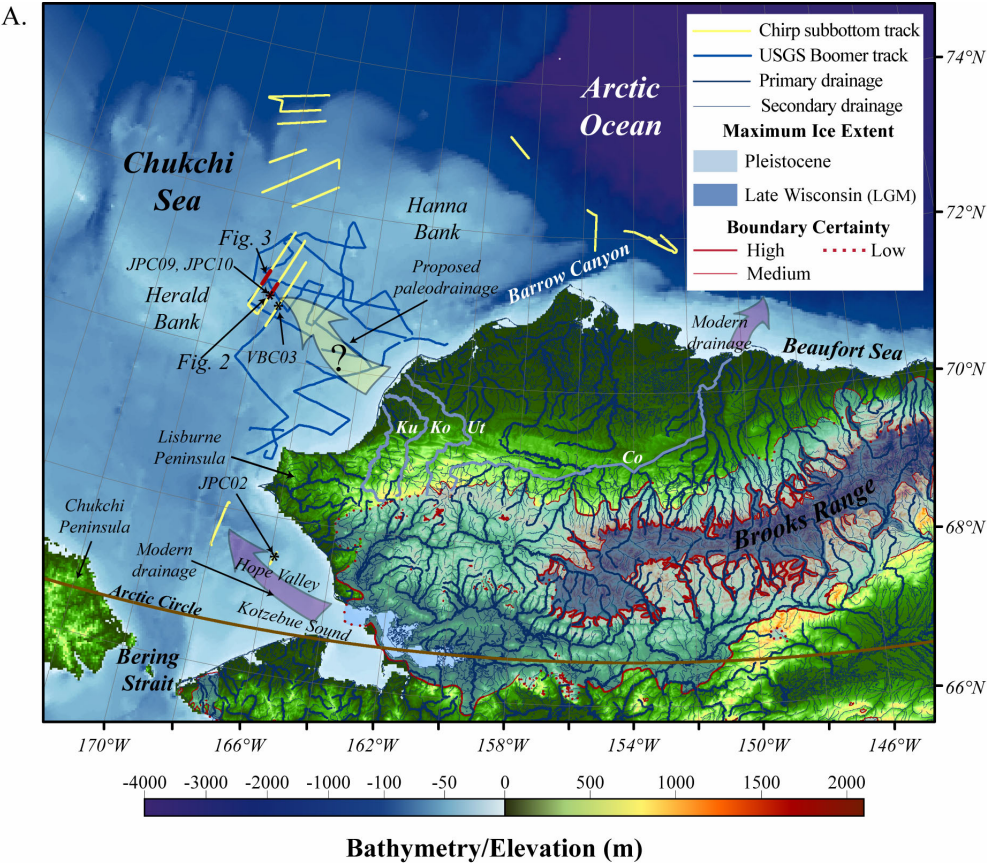
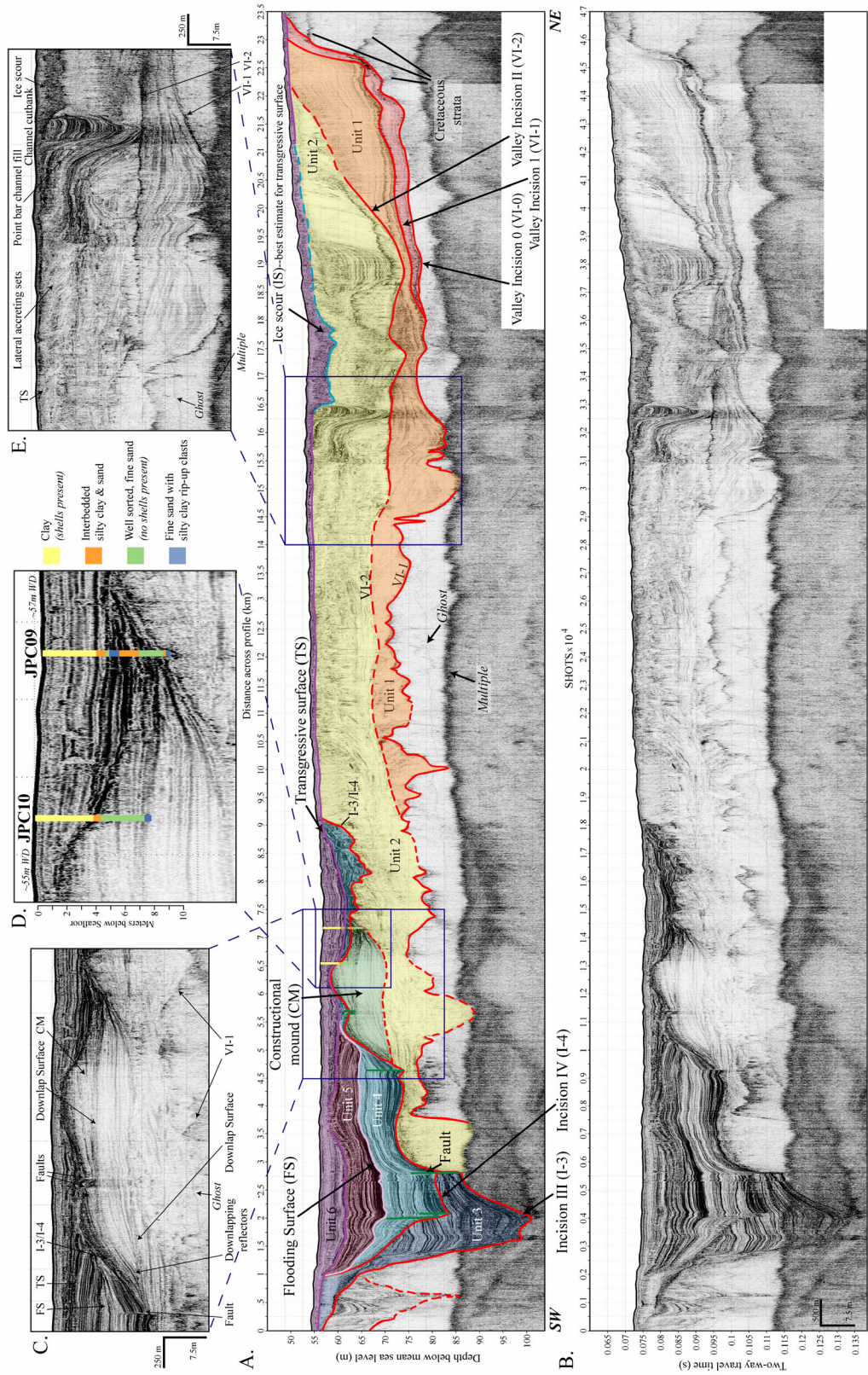


Figure 3.2 CHIRP subbottom profile across the incised valley (Line 2, see Figure 1 for location). *a.* Interpreted profile with the reflectors color coded as follows : *Red* – Valley Incision 0 (VI-0), Valley Incision I (VI-1), Valley Incision II (VI-2), Incision III (I-3) and Incision IV (I-4); *Light purple* –Flooding surface (FS); *Dark Purple* –Most recent transgressive surface (TS); *Blue* –Most recent ice scour (IS), also the best estimate for TS in that area; *Green* –Post-depositional faulting. CM indicates a constructional mound feature. Sedimentary units are also labeled. The dimensions of the I-3/I-4 valleys were measured between shotpoints ~2000 to ~18000. *b.* Same profile as 2a, with no interpretation. *c.* Constructional mound (CM). Downlapping reflectors indicate build up of positive relief. *d.* Sedimentary facies of piston cores JPC09 and JPC10 in the incised valley. Both cores have a similar stratigraphy of well sorted, fine sand with silty clay rip-up clasts in the base, grading upward into interbedded sand and silty clay, with silty marine clay at the top. JPC09 was collected ~60 m to the NW of the profile. JPC10 was collected ~15 m to the SE. The core positions have been projected orthogonally onto the subbottom profile to represent the most accurate correlation of sediment facies. *e.* Characteristic fluvial cut-and-fill stratigraphy. Unit 2 displays lateral accreting sets as well as fluvial point bar deposition on the SW bank, with cutbank erosion on the opposite side.



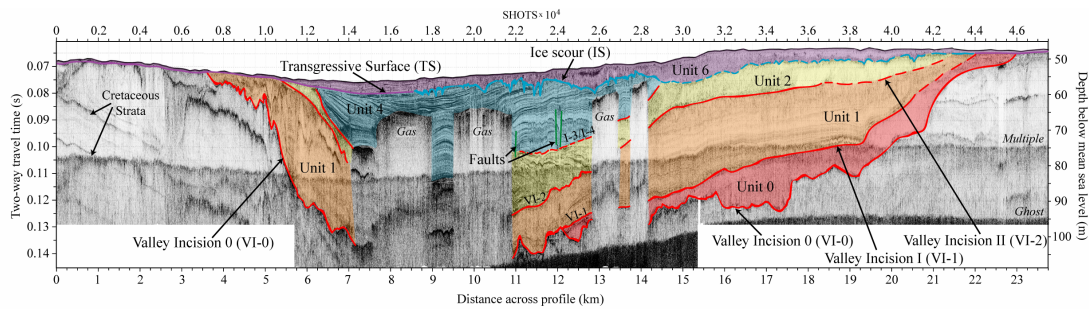


Figure 3.3 CHIRP subbottom profile across the incised valley (Line 3, see Figure 1 for location). **Bottom:** Uninterpreted profile. **Top:** Interpreted profile with the reflectors color coded as follows : *Red* –Valley Incision 0 (VI-0), Valley Incision I (VI-1), Valley Incision II (VI-2), Incision III (I-3) and Incision IV (I-4); *Light purple* –Flooding surface (FS); *Dark Purple* –Most recent transgressive surface (TS); *Blue* –Most recent ice scour (IS), also the best estimate for TS in that area. Sedimentary units are also labeled. Gas in the shallow sediment results in acoustic wipeouts that obscure deeper reflectors.

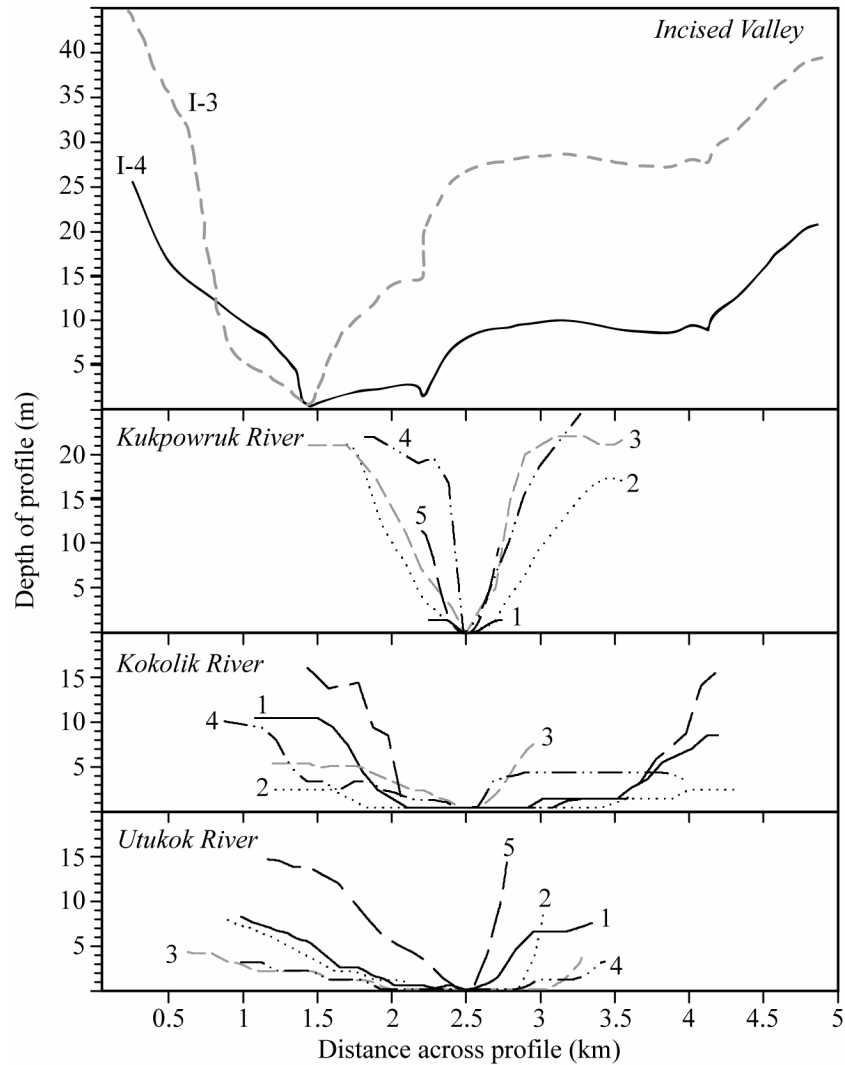
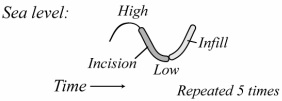
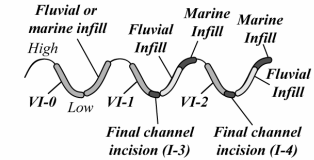
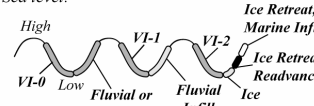
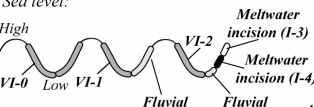
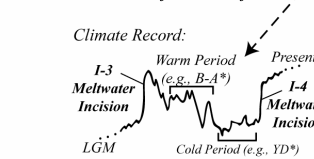


Figure 3.4 Profiles across the I-3 and I-4 reflectors compared with floodplain profiles across the three dominant northwestern Alaskan rivers believed to have sourced the midshelf valley. The river profiles were measured from a 100 m resolution DEM of northern Alaska (Manley, 2001). The river profile locations are shown in Figure 1b. Note the I-3 and I-4 valleys are much wider than the corresponding river valleys onshore.

Table 3.1 Options for explaining observed stratigraphy

	Options:	Description:	Concerns:
1	<p>5 Sea level cycles</p> <p>Sea level: </p> <p>Time → Repeated 5 times</p>	Each incision (VI-0, VI-1, VI-2, I-3, I-4) represents a separate sea level cycle: fluvial incision during sea level fall; infill as sea level begins to rise.	The character and infill of the last two incisions (I-3, I-4) is markedly different than previous incisions VI-0, VI-1, VI-2), which is difficult to explain if each erosional surface represents a different sea level fall
2	<p>3 Sea level cycles</p> <p>Sea level: </p>	<p><i>Sea level cycle 1:</i> VI-0 fluvial incision; fluvial or marine infill</p> <p><i>Sea level cycle 2:</i> a. VI-1 fluvial incision; predominantly fluvial infill b. I-3 represents the last channel location during valley incision; marine infill as sea level rises</p> <p><i>Sea level cycle 3:</i> a. VI-2 fluvial incision; predominantly fluvial infill b. I-4 represents the last channel location during valley incision; marine infill as sea level rises</p>	<p>I-3 appears to be younger than VI-2 indicating that it can not be associated with the VI-1 SL cycle</p> <p>I-3 and I-4 do not appear to have any fluvial infill prior to marine incursion</p>
3	<p>3 Sea level cycles and ice present on the shelf</p> <p>Sea level: </p>	<p><i>Sea level cycle 1:</i> VI-0 fluvial incision; fluvial or marine infill</p> <p><i>Sea level cycle 2:</i> VI-1 fluvial incision; predominantly fluvial infill</p> <p><i>Sea level cycle 3:</i> a. VI-2 fluvial incision; predominantly fluvial infill b. Grounded ice shelf advances shelf and incises I-3 c. Ice retreats; I-3: glacial lacustrine or marginal marine infill d. Shelf ice readvances; I-4 incised e. Ice retreats; I-4: glacial lacustrine or marginal marine infill</p>	<p>CM then is an ice contact feature (e.g. esker or lateral moraine) formed in association with I-4 ice advance.</p> <p>Requires shelf glaciation sourced from the Alaskan margin</p> <p>Expect more local sediment deformation with ice advance</p>
4	<p>2 Sea level cycles and 2 meltwater pulses</p> <p>Sea level: </p> <p><i>Climate Record:</i> </p>	<p><i>Sea level cycle 1:</i> VI-0 fluvial incision; fluvial or marine infill</p> <p><i>Sea level cycle 2:</i> VI-1 fluvial incision; predominantly fluvial infill</p> <p><i>Sea level cycle 3:</i> a. VI-2 fluvial incision; predominantly fluvial infill b. I-3 incised by glacial drainage as climate warms c. Climate cools (e.g., Younger Dryas); glacial meltwater diminishes; possible glacial readvance d. I-3: Bathymetric low infilled with lacustrine or marginal marine sediment e. Climate warms and I-4 incised by glacial meltwater drainage; marine infill as sea level rises</p> <p>*B-A=Bølling-Allerød, YD=Younger Dryas</p>	<p>Suggests there are two major discharge events, which are triggered by climatic variations rather than sea level</p> <p>The fills above I-3 and I-4 appear very similar, but I-3 infill may be glacial lacustrine or marginal marine, while I-4 infill is marine</p>

References

- Dalrymple, R. W., R. Boyd and B. A. Zaitlin (Eds.), 1994. *Incised-valley systems: Origin and sedimentary sequences*, Society for Sedimentary Geology Special Publication 51, 391 p.
- Benito, G. and O'Connor, J. E., 2003. Number and size of last-glacial Missoula floods in the Columbia River valley between the Pasco Basin, Washington, and Portland, Oregon. *GSA Bulletin*, 115: 624-638.
- Brigham-Grette, J., 2001. New perspectives on Beringian Quaternary paleogeography, stratigraphy and glacial history. *Quaternary Science Reviews*, 20: 15-24.
- Brigham-Grette, J., Lozhkin, A. V., Anderson, P. M. and Glushkova, O. Y., 2004. Paleoenvironmental conditions in western Beringia before and during the Last Glacial Maximum, In: Madsen, D. B. (Ed.), *Entering America: Northeast Asia and Beringia before the Last Glacial Maximum*, Salt Lake City: University of Utah Press, pp. 29-61.
- Childers, J. M., Kernodle, D. R. and Loeffler, R. M., 1979. Hydrologic reconnaissance of western Arctic Alaska, 1976 and 1977. U.S. Geological Survey Open-File Report 79-699.
- Christie-Blick, N. and Driscoll, N. W., 1995. Sequence Stratigraphy. *Annual Review of Earth and Planetary Sciences*, 25: 451-478.
- Edwards, M. E., Mock, C. J., Finney, B. P., Barber, V. A. and Bartlein, P. J., 2001. Potential analogues for paleoclimatic variations in eastern interior Alaska during the past 14,000 yr: atmospheric-circulation controls of regional temperature and moisture response. *Quaternary Science Reviews*, 20: 189-202.
- Fairbanks, R. G., 1989. A 17,000-year glacio-eustatic sea level record; influence of glacial melting rates on the Younger Dryas event and deep-ocean circulation. *Nature*, 342: 637-642.
- Grosswald, M. G. and Hughes, T. J., 2004. Chlorine-36 and 14C chronology support a limited last glacial maximum across central Chukotka, northeastern Siberia, and no Beringian ice sheet; discussion. *Quaternary Research*, 62: 223-226.
- Hamilton, T. D., 2001. Quaternary, glacial, lacustrine, and fluvial interactions in the western Noatak Basin. *Quaternary Science Reviews*, 20: 371-391.

- Keigwin, L. D., Donnelly, J. P., Cook, M. S., Driscoll, N. W. and Brigham-Grette, J., 2006. Rapid sea-level rise and Holocene climate in the Chukchi Sea. *Geology*, 34: 861-864.
- Manley, W. F., 2001. Alaska North Slope 100 m Digital Elevation Model (DEM). National Snow and Ice Data Center, Boulder, CO. Digital media.
- Manley, W. F. and Kaufman, D. S., 2002. Alaska PaleoGlacier Atlas, v. 1. Institute of Arctic and Alpine Research (INSTAAR), University of Colorado http://instaar.colorado.edu/QGISL/ak_paleoglacier_atlas.
- Mann, D. H., Peteet, D. M., Reanier, R. E. and Kunz, M. L., 2002. Response of an arctic landscape to Lateglacial and early Holocene climatic changes: the importance of moisture. *Quaternary Science Reviews*, 21: 997-1021.
- Marren, P. M., 2005. Magnitude and frequency in proglacial rivers: a geomorphological and sedimentological perspective. *Earth-Science Reviews*, 70: 203-251.
- McManus, D. A., Creager, J. S., Echols, R. J. and Holmes, M. L., 1983. The Holocene transgression of the flank of Beringia: Chukchi valley to Chukchi estuary to Chukchi Sea, In: Masters, P. M. and N. C. Flemming (Eds.), *Quaternary coastlines and marine archaeology: towards the prehistory of land bridges and continental shelves*, London: Academic Press, pp. 365-388.
- Mock, C. J. and Anderson, P. M., 1997. Some perspectives on the late Quaternary paleoclimate of Beringia. In: Isaacs, C. M. and V. L. Tharp (Eds.), *Proceedings of the thirteenth annual Pacific climate (PACCLIM) workshop*.
- Phillips, R. L., Barnes, P., Huner, R. E., Reiss, T. E. and Rearic, D. M., 1988. Geologic investigations in the Chukchi Sea, 1984, NOAA ship SURVEYOR cruise. U.S. Geological Survey Open-File Report 88-25.
- Posamentier, H. W. and Vail, P. R., 1988. Eustatic controls on clastic deposition II--Sequence and systems tract models, In: Wilgus, C. K., B. S. Hastings, C. G. S. C. Kendall, H. W. Posamentier, C. A. Ross and J. C. Van Wagoner (Eds.), *Sea-level changes: An integrated approach*, Tulsa: Society of Economic Paleontologists and Mineralogists Special Publication 42, pp. 125-154.
- Schumm, S. A., Mosley, M. P. and Weaver, W. E., 1987. *Experimental fluvial geomorphology*, New York: Wiley, 413 p.

Uchupi, E., Driscoll, N., Ballard, R. D. and Bolmer, S. T., 2001. Drainage of late Wisconsin glacial lakes and the morphology and late quaternary stratigraphy of the New Jersey-southern New England continental shelf and slope. *Marine Geology*, 172: 117-145.

Chapter 4

Evidence for Iceberg Armadas on the Chukchi Shelf during the Younger Dryas

4.1 Abstract

Ice extent in the Arctic Ocean and surrounding margins during recent glaciations, as well as deglaciation history for the region, remains poorly understood, especially in the western Arctic basin. While geomorphic evidence has been employed to argue for limited glaciation across northern Alaska during the Last Glacial Maximum (LGM; e.g., Brigham-Grette, 2001), new offshore evidence suggests icebergs were sourced from this margin (Polyak et al., 2001; Jakobsson et al. 2005). Here we present new CHIRP subbottom data from the shallow (<100 m) Chukchi shelf that reveals a regionally extensive, heavily ice scoured surface ~5-8 m below the modern seafloor. Above this surface there is little to no evidence of additional iceberg scour, indicating there was a discrete event where a large number of icebergs were discharged followed by predominately iceberg free conditions. Radiocarbon dating of samples above and below the ice scour surface suggests the iceberg discharge event occurred during the Younger Dryas between 10,600 and 11,900 ^{14}C yr BP. Evidence for concomitant large glacial meltwater discharge is also observed on the Chukchi midshelf (Hill, et al., in press). Both the iceberg scours and meltwater discharge appear to be sourced from the local northwestern Alaskan margin, suggesting that continental glaciation in this region may have been more extensive than previously recognized.

4.2 Results and Discussion

While recent studies of ice grounding have been conducted along the Chukchi borderland and greater Arctic Ocean regions (e.g., Jakobsson et al. 2001, 2005;

Polyak et al. 2001), the shallow Chukchi shelf remains relatively unexplored. Numerous questions persist concerning the extent of glaciation in northwestern Alaska during the Last Glacial Maximum (LGM), the source of sediment supply to the Chukchi shelf, and the movement of sea ice and/or icebergs across the shelf. Regional ice cover in the Arctic strongly affects albedo, which has climatic feedbacks that can play an important role in oceanic and atmospheric circulation (Aagard and Carmack, 1989). The question of ice extent during the Last Glacial Maximum (LGM) has particular significance in the coherence of global circulation models for glacial periods, the results of which are strongly influenced by ice extent input parameters (e.g., Smith, et al., 2003; Zweck and Huybrechts, 2005).

CHIRP subbottom data collected aboard the USCGC Healy in 2002 show evidence of numerous ice scours along a surface as much as 7 m below the modern seafloor on the Chukchi shelf. This is the first of evidence of such regionally extensive ice grounding at shallow depths (60 -100 m) on the shelf. The individual scours are represented by v-shaped incisions, ranging from 50-100 m wide and averaging 5 m deep, with some plough marks > 8 m deep. Similar ice scour morphology has been identified from glaciated margins worldwide (Davies, et al., 1997). There is little to no evidence of additional ice scour above this surface, which suggests these features were formed by a single, unrepeated event. If the scour depressions were derived from grounded sea ice, we would expect repeated scouring of the seafloor as the sea ice surges and retreats seasonally. This should create a stratigraphic record with ice scours present throughout the sediment column; a scenario that is not observed in the data. Additionally, the individual ice scour

dimensions observed here are much larger than that observed from modern sea ice gouges on the Chukchi and Beaufort shelves, which average 1 m or less in depth, with maximum incision of 3-4 m (Barnes , et al., 1984; Phillips , et al., 1988). Therefore, we suggest the regional scour surface was formed by discharge of a large number of icebergs over a relatively short period of time, rather than seasonal or multiyear sea ice movement, followed by generally iceberg-free conditions.

Sediment drape above the scour surface is thickest in the western portion of the profiles (~7 m), and systematically diminishes toward the east (Fig. 2). The buildup of sediment to the west mantles a preexisting bathymetric high and records the westward flow of the Beaufort Gyre. The acoustic character below the scour surface is chaotic and generally featureless. In contrast, the scour infill is highly reflective and acoustically laminated at the base, becoming less reflective upsection, especially above the crest of the scours.

In addition to the CHIRP subbottom data, we acquired 11 piston cores in the ice scour region. While the overall grain size in the cores is dominated by silt, the coarsest-grained intervals correlate with the highest amplitude subbottom reflectors, in the base of the ice scour (Fig. 3). Several of the cores penetrated the base of the ice scour surface, allowing us to examine sediments above and below the erosive horizon (Fig. 3). Samples from each of the piston cores at 20 cm intervals and the >150 μm fraction were examined. While there is a relatively small sand fraction and only occasional grains > 2mm, several trends are apparent in the composition. Overall the sand fraction is dominated by quartz, but there appears to be at least two distinct mineralogical zones in the cores. The basal section is characterized by an assemblage

of blueschist minerals (e.g., glaucophane, epidote). The flooding surface (FS) at 5-6 m depth within the cores separates blueschist minerals below from authigenic pyrite above, with the upper few meters show no distinguishing grains (Fig. 3). The foraminifer, *elphidium excavata*, which prefers brackish, estuarine environments, is most often observed in the base of the cores, coincident with the zone of metamorphic minerals. The blueschist facies minerals, in combination with the elphidium, appear to suggest relatively shallow water conditions, with a more pronounced terrigenous signal in the base of the cores, most likely sourced from the nearby Brooks Range of northern Alaska. The flooding surface, interpreted to be caused by a rapid rise in sea level, records the transition to more open marine conditions as evidenced by the presence of authigenic pyrite and decreased elphidium abundance upsection. A rapid rise in sea level might also explain the absence of additional scours above the 7 m subbottom surface.

Despite limited biogenic material in the cores, we were able to collect sufficient material from piston cores JPC26, JPC27 and JPC30 for reliable radiocarbon dating. The scour surface represents an erosional event, (i.e. a hiatus) therefore we acquired samples from horizons directly above and below the surface to constrain the timing of incision. All but one of the radiocarbon dates were determined from the most abundant foraminifera, *elphidium excavata*. In JPC27, the section with the highest terrigenous component (i.e. blueschist) at the base of the core is inferred to be below the iceberg scour surface, which is consistent with the location of the core section as projected onto the subbottom data. Radiocarbon dates from this interval yield an age of $12,850 \pm 220$ ^{14}C yr BP. Radiocarbon dates from the more

reflective, laminated sequence that infills the base of scours yields ages of $10,400 \pm 140$ and $10,650 \pm 170$ (JPC27; Fig. 3). The radiocarbon dates from JPC30 are slightly more equivocal. The dated interval at 6.8 m ($11,900 \pm 160$ ^{14}C yr BP; Fig. 3) appears to be below the ice scour surface as projected on the subbottom profile; however, this interval is above the section characterized by the highest terrigenous component observed in the core. Despite this, the age-depth pair is consistent with global sea level records, which suggests deposition at or near the time of flooding. Therefore we interpret the age of $11,900 \pm 160$ ^{14}C yr BP to be older than the ice scour surface. The radiocarbon age on a mollusk from JPC30 ($11,000 \pm 50$ ^{14}C yr BP, 7.2 m; Fig. 3) also confirms the relative age for the surrounding sediments, but appears chronologically out of context with the other dated samples. Given these constraints, our preferred timing for the iceberg discharge event and consequent scour formation is between $10,650 \pm 170$ and $11,900 \pm 160$ ^{14}C yr BP, but it may extend from $10,650 \pm 170$ to $12,850 \pm 220$ ^{14}C yr BP (Fig. 3). Sea level at this time would have been at least ~60 m lower than present (Bard, et al., 1998), which is consistent with the depth of the scour surface observed in the CHIRP data (Fig. 2). CHIRP profiles at shallower depths on the shelf show no evidence of the scour surface.

There appears to be small quantities of sediment at the base of the ice scours with grain size > 250 μm , indicating the possible presence of ice-rafted debris (IRD). These deposits may be analogous to the Heinrich layers of the North Atlantic, which record large outbursts of icebergs during deglaciation (Bond, et al. 1992). The proposed timing of the scour surface indicates the iceberg discharge event occurred during the Younger Dryas and maybe an expression of Heinrich event 0 on the

Chukchi Shelf (~10,500 to 11,000 ^{14}C yr BP; Bond, et al., 1993). Heinrich events generally occur during cold stadials and have been frequently invoked for climatic forcing through freshwater input and disruption of thermohaline circulation (e.g., Broecker, 1994; Clark, et al, 2001).

It is important to note, however, there is no detrital carbonate in the sediments collected. This result is somewhat surprising as most icebergs and subsequent IRD deposits in the western Arctic basin are generally believed to be sourced from the carbonate rich Canadian Arctic Archipelago (CAA; e.g., Bischof, et al., 1996; Darby, et al. 2002). One of the primary western outlets for ice streams and icebergs emanating from large Pleistocene ice sheets across North America during deglaciation was through the dolostone-rich Banks Island and Victoria Island regions of northern Canada, as well as the Mackenzie river valley (Stokes and Clark, 2005; Dyke, et al. 2002). These late stage icebergs on the Chukchi shelf may have been sourced from glaciated regions of Canada; however, the absence of carbonate IRD here suggests provenance from a less carbonate rich region, most likely west of the Mackenzie River district.

It is somewhat difficult to understand how continental ice in eastern Alaska might be transferred to the marine environment due to the lack of coastal embayments in the region. West of the Mackenzie valley, the largest embayment on the margin is the Barrow Canyon (Fig. 1). Sea level during the ice scour event would have been ~60 m below present (Bard, et al., 1998), at this depth most of the canyon would remain flooded (Fig. 1). CHIRP seismic profiles on the upper slope of Barrow Canyon (~145 m to > 220 m WD) show evidence of a buried ice scour surface very

similar to the surface observed on the outer shelf. There is almost no sediment cover in the upper part of the canyon, increasing to >20 m in the lower portion where there is a much higher sedimentation rate (Keigwin, et al. 2006). The relatively thin sediment cover suggests these are recent features and may indicate iceberg activity during the last deglaciation. Since these scours are at much greater depths in the canyon than those observed on the outershelf, we interpret these features to be related to earlier phases of deglaciation, during a period when sea level was lower. The presence of iceberg scours in the Barrow Canyon supports our hypothesis that this may have been an important conduit for iceberg discharge.

Another scour field of LGM age has been identified on the Chukchi borderland (Polyak, et al., 2001; Jakobsson, et al., 2005; Polyak, et al., 2007). This outer region has scours with scales similar to that observed on the shelf and estimates of their orientations suggest the icebergs may have been sourced from the shallow Chukchi shelf (Jakobsson, et al., 2005). Examining these features, Polyak, et al. (2001) postulated the presence of Chukchi shelf ice that may have deflected westward flowing ice streams emanating from the Alaska/Canada margin. Polyak, et al. (2007) also noted a distinct absence of carbonate-rich IRD in Chukchi borderland sediments prior to 13,000 cal yr BP. In the eastern region, where there is little to no sediment cover above the scour surface, swath bathymetry data coregistered with the Chirp profiles suggest a WNW iceberg trajectory. This trend is consistent with iceberg discharge from the Beaufort margin, either Barrow Canyon or the Mackenzie region, flowing along the shoreline. The absence of the carbonate-rich IRD in both outer shelf and borderland sediments at this time favors a more proximal iceberg source

(e.g., northwestern Alaska) with the discharge potentially deflecting CAA-sourced icebergs as suggested by Polyak, et al. (2007).

If the scour forming icebergs on the outer shelf were indeed sourced from the northwest Alaskan margin, this raises important questions about the mapped extent of continental glaciation in northern Alaska during the LGM. Compared with much larger scours observed in the greater Arctic basin (e.g., Polyak, et al., 2001; Jakobsson, et al., 2005) the iceberg scours on the outer shelf are relatively small and do not indicate extremely large volumes of ice on the margin. It is unclear when the ice buildup was initiated, whether it was during Marine Isotope Stage 3 or 4, a period interpreted to be fairly arid, or perhaps during waning stages of glaciation when the moisture supply would have been more plentiful. Climate records indicate an increase in effective moisture $\sim 12,500$ ^{14}C yr BP (Mann, et al., 2002), which appears to correlate with glacial readvance in the Brooks Range between 13,000 to 11,500 ^{14}C yr BP (Hamilton, 1986, 2004).

Previous authors have argued for extremely limited glaciation across the Brooks Range, restricted primarily to montane glaciers in the eastern region (Hamilton, 1986; Kaufman and Manley, 2004). Many of these arguments are based on field observations of glacial geomorphology and biogenic proxies; however, very few studies have been conducted in northwestern Alaska and recent evidence has begun to suggest there may have more variability in this region than previously recognized. Large meltwater discharge channels present on the mid Chukchi shelf appear to link up with drainage patterns sourced from the northwest Alaskan margin (Hill, et al., in press) (Fig. 1). Furthermore, these channels appear to have been

incised during the most recent period of sea level rise and may record catastrophic drainage that was coincident with the iceberg discharge event. High sedimentation rates on the shelf from 11 ka - 7 ka, are also consistent with glacial drainage from the margin (Keigwin, et al., 2006; Hill, et al., in press). Additional investigation of the northwestern Alaskan margin, both on and offshore, will help illuminate the complex glacial history and provide insight into Arctic ice sheet dynamics and their role in global climate interactions.

4.3 Chapter acknowledgement

Chapter 4, in full, is the material as submitted to Science: Hill, J.C. and Driscoll, N.W., 2007. Evidence for iceberg armadas on the Chukchi shelf during the Younger Dryas. *Science, submitted*.

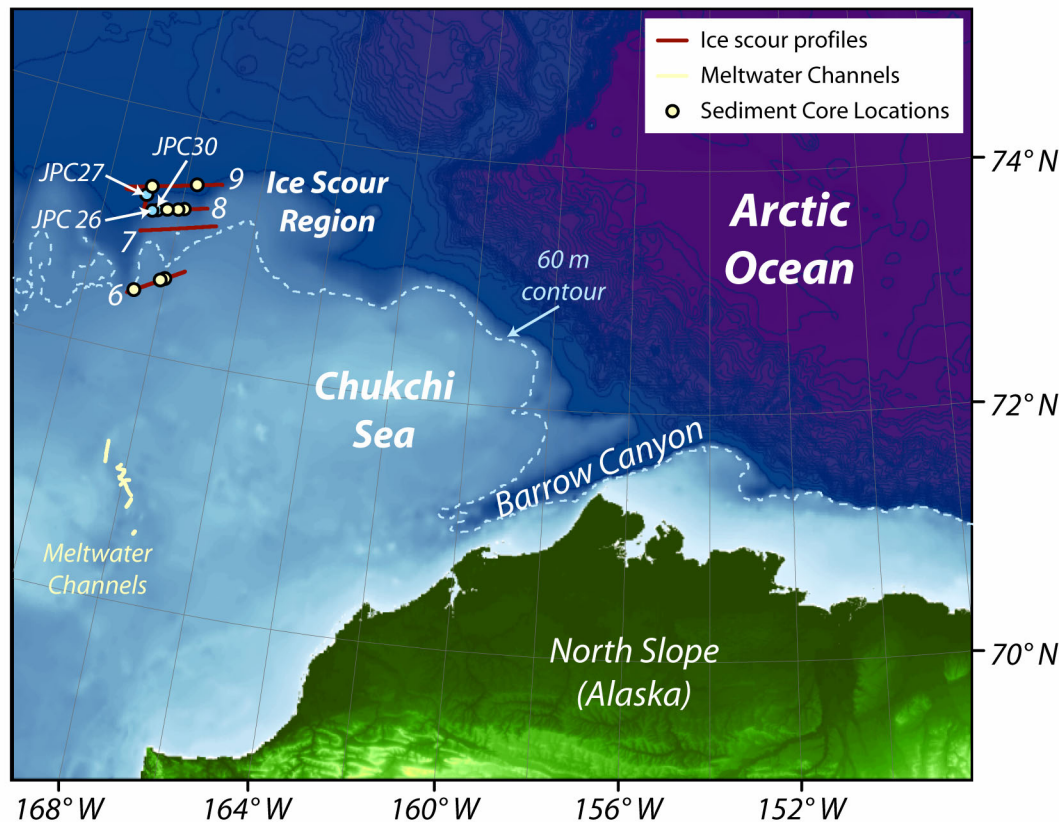


Figure 4.1 Map of the eastern Chukchi margin showing CHIRP profiles across the ice scour surface and sediment core locations. Profiles locations of midshelf meltwater drainage (*Hill et al.*, in press) discussed in the text are shown. At the time of ice scour incision, sea level was ~60 m below present. We suggest Barrow Canyon may have served as an embayment directing iceberg discharge from the Alaskan North Slope to the outer shelf.

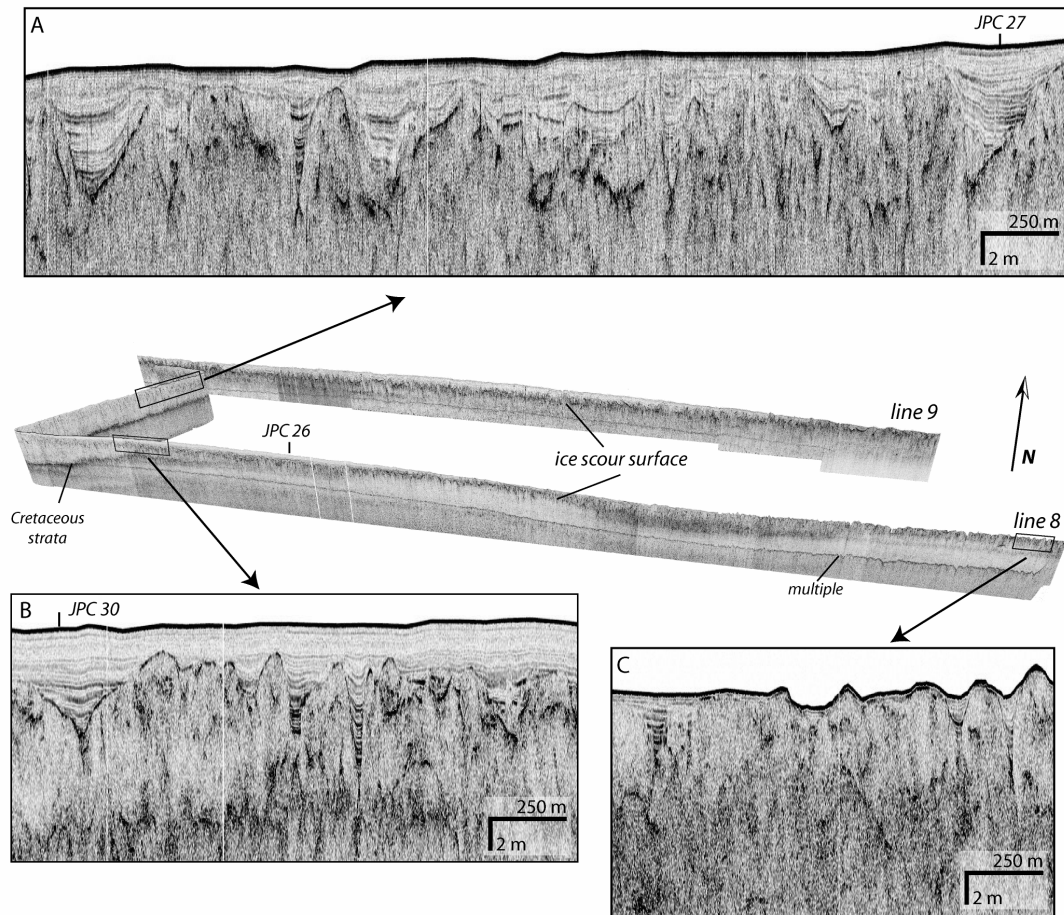


Figure 4.2 3-D perspective view of CHIRP profiles across the ice scour region. Sediment cover is thickest in the western portion of the profiles. Boxes A, B and C show insets. The ice scour morphology has a distinctive v-shaped morphology, with elevated ridges on either side, infilled with highly reflective, acoustically laminated sediment. Above the localized scour infill the acoustic character becomes more transparent. Box C, in the eastern region, shows very little sediment cover. Profile locations are shown in Figure 4.1.

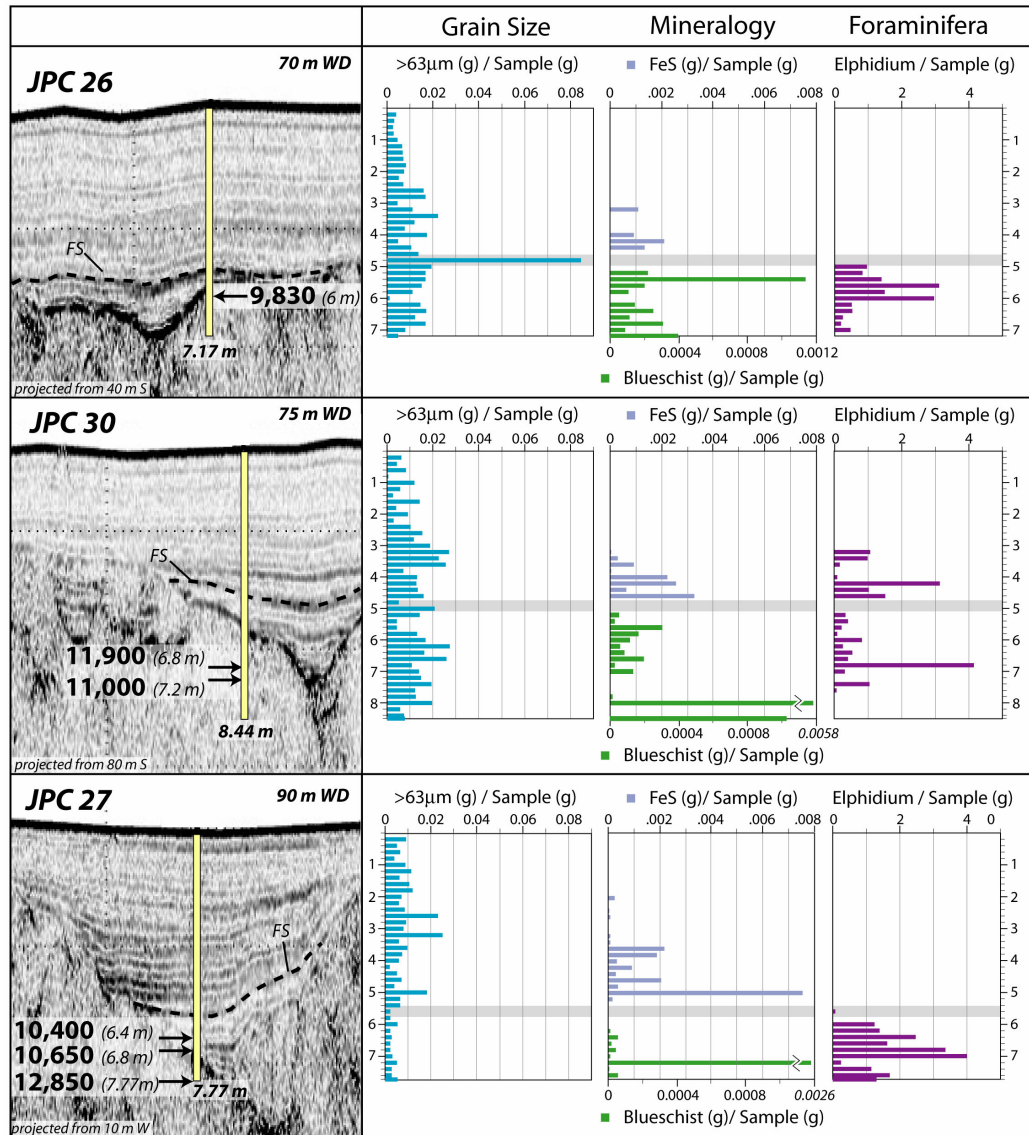


Figure 4.3 Sediment core locations projected onto the CHIRP profiles, along with sediment analyses (each plot is scaled to the length of the core). Radiocarbon dates were collected (shown in bold) above and below the scour surface to constrain the age of the ice-scour event to between 10,600 and 11,900 ^{14}C yr BP. Sediment composition exhibits a marked transition from blueschist facies minerals near the scour surface to pyrite precipitation above. Note the break in scale for high abundances of blueschist facies minerals in JPC27 and JPC30. The grey bar indicates a flooding surface that separates the two mineralogical zones. The flooding surface appears to represent a period of rapid sea level rise and the transition from estuarine to open marine conditions. Elphidium, which prefer brackish environments, are most abundant in the basal section of each core. JPC30 has some additional elphidium above the basal flooding surface; there appears to be another flooding surface above that might explain this signal.

References

- Aagaard, K. and Carmack, E., 1989. The role of sea ice and other fresh water in the Arctic circulation. *Journal of Geophysical Research*, 94: 14,485-14,498.
- Bard, E., Hamelin, B., Tisnerat-Laborde, N. and Cabioch, G., 1988. Radiocarbon calibration by means of mass spectrometric $^{230}\text{Th}/^{234}\text{U}$ and ^{14}C ages of corals: An updated database including samples from Barbados, Muroroa and Tahiti. *Radiocarbon*, 40: 1085-1092.
- Barnes, P., Rearic, D. and Reimnitz, E., 1984. Ice gouging characteristics and processes, In: Barnes, P., D. Schell and E. Reimnitz (Eds.), *The Alaskan Beaufort Sea - Ecosystems and Environments*, Orlando: Academic Press, pp. 185-213.
- Bischof, J., Clark, D. L. and Vincent, J., 1996. Origin of ice-rafted debris: Pleistocene paleoceanography in the western Arctic Ocean. *Paleoceanography*, 11: 743-756.
- Bond, G., Heinrich, H., Broecker, W., Labeyrie, L., McManus, J., Andrews, J., Huon, S., Jantschik, R., Clasen, S., Simet, C., Tedesco, K., Klas, M., Bonani, G. and Ivy, S., 1992. Evidence for massive discharges of icebergs into the North Atlantic ocean during the last glacial period. *Nature*, 360: 245-249.
- Brigham-Grette, J., 2001. New perspectives on Beringian Quaternary paleogeography, stratigraphy and glacial history. *Quaternary Science Reviews*, 20: 15-24.
- Darby, D. A., Bischof, J. F., Spielhagen, R. F., Marshal, S. A. and Herman, S. W., 2002. Arctic ice export events and their potential impact on global climate during the late Pleistocene. *Paleoceanography*, 17: doi:10.1029/2001PA000639.
- Davies, T. A., T. Bell, A. K. Cooper, H. Josenhans, L. Polyak, A. Solheim, M. S. Stoker and J. A. Stravers (Eds.), 1997. *Glaciated Continental Margins: an Atlas of Acoustic Images*, London: Chapman and Hall, 314 p.
- Dyke, A. S., Andrews, J. T., Clark, P. U., England, J. H., Miller, G. H., Shaw, J. and Veillette, J. J., 2002. The Laurentide and Innuitian ice sheets during the Last Glacial Maximum. *Quaternary Science Reviews*, 21: 9-31.
- Hill, J. C., Driscoll, N. W., Donnelly, J. P., Brigham-Grette, J., Gayes, P. T. and Keigwin, L. D., 2007. New evidence for high discharge to the Chukchi shelf since the Last Glacial Maximum. *Quaternary Research*, in press.

- Jakobsson, M., Løvlie, R., Arnold, E. M., Backman, J., Polyak, L., Knutsen, J.-O. and Musatov, E., 2001. Pleistocene stratigraphy and paleoenvironmental variation from Lomonosov Ridge sediments, central Arctic Ocean. *Global and Planetary Change*, 31: 1-22.
- Jakobsson, M., Gardner, J. V., Vogt, P. R., Mayer, L. A., Armstrong, A., Backman, J., Brennan, R., Calder, B., Hall, J. K. and Kraft, B., 2005. Multibeam bathymetric and sediment profiler evidence for ice grounding on the Chukchi Borderland, Arctic Ocean. *Quaternary Research*, 63: 150-160.
- Kaufman, D. S. and Manley, W. F., 2004. Pleistocene maximum and Late Wisconsin glacier extents across Alaska, U.S.A., In: Ehlers, J. and P. L. Gibbard (Eds.), *Quaternary Glaciations—Extent and Chronology, Part II: North America*, Amsterdam: Elsevier, pp.9-27.
- Keigwin, L. D., Donnelly, J. P., Cook, M. S., Driscoll, N. W. and Brigham-Grette, J., 2006. Rapid sea-level rise and Holocene climate in the Chukchi Sea. *Geology*, 34: 861-864.
- Mann, D. H., Peteet, D. M., Reanier, R. E. and Kunz, M. L., 2002. Response of an arctic landscape to Lateglacial and early Holocene climatic changes: the importance of moisture. *Quaternary Science Reviews*, 21: 997-1021.
- Phillips, R. L., Barnes, P., Huner, R. E., Reiss, T. E. and Rearic, D. M., 1988. Geologic investigations in the Chukchi Sea, 1984, NOAA ship SURVEYOR cruise. U.S. Geological Survey Open-File Report 88-25.
- Polyak, L., Edwards, M. E., Coakley, B. J. and Jakobsson, M., 2001. Ice shelves in the Pleistocene Arctic Ocean inferred from glaciogenic deep-sea bedforms. *Nature*, 410: 453-457.
- Polyak, L., Darby, D. A., Bischof, J. F. and Jakobsson, M., 2007. Stratigraphic constraints on late Pleistocene glacial erosion and deglaciation of the Chukchi margin, Arctic Ocean. *Quaternary Research*, 67: 234-245.
- Smith, L. M., Miller, G. H., Otto-Bliesner, B. and Shin, S.-I., 2003. Sensitivity of the Northern Hemisphere climate system to extreme changes in Holocene Arctic sea ice. *Quaternary Science Reviews*, 22: 645-658.
- Stokes, C. R., Clark, C. D., Darby, D. A. and Hodgson, D. A., 2005. Late Pleistocene ice export events into the Arctic Ocean from the M'Clure Strait Ice Stream, Canadian Arctic Archipelago. *Global and Planetary Change*, 49: 139-162.

Zweck, C. and Huybrechts, P., 2005. Modelling of the northern hemisphere ice sheets during the last glacial cycle and glaciological sensitivity. *Journal of Geophysical Research*, 110: doi:10.1029/2004JD005489.

Chapter 5

**Paleodrainage on the Chukchi shelf reveals
sea level history and meltwater discharge**

5.1 Abstract

CHIRP subbottom data collected across the Chukchi shelf, offshore NW Alaska, imaged numerous paleochannels and valleys that appear to have been downcut and incised during sea level falls associated with glacial intervals. In contrast, the two most recent incisions appear to have been formed during the period of sea level rise following the Last Glacial Maximum (LGM). The architecture and infill associated with these two incisions suggests they were formed by an increase in discharge. These events appear to be unrelated to sea level fluctuations, but rather triggered by climatic variations during the most recent deglaciation (i.e. meltwater discharge). Radiocarbon dates from sediment cores within the southern incised valley suggest the two episodes of meltwater discharge may correlate with Meltwater Pulse 1-A (~14,000 yrs BP) and the Chukchi iceberg scour event (~12,000 to 13,000 yrs BP; *Hill and Driscoll*, in prep), respectively. Regional transgression across the interfluvies on the middle Chukchi shelf appears to postdate the second meltwater discharge and may correlate with Meltwater Pulse 1-B (11,500 yrs BP). This evidence suggests that in glacially dominated landscapes, episodes of large discharge to the shelf might be out of phase with the sea level cycle. In addition, the presence of glacial meltwater drainage on the shelf implies a greater volume of continental glaciation during the LGM than previously recognized.

5.2 Introduction

The Chukchi Sea overlies a broad, shallow shelf between northern Alaska and Siberia that has been repeatedly exposed during periods of lowered sea level (Figure

1). CHIRP subbottom data imaged extensive buried paleochannel networks on the shelf offshore NW Alaska that appear to record several sea level falls. Incision and downcutting are often interpreted to occur as result of base level lowering (*Christie-Blick and Driscoll, 1995*); however, along glaciated margins fluctuations in discharge associated with glacial lake breaching, meltwater discharge and climatic oscillations can lead to renewed incision and downcutting independent of base level change. While most of the fluvially incised valleys observed on the Chukchi shelf appear to be related to variations in sea level, the two most recent incisions appear to represent glacial meltwater pulses. Similar observations have been made on other glaciated margins where glacial lake breaching has played an important role in shaping margin morphology (e.g., *Uchupi, et al., 2001* and references within). Glacial outburst floods from ice dammed lakes in southern New England produced sheet flows that deposited large sediment lobes across the New York-New Jersey margin and emplaced numerous large glacial erratics on the outershelf (*Uchupi, et al., 2001*). The Hudson Shelf Valley is also believed to have been incised by high discharge flows from glacial meltwater that scoured the channel, contributing to incision and sediment bypass (*Uchupi, et al., 2001; Donnelly, et al., 2005*). Massive floods from Glacial Lake Missoula carved the Channeled Scabland topography of Washington and induced hyperpycnal flows with turbidite deposits that can be traced more than 1000 km offshore (*Bretz, 1969; Normark and Reid, 1998; Zuffa, et al., 2000*).

It is important to recognize how the morphology of glaciated margins differs from non-glaciated, temperate and low latitude regions in order to understand the

processes that can lead to renewed incision and downcutting in the absence of base level lowering.

The channel formation and evolution presented in *Hill, et al., (2007)* is expanded upon here, with additional CHIRP and Boomer subbottom data, as well as sediment core data and radiocarbon ages that corroborate the initial interpretations and place important constraints on channel development and drainage evolution across the Chukchi margin. Evidence presented here also implies a greater extent of glaciation than previously recognized (*Brigham-Grette, 2001*), which has important implications for development of global climate models (*Smith, et al., 2003; Zweck and Huybrechts, 2005*), the understanding of freshwater balances in the Arctic (*Aagard and Carmack, 1989*) and the degree of climate variability across the region (*Keigwin, et al., 2006*).

5.2 Regional Setting

5.2.1 Tectonics

The complex tectonic history of Arctic Alaska and the surrounding shelves is comprised of a number of rifting, subduction and uplift events (*Moore, et al., 1994*). Uplift in the mid-Jurassic to late Cretaceous produced much of the modern topography observed in northern Alaska. The Barrow Arch, which forms a broad structural high trending along the Beaufort coast, developed as a result of the late Cretaceous rifting that opened the Canada Basin (Fig. 2) (*Moore, et al., 1994*). Around the same time, subduction of the Arctic Terrane along the northern margin transitioned into uplift along the northward verging Brooks Range thrust zone and the

southern flank of the Barrow Arch became the foreland basin for the nascent orogenic belt (Moore, *et al.*, 1994). The E-W trending Brooks Range dominates the modern topography and exposed imbricate folds of the northern foothills transition into the broad, flat topography of the Arctic Coastal Plain that comprises most of the North Slope.

Offshore, uplift along the Herald thrust has created a structural high that separates the northwestern Chukchi margin from the Hope Basin to the south (Fig. 2). The NE verging Herald thrust trends NW-SE across the Chukchi shelf and converges with the Brooks Range thrust on the Lisburne Peninsula in the Chukchi syntaxis (Moore, *et al.*, 2002). On the northern side of the Herald Arch, the Hanna wrench fault zone, a complex, north trending, failed rift basin, covers a large portion of the northwestern shelf, while a series of listric normal faults related to rifting along the Beaufort margin makes up the North Chukchi Basin in the east (Thurston and Theiss, 1987). The Hope Valley to the south is a an extensional drop-down basin made up of half-grabens that originated through transtension on a dextral-slip fault system in the Eocene (Tolson, 1987).

5.2.2 Drainage patterns

The Brooks Range is the drainage divide for northern Alaska. Most of the southwestern foothill drainage flows through Kotzebue Sound into the Chukchi Sea, while the northern foothills predominantly discharge into the Beaufort Sea. The Colville River drains a large portion of the North Slope ($\sim 60,000 \text{ km}^2$; Lamke, *et al.*, 1995) and flows axial parallel through much of the foreland basin of the thrust belt

before emptying into the Beaufort Sea. The few northern rivers that drain west into the Chukchi Sea (e.g., Kukpowruk, Kokolik, and Utukok Rivers) have a combined drainage area of only $\sim 25,000 \text{ km}^2$ (Lamke, *et al.*, 1995). The northwestern rivers also have very low discharge, ranging from 500 to $1750 \text{ m}^3\text{s}^{-1}$, compared with a discharge of $6,700 \text{ m}^3\text{s}^{-1}$ for the Colville River (Childers, *et al.*, 1979).

Previous authors have suggested the primary drainage to the Chukchi Sea during periods of lowered sea level was derived from southwestern Brooks Range and flowed northwest through Hope Valley, emptying into the Arctic Ocean via the Herald Canyon (McManus, *et al.*, 1983). While this may be true for the southern Chukchi Sea, the structural high of the Herald Arch effectively prevents drainage from the Hope Basin from reaching the northeastern shelf. Paleochannels linked to rivers in the northernmost part of Alaska appear to trend northward, bypassing the shelf and flowing down Barrow Canyon (Phillips, *et al.*, 1988). The small rivers of the northwest Alaska appear to be the sole source of discharge to the region northeast of the Herald Arch.

5.2.3 Recent glaciations

Controversy exists regarding the extent and volume of glaciation across the western Arctic during the LGM. Several authors have argued that the Beringian landmass remained largely ice-free throughout the LGM, with small glaciers restricted to upland regions (e.g., Brigham-Grette, 2001; Brigham-Grette, *et al.*, 2004). The Alaska Paleoglacier Atlas (Manley and Kaufman, 2002) indicates glaciation was limited to alpine and montane regions during the LGM, while the

maximum extent of glaciation is proposed to have occurred during the late Pleistocene, with ice extent mapped to edge of the Brooks Range foothills (Fig. 1). Note the Alaska Paleoglacier Atlas assigns a low level of certainty to the western extent of glacial boundaries, including the northwestern foothills, due to a lack of detailed air photograph or field based studies in this region (Fig. 1). Alternatively, Grosswald and Hughes (2002; 2004) suggest a large ice shelf extended from eastern Siberia across the western Arctic that would have abutted surrounding continental margins and moved south through the Bering Strait.

5.3 Data Acquisition

CHIRP subbottom data were acquired aboard the USCGC Healy on the Chukchi mid-shelf (Fig. 1) in 2002, using the Scripps Institution of Oceanography EdgeTech X-Star CHIRP subbottom reflection sonar with sub-meter vertical resolution. Data were acquired at a ship speed of ~4-5 knots. Towfish navigation was obtained by monitoring fish depth and the winch cable payout in relation to topside DGPS receivers. The subbottom reflection profiles were acquired using a 1-6 kHz CHIRP signal with a 50 ms sweep. The CHIRP subbottom data were processed using SIOSEIS (*Henkart, 2006*) and Seismic Unix (*Cohen and Stockwell, 1999*) seismic processing software packages. Boomer subbottom data were collected by the U.S. Geological Survey (R. Lawrence Phillips, chief scientist) aboard the R/V Surveyor and R/V Discoverer in 1984 and 1985, respectively. The USGS Boomer data were collected using an ORE Geopulse subbottom profiler at 100, 150, 175 and 200 joules with single channel 25 or 50 element hydrophones. The Boomer

subbottom profiles presented here were digitally scanned from paper records. For more information about the USGS expeditions, see Phillips, et al. (1988) and Miley and Barnes (1986).

The CHIRP subbottom profiles were used to select piston and vibracore locations across the shelf to construct a relative sea level curve and drainage history for the region. Difficulties with station keeping abilities in sea-ice free conditions limited the number of cores we were able to acquire and in some cases drift in the ship position caused the core locations to be offset from the profiles.. Grain size analyses were performed on selected core sections with a 1 cm sampling interval using a Beckman-Coulter Laser Diffraction Particle Size Analyzer LS13320. Articulated bivalve mollusks and benthic foraminifera samples were collected for ^{14}C dating at the National Ocean Sciences Accelerator Mass Spectrometer (NOSAMS) facility in Woods Hole, Mass. Radiocarbon dates were calibrated to calendar years using the Fairbanks0805 calibration curve (*Fairbanks, et al.*, 2005) with a ΔR of 300 as in the Bering Sea (*Cook, et al.*, 2005).

5.4 Results

5.4.1 Acoustic Facies

Cretaceous strata

The deepest unit imaged on the shelf consists of steeply inclined, folded and faulted strata with a predominantly northward dip. The tilted strata are most prominent in close proximity to the Herald Arch, where they commonly outcrop at the seafloor or have very thin (<1 m), discontinuous sediment cover (Fig. 3). Strata

in the north are more acoustically transparent and appear truncated horizontally, with a highly reflective, uneven erosional surface that may have up to 25 m of sediment above. Previous authors interpret this deposit as Cretaceous age strata deformed as a result of thrusting along the Herald front (*Phillips, et al.*, 1987; 1988; *Thurston and Theiss*, 1987).

Southern Valley

A large incised valley (~24 km wide) trends along the axis of the Herald Arch for at least ~90 km across the midshelf, downcutting the underlying Cretaceous strata by 50 m (Fig. 4). Subbottom profiles on the landward side of the incised valley suggest multiple smaller valleys may converge to form the large midshelf valley, which appears to widen and deepen offshore. The valley has a compound fill made up of several distinct depositional units that are defined by six regionally extensive erosional surfaces. In many cases, these erosional surfaces appear to coalesce along the boundaries of the incised valley.

The deepest incision, Valley Incision 0 (VI-0), truncates underlying Cretaceous strata and defines northeastern limit of the incised valley (Figs. 5, 6, 7). The sediment above this reflector (Unit 0) appears acoustically transparent in the CHIRP subbottom data, but displays some inclined bedding with cross-cutting relationships farther offshore in the Boomer subbottom data. Unit 0 deposits are observed only on the NE side of the incised valley (Figs. 5, 6, 7). Most of the Unit 0 strata appear to be truncated or removed by incision along a second erosional surface, Valley Incision I-1 (VI-1) (Fig. 8). Strata overlying VI-1 (Unit 1) mostly consists of

acoustically laminated, low reflectivity unit that is continuous over long distances and drapes the underlying topography (Figs. 5, 6, 7). Some internal truncation of reflectors and small channels are present within the unit on the most landward subbottom profiles (Figs. 5, 6).

Erosion by Valley Incision II (VI-2) truncates and downcuts Unit 1 strata across most of the valley (Figs. 5, 6, 7). Incision along VI-2 appears to deepen offshore. The most nearshore profiles show maximum incision of ~15 m, which increases to ~40 m farther offshore. Infill above VI-2 (Unit 2) exhibits a very complex stratigraphy that displays characteristic fluvial cut and fill geometry made up of numerous cross-cutting channels with inferred point bars, cutbanks and lateral accreting sets. Individual channels in Unit 2 are several hundred meters wide with 10-15 m of incision (Figs. 5, 6).

The two most recent incisions, Incision III (I-3) and Incision IV (I-4), downcut into Unit 2 strata. I-3 has a maximum incision of ~45 m into Unit 2 strata, while I-4 downcuts at least 20 m within I-3 (Fig. 6) and the incision deepens offshore. The two incision surfaces are sometimes difficult to differentiate and may coalesce seaward. Both I-3 and I-4 appear to be restricted to the southwestern side of the incised valley, with widths ranging from 3 km on landward profiles to 15 km seaward (Figs. 4, 8). The sediments above I-3 (Unit 3) and I-4 (Units 4 and 5) have a very similar acoustically laminated character and are much more reflective than lower units (Figs. 5, 6, 7, 8). Unit 3, 4 and 5 strata infill the valley with slight thickening observed toward the basin depocenter. In some profiles, the contact between Unit 4 and Unit 2 is characterized by a relatively rough erosional surface (Fig. 6). In

addition, there is some small, localized post-depositional faulting in Unit 4 (Figs. 6, 7). Units 4, 5 and 6 are separated by local flooding surfaces (FS1, FS2) identified most clearly on CHIRP line 2 (Fig. 6).

A large constructional mound (~2 km wide, 15 high) is observed on the southwestern side of the southern incised valley, situated above Units 1 and 2 (CM; Figs. 5, 6, 8). The feature is adjacent to I-3/I-4 and onlapped by strata within Unit 4. Sediment within CM exhibits downlapping along two surfaces. The upper internal downlap surface occurs roughly mid-section, while the lower downlap surface defines the contact between CM and the underlying sediment (Figs. 5, 6). The uppermost reflectors on the NE side of the feature show minor truncation by I-3/I-4 and the feature is onlapped by Unit 3 and/or 4 (Figs. 5, 6). CM is present in multiple subbottom profiles, including an orthogonal crossing of two Boomer subbottom profiles that provides evidence of a three dimensional structure (Fig. 8).

Northern Valley

Another heavily channelized region is observed on the northern Chukchi midshelf. Compared with the incised valley to the south, drainage in this area appears to less confined, with multiple individual channels and valleys cut into the Cretaceous strata (Fig. 4, 9). The largest valley in the region, termed the northern valley, downcuts and incises the Cretaceous strata by ~35 m, with widths ranging from 5 to 8 km (Fig. 9). Unlike the incised valley to the south, the northern valley only exhibits one acoustic fill, Unit N1. Unit N1 is acoustically laminated with low reflectivity, an acoustic character similar to Unit 1 observed in the southern valley. There is a ~15 m

thick inclined wedge of sediment at the base of N1 on the SW edge. The overlying strata onlap this wedge and infill the valley. Reflectors in the upper few meters of N1 sediment appear somewhat chaotic and are disrupted by abundant small v-shaped incisions. Several smaller channels and valleys are present surrounding the northern valley (Fig. 4, 9); however, given the diffuse drainage and lack of stratigraphic overlap, it is difficult to trace regional surfaces across the valleys or distinguish individual depositional units outside of N1.

Incision of small channels and valleys

Numerous individual paleochannels and small valleys (1-2 km width) are observed across the Chukchi shelf from the most nearshore subbottom profiles out to at least ~55 m water depth (Fig. 4). Incision depths in the channel thalwegs range from 10-35 m. The maximum depth of channel base with respect to modern sea level averages ~55 m in the nearshore region, whereas the depth to the channel thalweg is 85-100 m below modern sea level in the northern and southern valleys (Fig. 10). Note there is a marked change in channel depth at approximately 175 km from the coastline, between the paleo- Kokolik/ Kukpowruk and the southern valley and the paleo- Utukok and the northern valley. The large profile spacing and lack of stratigraphic overlap makes it difficult to draw any conclusions about relative ages or depositional units between the southern and northern channel systems. There appear to be two drainage pathways emanating from the northwestern Alaskan margin. One series of paleochannels appears to link the Kokolik and/or Kukpowruk Rivers with

the southern valley, while the other may link the Utukok River with the northern valley (Fig. 4).

Regional transgressive surface

The uppermost erosional surface (TS) observed in the subbottom profiles truncates strata along the boundaries of both the northern and southern valleys as well the surrounding shelf (Figs. 5, 6, 7, 8, 9). In some areas reflector TS is interrupted by small, discrete, v-shaped downcutting events on the NE side of the southern incised valley (IS; Figs. 6, 7). The sediments above TS (Unit 6) are acoustically laminated with low reflectivity. Unit 6 infills bathymetric lows and exhibits thickness variations ranging from <1 m on the interfluvies to > 5 m in some of the paleochannels (Fig. 8). The transgressive surface in portions of the southern valley separates Unit 6 from the older underlying Units 1 and 2 (Figs. 5, 6). Along the southern edge of the valley, TS coalesces with I-3 (Figs. 5, 6).

5.4.2 Sediment Facies

Southern Valley

Six sediment cores were collected within the southern incised valley. VBC03 (8.66 m) recovered sediment from Units 3 and 6 on the southwestern side of the southern incised valley (Figs. 5, 11). The base of VBC03, just above I-3, consists of well-sorted medium sand above interbedded sand and silt. This section contains some of the coarsest sediment collected across the shelf. In addition, there is a large (~3 cm diameter) mudclast in the basal section, which is coincident with an

articulated bivalve mollusk, identified as *Portlandia arctica* (Fig. 11). Radiocarbon dating of this shell yielded an age of $12,300 \pm 65$ ^{14}C yrs BP ($\sim 13,500$ calendar yrs BP). The upper portion of Unit 3 is composed of a several meter thick section of silt with occasional sand layers. Upsection, interbedded sand and silt delineates the contact between Unit 3 and Unit 6. The uppermost section of Unit 6 is a silty clay with abundant shell, wood and charcoal fragments.

VBC04 (5.82 m) and VBC05 (6.94 m) both sampled sections of Unit 2 from the center of the southern valley (Fig. 11). VBC05 also has a cap of Unit 6 silt at the surface, while the upper section (presumably Unit 6) of VBC04 was not recovered due to coring difficulties. Unit 2 sediment from VBC05 primarily consists of silty clay, but also contains a several meter thick section of interbedded sand and silt in the upper section and a thin layer of small clay rip-up clasts mid-core, as well as a layer of fine sand at the base. A thin layer of blocky sand marks the TS surface between Unit 2 and Unit 6 in VBC05. In contrast, VBC04 consists entirely of well-sorted fine sand with a slight downcore coarsening. Neither VBC05 nor VBC04 recovered any biogenic material.

JPC08 (3.67 m) recovered sediment from Units 3 and 6 (Fig. 12). The upper ~ 1 m of JPC08 consists of silty, shell rich clay from Unit 6. Just beneath Unit 6, Unit 3 contains interbedded fine sand and silt that grades downward into visually homogenous silty clay in the basal section, but shows faint laminations on an X-ray image. JPC09 (8.92 m) and JPC10 (8.13 m) both recovered sediment from Units 4 and 6, as well as from the northeastern edge of the CM feature below I-4 (Fig. 12). The base of JPC09 is comprised of fine sand with clay rip-up clasts that are

coincident with the contact between the CM feature and Unit 2. Above is a thin layer of interbedded silt and sand overlain by ~2 m of well-sorted medium-fine sand (median grain size ~175 μm) that correlates with the CM feature. Similar to JPC09, the lower section of JPC10 consists of ~4 m of well-sorted sand that also corresponds to the CM feature; however the JPC10 sand is slightly finer (median grain size ~150 μm) than the sand in JPC09. Clay-rip clasts (2-10 cm) at the base of JPC10 are coincident with an internal downlap surface in the CM feature. Both cores exhibit a slight fining upward at the top of the sand sections before transitioning to the interbedded sand and silty clay at the interface between the CM feature and Unit 4. JPC09 has a more expanded Unit 4 section than JPC10, characterized by a thin layer of clay rip-up clasts, in between sections of interbedded sand and silt. The upper ~4 m of both cores consists of the silty/sandy clay of Unit 6 with shell fragments. Radiocarbon dates were obtained from articulated bivalve mollusks at several depths within the Unit 6 section of JPC10 (Fig. 12). The ages yield an average sedimentation rate of ~1.45 m/kyr, from 8,000 – 10,700 yrs BP, decreasing to ~ 0.05 m/kyr in the last 8,000 yrs.

Hope Valley

A piston core (JPC02) in the central Hope Valley recovered a ~9.5 m thick Holocene section (Fig. 13). The base of the core contains interbedded sand and silt that coarsens upward to a 55 cm thick well-sorted sand section, with a slight fining upward. A much finer section of interbedded silt and sand creates an abrupt transition at the top of the sand. This section is overlain by 8.5 m of silt that

correlates with Unit 6. Two abundance peaks of the foraminifer, *elphidium excavata*, yielded radiocarbon dates of 10900 ± 140 ^{14}C yrs. BP ($\sim 11,900$ calendar yrs BP) at 845.5 cm, just above the TS transition, and 6920 ± 75 ^{14}C yrs. BP ($\sim 7,100$ calendar years) at 69.5 cm (Keigwin, et al., 2006). X-ray fluorescence (XRF) analysis of the basal section shows a major shift in elemental components (Cu, Fe, Ni, Zn and S) at the transition from sand to silt. Keigwin, et al. (2006) also report a large increase in $\delta^{18}\text{O}$, along with a decrease in $\delta^{13}\text{C}$, at this same level.

Outer shelf sedimentation

A suite of six cores on the mid to outer shelf (49-62 m water depth) each recovered several meters of Unit 6 sediment (Fig. 14). All of the cores recovered several meters of silty clay above a fine sand or interbedded sand and silt that correlates with a flooding surface observed in the CHIRP subbottom profiles (Fig. 14). Grain size analyses were conducted on the basal sections of VBC39 and VBC40. VBC39 (4.4 m) sampled a well sorted, fine sand (median grain size ~ 125 μm) at the base, overlain by an interbedded sand and silt. VBC40 (3.7 m) consists of a bedded, well-sorted fine sand (median grain size ~ 75 μm) at the base mantled by a unit of interbedded fine and coarse sands, which creates a sharp contact with the basal sands. Overlying the interbedded fine and coarse sands is a silty clay unit in the uppermost section (Fig. 14).

5.4.3 Onshore drainage

Drainage in northern Alaska is in large part structurally controlled by the Brooks Range. The Colville River appears to have captured most of the northern foothill drainage along the axis of the foreland basin. A low lying drainage divide (~10 m high) near the headwaters of the Colville separates the headwaters for the Utukok, Kukpowruk and Kokolik rivers, which flow westward into the Chukchi Sea (Fig. 15). The northwestern rivers have much lower discharge and smaller combined drainage area than the Colville River, yet appear to be more deeply incised. The headwaters of the northwestern rivers cut across exposed folds of the foothills to form a trellis drainage network. The coastal plain in this region is characterized by numerous thermokarst lakes (Fig. 15c). Both the Utukok and Kokolik Rivers display broad floodplains characteristic of low gradient, meandering rivers. Profiles across portions of these rivers on the coastal plain shows floodplain valley widths of 1-3 km (Fig. 15a). The active flow occupies a small channel surrounded by meander cutoffs and oxbow lakes while the remaining floodplain is heavily sedimented with fluvial deposits. The Kokolik River is the most deeply incised of the three, but also has the narrowest valley (~1 km width; Fig. 15a). The Kokolik River is also much less sinuous and may have a structural barrier on the eastern side (Fig. 15d).

5.5 Discussion

5.5.1 Multiple sea level cycles

The southern incised valley contains three regional erosional surfaces that appear to represent fluvial downcutting during multiple sea level lowering events.

Each of these incision surfaces defines a sequence boundary underlying a succession of lowstand systems tract deposits (LST) followed by transgressive systems tract deposits (TST). In classic sequence stratigraphic incised valley fill models (e.g. *Vail* 1987; *Van Wagoner, et al.*, 1990; *Zaitlin, et al.*, 1994), the valley undergoes net fluvial erosion and sediment bypass during the relative sea level fall. During the late part of the lowstand, as the rate of relative sea level fall slows and the rise begins, the valley is filled with backstepping fluvial deposits of the LST, assuming there is sufficient sediment supply. As the valley is flooded, estuarine and open marine deposits of the TST downlap onto the underlying fluvial strata. Typically the TST would be overlain by deposits of the highstand systems tract (HST); however, we do not commonly observe HST deposits across the southern valley region due to a combination of processes. Within the valley, multiple fluvial incisions have reworked and removed any highstand deposits, while on the interfluvies highstand deposits are reworked with each transgression due to the limited accommodation space.

The deepest surface, VI-0 (~50 mbsf), represents the oldest phase of incision into the underlying Cretaceous strata. While the acoustically transparent character of Unit 0 in the CHIRP data is difficult to classify, Boomer subbottom profiles across Unit 0 farther offshore exhibit well-defined, inclined beds that may represent fluvial deposition. The majority of Unit 0 has been eroded during a second period of sea level lowering that corresponds to incision along VI-1. Unit 1 contains small channels on CHIRP line 1 (Fig. 5) and some inclined beds in the basal part of the unit along CHIRP line 2 (Fig. 6). The majority of Unit 1, though, contains parallel,

draping strata that appear more representative of quiescent deposition. Both Units 0 and 1 appear to represent the classic succession of fluvial deposition within the LST as sea level begins to rise, transitioning upward to estuarine and marine deposition within the TST, creating a drowned valley estuary at the seaward end of the system. The transition from fluvial to marine is predominantly concordant in the incised channels as sediments are infilling the lows and there is little to no erosion across the transgressive surface.

A third phase of sea level lowering is represented by regional erosional surface VI-2 that downcuts and truncates Unit 1 strata. The fluvial strata that make up the majority of Unit 2 appear to record lateral channel migration within the valley. On CHIRP lines 1 and 2 (Figs. 5, 6), several individual channels can be identified within the deposit that exhibit characteristic fluvial features (e.g., point bars and cutbanks). The upper part of these channels is filled with acoustically laminated, sediment that may represent meander cutoff deposits or localized backfilling with marine sediment during the sea level rise. Cut and fill channel architecture is far more common in Unit 2 than Units 0 or 1. Furthermore, there does not appear to be any regionally extensive laminated sequences within Unit 2 as observed in Unit 1. One possible explanation is that rate of sedimentation during this interval may have been high enough to outpace the rate of sea level rise. In such a scenario, nearly the entire valley would be filled with fluvial deposits leaving little accommodation for marine deposits.

The uppermost surface, TS, which truncates strata across both the edges of the northern and southern valleys as well as the surrounding shelf, is interpreted to be a

regional transgressive surface. On some subbottom profiles within the southern incised valley, reflector TS is disrupted by numerous v-shaped incisions (IS), indicative of sea ice scouring following the transgression, that obscure the exact location of TS. In these instances, reflector IS is taken as the best estimate for the transgressive surface. TS is overlain by marine strata of Unit 6, which represents post-transgressive Holocene sedimentation associated with the TST. In the southern valley, the TS surface identified in the CHIRP data correlates to a shift from sand or interbedded silt and sand to more homogeneous silt and clay (Figs. 11, 12). JPC02 in the Hope Valley exhibits similar change in grain size and XRF analyses of the basal section shows a concomitant shift in elemental composition at the grain size boundary. Keigwin, et al. (2006) also report a shift in $\delta^{18}\text{O}$ that is indicative of a switch from estuarine to open marine conditions at this same level. Radiocarbon dating of the TS within the Hope Valley yields an age of $10,900 \pm 140$ ^{14}C yrs. BP ($\sim 11,900$ calendar yrs BP). The oldest radiocarbon date from material within Unit 6 of JPC10 yields an age of $10,200 \pm 55$ ^{14}C yrs. BP ($\sim 10,700$ calendar yrs BP), approximately 1 m above TS. Using the JPC10 sedimentation rate of ~ 1.45 m/kyr for this interval to extrapolate the age of TS in both JPC10 and JPC09 yields an age estimate of $\sim 11,500$ yrs BP, which roughly correlates with the timing of the inferred MWP-IB (Fig. 16).

In general, Unit N1 within the northern valley has a similar acoustic character to Unit 1 in the southern valley. Both deposits exhibit inclined beds at the base that may represent initial fluvial deposition, but are primarily comprised of acoustically laminated strata that are continuous across much of the valley and appear to drape the

underlying strata (Figs. 5, 6, 7, 9). The dipping strata in both Units 1 and N1 are onlapped by a channel filling sequence that is obscured at the top by multiple ice scouring events. Without stratigraphic overlap between the northern and southern valleys or core information in the northern valley, correlation of these two units is speculative; however, based on acoustic character and these three observed packages (i.e. basal dipping, middle infilling and onlapping, and the upper ice scoured section), we suggest incision of the northern valley and VI-1 and the overlying fill may record the same sea level cycle.

The exact age of the valley incisions remains unknown; however, several lines of evidence suggest the features are relatively recent. In the southern valley, VI-0 truncates the northward dipping Cretaceous strata. These underlying strata were tilted as a result of thrusting along the Herald Arch, a feature which may have been active as recent as the early Tertiary (*Phillips, et al.*, 1988; *Moore, et al.*, 1994). The strata within the southern valley are not deformed, suggesting they must be younger than the age of deformation. The seafloor above the southern valley exhibits ~6 m of negative relief. If the valley was formed in the distant past, we would expect this depression to have since filled with sediment. Additionally radiocarbon dating across the shelf indicates TS is related to the most recent marine transgression (e.g., JPC02, JPC10). Without deep core information from Units 2 and older, the simplest explanation appears to be that the sea level cycles represented by VI-1 and VI-2 correlate to the Illinoian (Marine Isotope Stage 6) and Wisconsin (Marine Isotope Stage 2) glaciations, respectively (Fig. 16). VI-0 appears to represent an even older phase of sea level lowering, perhaps dating back to Marine Isotope Stage 12. We

expect maximum downcutting to have occurred during the period of most rapid sea level lowering, with subsequent deposition of overlying units as sea level began to rise (Fig. 16). By analogy with VI-1, the northern valley may also correlate with MIS 6 and other incisions in the region may be MIS 12 or older.

5.5.2 Meltwater discharge

Reflectors I-3 and I-4 both exhibit large downcutting relief that truncates underlying Units 1 and 2; however, these two surfaces do not appear to represent sequence boundaries. Units 3 and 4 strata onlap Unit 2, indicating I-3 and I-4, along with the subsequent fill, must be younger than VI-2 and Unit 2. If VI-2 was indeed incised during MIS 2, I-3 and I-4 must have been downcut during the period of sea level rise following the LGM. Sequence stratigraphic models commonly invoke base level lowering as the primary cause of fluvial incision and downcutting across the shelf; however climatic factors, such as increased discharge or decreased sediment input, or a combination of both, may generate incision in the absence of relative sea level fall (*Schumm, et al., 1987; Dalrymple, et al., 1994*). While sedimentation is generally expected to decrease during the transgression, estimates from both the southern valley (JPC10) and the Hope Valley (JPC02) (*Keigwin, et al., 2006*) indicate sedimentation rates were relatively high during the most recent transgression and decreased dramatically ~7,000 yrs BP. In the absence of base level lowering or decreased sedimentation, our preferred interpretation is that the incision resulted from increased discharge in response to meltwater runoff during deglaciation.

Unlike Units 0, 1 and 2, the highly reflective, acoustically laminated sediment of Units 3, 4, and 5 shows no evidence of fluvial structures. VBC03 recovered entirely marine sediment from within Unit 3. The basal section of this core also exhibits relatively coarse grained layers that may represent lag deposits in the base of the channel (Fig. 11b). Therefore we interpret Units 3, 4 and 5 as estuarine or marine deposits, infilling localized coastal embayments that were flooded in advance of the regional transgression of the interfluvies. Thus, the TS that separates marine above from nonmarine below must coalesce with I3 and go beneath Unit 3. The timing of the regional flooding is best recorded by FS2 that separates Unit 5 and 6 because the hiatus is minimized. FS1 is interpreted to be a local flooding surface that represents a period of rapid sea level rise separating Units 4 and 5. The lack of lateral fluvial deposition in Units 3, 4, and 5 indicates this segment of the valley was predominantly undergoing erosion and sediment bypass during the downcutting of I-3 and I-4. High discharge events, such as meltwater outbursts during deglaciation, would scour the upper reaches of the channel, transporting the sediment farther offshore, and may explain the lack of fluvial fill observed in the subbottom data (Figs. 5, 6, 8).

The large CM feature is elevated above Unit 2 and shows markedly different geometry than the strata beneath. The three dimensional morphology and internal downlapping stratigraphy suggest a constructional feature rather than an erosional remnant. CM is onlapped by both Units 3 and 4, suggesting it may be associated with I-3/I-4 processes. The large size (~15 m high; 2 km wide), stratal geometry and sediment facies of CM is consistent with a fluvial origin, e.g. bar or braided island, in a high discharge environment. The CM section of both JPC09 and JPC10 is

comprised of well-sorted fine sand with small clay rip-up clasts on each of the downlapping surfaces (Fig. 12). CM pinches out to the NE and the sand recovered in JPC09 is slightly coarser than JPC10 sand from the upper part of the feature, suggesting the edges may be a lag deposit, with the finer sediment building up on the high. Geochemical analyses of JPC10 also indicate a relatively high percentage of organic carbon in the sandy CM section, transitioning upward to very low organic content in Unit 6 (*Lundeen, 2005*), which points to a more terrestrial signal at the base overlain by marine sediment.

The marine shell dated at 13,500 yrs BP in Unit 3 is 1.24 m above I-3. Extrapolation with the sedimentation rate determined from JPC10 implies I-3 was formed 14,300 yrs BP, which coincides with Meltwater Pulse 1A (Fig. 16). Thus we speculate I-3 was incised by meltwater discharge during post-LGM warming, with the open channel subsequently infilled by estuarine to marine sediment of Unit 3 (Figs. 5, 6, 8). Regional flooding of the interfluves across the Chukchi shelf, that is where Unit 6 overlies Unit 2 (Figs 5 and 6) appears to correlate with FS1 (separating Unit 4/5) or FS2 (separating Unit 5/6) within the paleochannel, which implies that I4 is older than the regional flooding (~11,500 yrs BP), but younger than I-3. If correct then I-4 incision occurred ~12,000-13,000 yrs BP. Evidence from a regionally extensive ice scour field on the outer Chukchi shelf suggests discharge of a large number icebergs, possibly sourced from the Chukchi margin of Alaska, during this time interval (Fig. 16) (*Hill and Driscoll, in prep*). Therefore, we speculate downcutting along I-4, which records a second phase of meltwater discharge, may be coincident with the release of the iceberg armada. The proposed timing of I-4 also

correlates with deglaciation following a late stage glacial advance across the central and southwestern Brooks Range that ended $\sim 11,500$ ^{14}C yrs BP (Hamilton, 1982; 1986). Since these most recent incisions appear to be unrelated to base level change, having occurred during a period of sea level rise, the I-3 and I-4 incision are not sequence boundaries formed by a base level fall. This evidence suggests that in glacially dominated landscapes, climatic factors can play an important role in creating incision and downcutting that is out of phase with sea level cycles.

5.5.3 Onshore and offshore drainage patterns

Structural controls from underlying bedrock may explain many of the drainage patterns observed across the Chukchi margin. Paleochannels incised into the Cretaceous strata appear to be controlled by *cuestas* and follow the strike of the underlying strata. Paleochannels and valleys mapped in this study appear to follow the same trend, flowing NNW along structural contours toward the shelf break and Chukchi borderland. The southern valley has been repeatedly excavated throughout multiple sea level cycles, creating the largest incised valley observed on the shelf. Drainage is concentrated in this region and flows axial parallel to the primary thrust of the Herald Arch, much like the Colville River onshore flows axial parallel to the Brooks Range. The Cretaceous strata outcrop at the seafloor near the southern valley, while the top of the Cretaceous strata is truncated beneath the modern seafloor in the north by as much as 25 m in some locations (Figs. 3, 8). Drainage on the outer shelf appears directed along the strike of the Hanna wrench fault zone, but similar to the northern valley region is relatively dispersed and does not appear to reoccupy the

same valleys during subsequent sea level cycles. It appears that with increasing proximity to the Herald thrust belt, drainage is more strongly controlled by the underlying bedrock. This may explain why the southern valley is reoccupied during multiple sea level cycles.

Modern rivers draining the northwestern margin exhibit similar structural control. Satellite imagery of the Utukok and Kokolik Rivers shows meandering rivers with broad floodplains and numerous meander cutoffs, while the Kukpowruk River exhibits the least sinuosity and strongest bedrock control (Fig. 15). Profiles across portions of the Kokolik, Kukpowruk and Utukokok Rivers on the coastal plain bear out these observations. The Utukok and Kokolik Rivers exhibit much larger valleys than the Kukpowruk River, but appear to be less incised (Fig. 15). The Kukpowruk River is the closest of the three to the onshore extension of the Herald Thrust, which trends NNW across the Lisburne Peninsula (Fig. 2). Some authors have also speculated that neotectonic activity in the region may have influenced the course of the river (*Cassavant and Miller, 2002*).

The paleochannels and valleys observed in the nearshore region appear to be much narrower and more distributed than their midshelf counterparts. This may be explained in part by sparse innershelf data coverage, the relatively poor resolution of many of the Boomer records in this region and the fact that many of the Boomer profiles trend parallel to the azimuth of the drainage. The midshelf may also be an important drainage confluence as flows are constricted, passing between the broad structural highs of the Herald and Hanna Banks. The most landward profiles suggest the southern valley may be split into two smaller valleys, a northern segment and a

southern segment (Fig. 8). Based on acoustic character, the southern segment appears to contain predominantly Unit 2 deposits, while the northern segment is filled with Units 0 and 1, but shows no evidence of Unit 2. The two smaller valleys appear to converge, creating the much larger valley observed in CHIRP line 2 (Fig. 8).

Across the shelf, comparison of channel incisions relative to modern sea level, which takes into account differing seafloor elevations, indicates there may be a knickpoint landward of the large incised valleys observed on the midshelf. With a few exceptions, channels and valleys imaged on the innershelf exhibit a base of incision around 55 m below modern sea level; this increases considerably to 85-100 m on the midshelf (Fig. 10). This suggests the incised valleys on the midshelf may have been migrating shoreward through headward erosion as they attempted to regrade following base level lowering. The knickpoint on the midshelf at ~40-45 m water depth may indicate the point beyond which fluvial rejuvenation of the system and farther landward incision was restricted. Thus it appears that a combination of headward erosion and drainage confluence may have contributed to the misfit of the large midshelf incised valleys relative to smaller channels and valleys observed on the midshelf. Unfortunately, a lack of additional data makes it difficult to fully constrain the extent of the incised valleys across the shelf or to ascertain how the individual channels correlate with various sea level cycles.

Drainage observed in the nearshore region appears to emanate from two sources on the northwestern Alaskan margin and may link modern rivers with the larger incised valleys observed on the midshelf. One set may represent the paleo-Kokolik/Kukpowruk channels that connect to the southern valley, while the other set

appears to flow between the Utukok River and the northern valley region (Fig. 4). The modern rivers draining the northwestern margin of Alaska (Fig. 1, 15) have very low discharge and relatively small drainage areas that suggest a misfit with the offshore drainage. Nevertheless, these rivers have steep banks and incised channel morphologies cut into the Brooks Range foothills, which suggest they may have been carved by much stronger flows in the past (Fig. 15). The dimensions of these northwestern river valleys are less than half the size of the valleys defined by I-3 or I-4 on the midshelf. The lack of fluvial fill in the I-3 and I-4 valleys makes it difficult to compare the offshore channel networks with the northwestern rivers. The onshore river valleys may be more deeply incised than they appear in the profiles since we were not able to measure unfilled valley dimensions. The northwestern river valleys were most likely carved by the same processes as on the midshelf, but are filled with fluvial sequences emplaced within the last 8,000 yrs, as the rate of sea level rise slowed and channels were able to regrade (Fig. 16).

5.5.4 *Climate*

The presence of glacial meltwater channels on the shelf implies a greater extent of glaciation in northwestern Alaska during the LGM than previously recognized. While the mapped extent of glaciation at this time is largely restricted to the central and eastern Brooks Range, some highland glaciation also been mapped in the southern Brooks Range foothills (Fig. 1). Throughout recent glacial periods ice masses repeatedly dammed the headwaters of the Noatak River, creating a succession of proglacial lakes, collectively termed Glacial Lake Noatak (Fig. 17) (*Hamilton,*

2001; 2003). The northern margin of this ice dammed lake was located just south of the western Brooks Range drainage divide. The headwaters of the northwestern rivers are located 15-20 km to the north of LGM age glacial lake deposits (Fig. 17). While very few field studies have been conducted along the northwestern rivers, hydrologic reconnaissance reports from the 1950s of the northwestern foothills indicates the presence of stream incised u-shaped valleys and north facing cirques across the region encompassing the Utukok, Kokolik and Kukpowruk headwaters (*Sable, et al.*, 1981). These features are tentatively attributed to older glaciations; however, it appears plausible that glacial lake damming similar to the Noatak region may have occurred on the northern side of the drainage divide as well. Geologic mapping in the Noatak region indicates the presence of a U-shaped pass of unspecified age, where glaciers flowed north from the edge of the interpreted region into the Utukok River headwaters (Fig. 17) (*Hamilton*, 2003).

Hamilton (2003) suggests Glacial Lake Noatak water levels commonly fluctuated throughout glaciation, leaving behind weakly developed shoreline features that are difficult to trace. Additionally, the underlying geology of the northwestern foothills is very different from the Noatak region, making it difficult to compare morphologies on the basis of DEMs alone and highlights the need for field mapping in the region.

The argument for limited Brooks Range glaciation during the LGM often focuses on a synoptic paleoclimate record for the region that emphasizes a lack of moisture necessary for significant ice buildup (e.g. *Brigham-Grette*, 2001). While it is likely that the general paleoclimatic trend of northern Alaska was toward

exceptionally aridity during the LGM, some studies have suggested there may have been considerable spatial heterogeneity (e.g., *Mock and Anderson, 1997; Edwards, et al., 2001*). Hamilton (2003) documents evidence of an “unusually large valley glacier” in the Avan River valley during the LGM and speculates that the Avan region, which is in close proximity to headwaters of the Kokolik and Kukpowruk Rivers (Fig. 18), must have been experiencing much higher snow fall at this time than the highlands to the east. This example highlights the role of small scale regional variability in moisture conditions across the northwestern margin during the LGM and implies similar paleoclimatic conditions may have also existed across the headwaters of the northwestern rivers. The evidence presented here for glacial meltwater drainage on the shelf does not necessarily suggest large ice sheets across the region, but rather indicates there may have been more extensive alpine glaciation during the LGM than previously recognized.

5.5.5 *Sea level and Holocene sedimentation*

Extrapolation of sedimentation in several of the midshelf cores allows us to place some new constraints on the timing of sea level rise across the Chukchi margin. The age of TS in JPC02 indicates marine inundation of the Hope Valley and nearby Bering Strait occurred ~12,000 yrs BP, nearly 1,000 years earlier than previous estimates (*Keigwin, et al., 2006*). The estimated age of TS in both JPC09 and JPC10 from the southern valley suggests this surface represent rapid flooding across the Chukchi mid shelf ~11,500 yrs BP and may correlate with globally recognized Meltwater Pulse 1-B (*Bard, et al., 1996*).

Sediment cores and CHIRP subbottom data from the mid to outer shelf show evidence of a prominent flooding surface (FS) near the base of Unit 6 (Fig. 14). Similar to the flooding surface transitions observed across the southern valley, each of the sediment cores exhibits a distinct shift in grain size from sand or interbedded sand and silt to silty clay at the FS boundary (Fig. 14). The coarser grains appear to represent a lag deposit accumulated during the flooding and wave-base reworking, followed by finer-grained sediment deposition above as the shoreline and associated facies migrates landward. While the age of the FS boundary is unknown, the paleodepth of the surface is roughly the same in each of the sediment cores. Plotting this surface on the global sea level curve and assuming it is marine allows us to place some constraints on the maximum age of the surface. The mid to outer shelf FS is at the same paleodepth as the regional transgressive surface (TS) observed across the southern incised valley and Hope Valley. This suggests FS may represent the transgressive surface across this portion of the shelf, corresponding to Meltwater Pulse-1B (Fig. 16). If the midshelf FS is younger, it most likely formed within several meters of the transgression and may represent a younger episode of rapid sea level rise.

Radiocarbon dating from cores in both the Hope Valley (JPC02) and the midshelf (JPC10) suggests the sedimentation rate across the Chukchi shelf was relatively high during the rapid sea level rise following the LGM, and decreased dramatically ~7000 yrs BP. Between 11 ka and 7 ka, portions of the Hope Valley accumulated as much as 10 m of Holocene sediment, with almost no sedimentation thereafter (Fig. 13). This is unusual, given that sequence stratigraphic models

commonly predict sediment starvation on the shelf during rapid sea level rise as the margin becomes inundated and sediment is trapped in shallow embayments (*Vail, 1987; Van Wagoner, et al., 1990*). Typically, as the rate of sea level rise begins to slow, we would expect sediment accumulation rates to slowly increase. This prediction is borne out in other river deltas around the world (*Stanley and Warne, 1994*), many of which show a prominent build out around 8,000 yrs BP, as the rate of sea level began to slow (*Fairbanks, 1989*). In contrast, sedimentation on the Chukchi margin appears to be highest during the rapid sea level rise, which suggests there must have been additional inputs. Precipitation and moisture levels across the continent began to increase during deglaciation, as sea level rise flooded the shelf and brought moister maritime climates to the region (*Edwards, et al. 2001*); however, paleoprecipitation was still 10-20% less than modern 6,000 yrs BP (*Barber and Finney, 2000*). Pluvial conditions during deglaciation may have increased glacial water storage and led to glacial readvances observed in the central and southwestern Brooks Range between 13,000 to 11,500 ^{14}C yrs BP (*Hamilton, 1986*). Increased moisture input would have also augmented glacial meltwater discharge, which would have maintained high sediment input during this period. The drop in sedimentation roughly coincides with the global cessation of meltwater discharge $\sim 8\text{ka}$ (*Barber, et al., 1999*). This evidence suggests local meltwater pulses to the Chukchi margin may be in phase with global meltwater patterns.

5.6 Conclusions

The Chukchi shelf appears to have been an important drainage pathway during periods of lowered sea level, as evidenced by the numerous paleochannels and valleys observed on the mid to outershelf. This is contrary to the assertion that most of the flow across the Chukchi was derived from the Hope Valley and escaped down the Herald Canyon offshore, largely bypassing the greater shelf region (*Mc Manus, et al.*, 1983). The southern incised valley shows evidence of multiple incisions, representing sequence boundaries that correlate with periods of lowered sea level, possibly as recent as the LGM. Sequence stratigraphic models for siliciclastic margins generally predict fluvial incision during the falling limb of sea level, as base level lowering leads to stream rejuvenation (*Christie-Blick and Driscoll*, 1995). In contrast, the two most recent incisions, I-3 and I-4, appear to have been downcut during the period of sea level rise following the LGM, and therefore do not represent sequence boundaries but rather are related to important climatic events. This evidence suggests that on glaciated margins it is important to realize that not all incisions represent sequence boundaries. In these cases, the timing of channel excavation and nature of the fill is very important in determining whether the incision is related to base level change or climatically driven.

Sea level records across the shelf indicate the regional transgression occurred 11,500 to 12,000 yrs. BP, coincident with Meltwater Pulse 1-B. Following transgression, shelf sedimentation appears to have remained unusually high throughout deglaciation and rapid sea level rise, most likely the result of the large volumes of fresh water input from melting glaciers following the LGM. The

meltwater drainage observed on the shelf may have been derived from glacial lake breaching; regardless it highlights the role of climatic heterogeneity across the region and implies a greater extent of continental glaciation during the LGM than previously proposed.

5.7 Chapter acknowledgement

Chapter 5, in full, is the material as submitted to Marine Geology: Hill, J.C. and Driscoll, N.W., 2007. Paleodrainage on the Chukchi shelf reveals sea level history and meltwater discharge. *Marine Geology, submitted*.

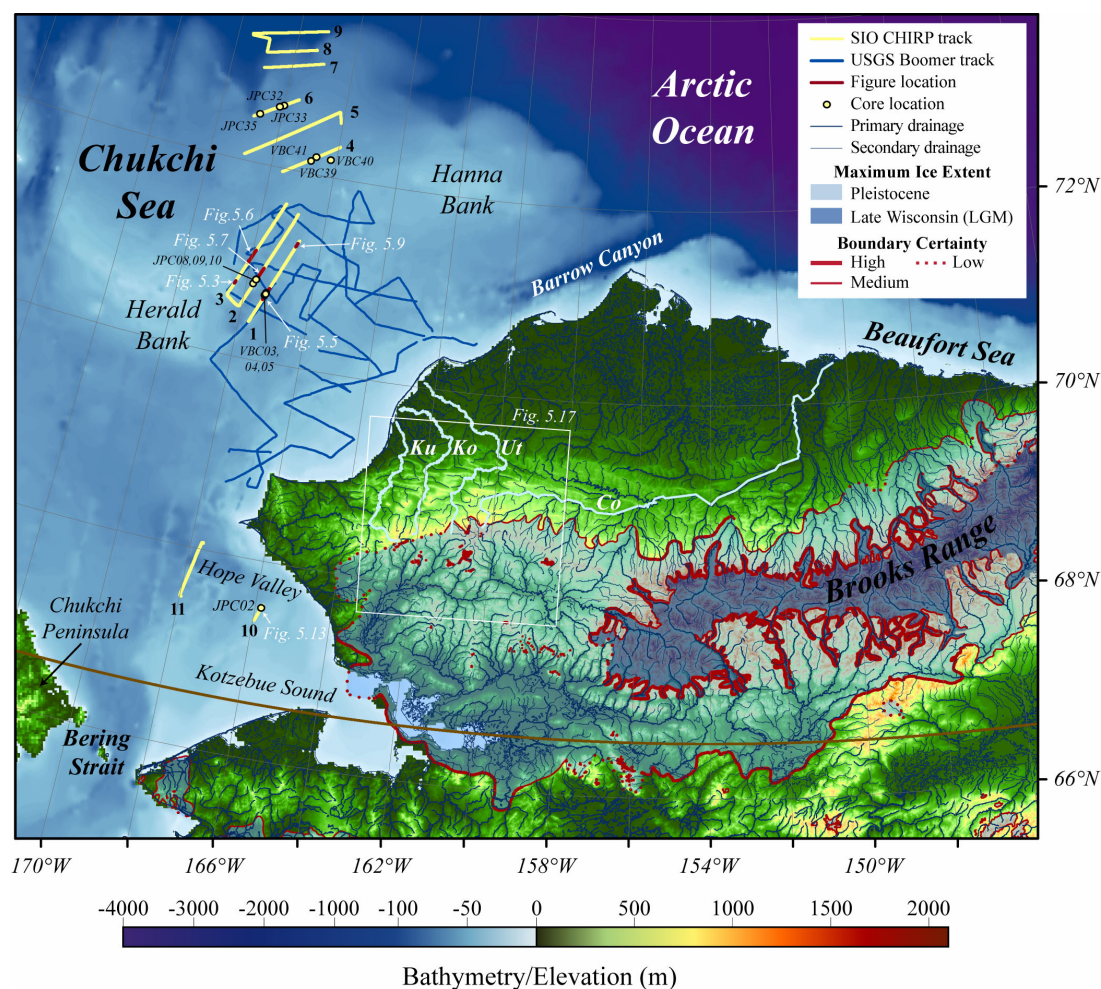


Figure 5.1 Location map of northern Alaska and the adjacent Chukchi margin showing SIO CHIRP and USGS Boomer subbottom tracks. CHIRP profile numbers are labeled in bold and piston core locations are also noted. Figure profiles discussed in the text are highlighted in red. Abbreviations: Ut – Utukok River, Ko – Kokolik River, Ku – Kukpowruk River, Co – Colville River. The primary modern drainage in northern Alaska flows NNE through the Colville River, while the southern Brooks Range drains through Hope Valley. The northwestern margin is drained by the small, low discharge Utukok, Kokolik and Kukpowruk Rivers. Also shown is the previously interpreted maximum ice extent for the Pleistocene and Late Wisconsin (LGM) glaciations (*Manley and Kaufman, 2002*). High certainty boundaries have well-defined chronologies, while low certainty boundaries may encompass areas lacking significant field or remotely sensed studies. Note that ice extent is uncertain along the NW Brooks Range foothills that comprise the headwaters of the Kukpowruk, Kokolik, and Utukok Rivers.

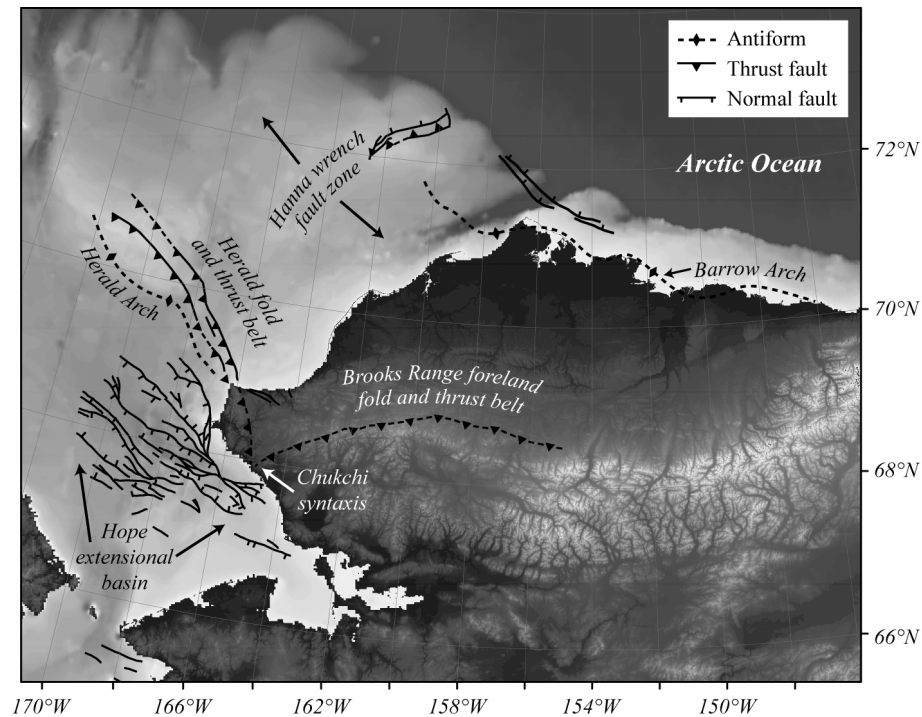


Figure 5.2 Simplified tectonic map of northern Alaska and adjacent Chukchi margin with data from *Miller, et al., 2002*. The modern topography is dominated by two northward verging thrust belts. Onshore, the Brooks Range orogenic front trends E-W and transitions northward into the exposed fold and thrust belt of the Brooks Range foothills in the foreland basin. Offshore the Herald Thrust and associated thrusting onshore in the Lisburne Peninsula have created uplift along the Herald Arch and Lisburne Hills trending at a high angle to the Brooks Range. To the north, the Herald fold and thrust belt gives way to the northward trending wrench fault zone. The Hope Valley is an extensional basin comprised of numerous half-graben features.

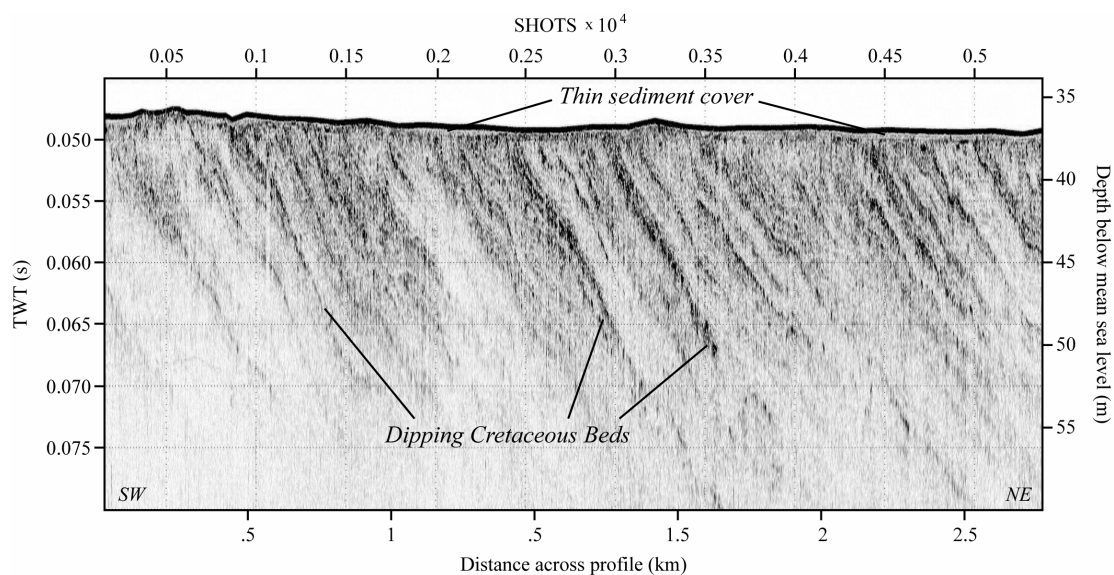


Figure 5.3 CHIRP subbottom profile (see Figure 5.1 for location) showing northward dipping Cretaceous strata. Outside of the channeled region, these strata outcrop at the seafloor with very little sediment cover.

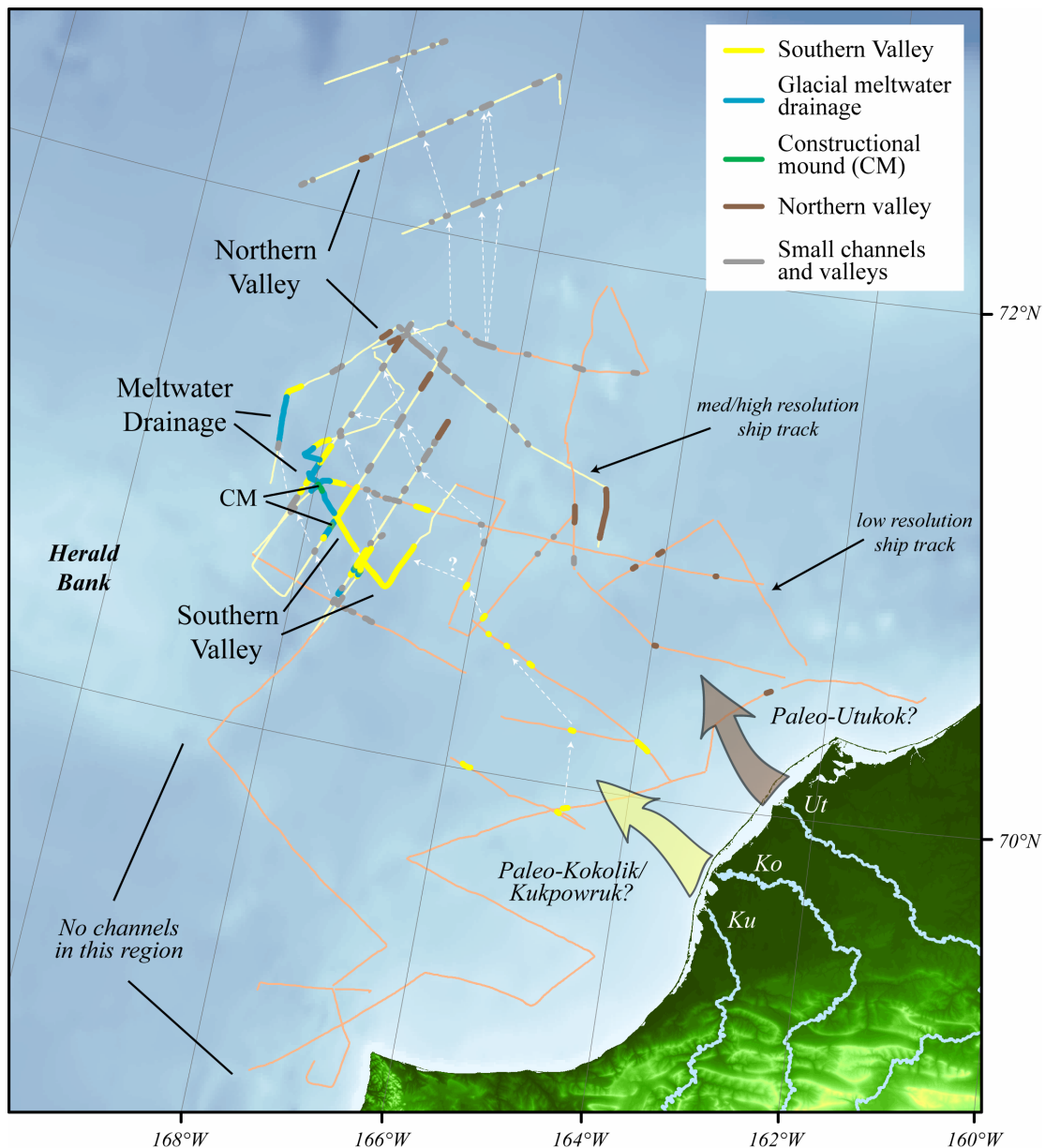


Figure 5.4 Interpreted channel map showing profiles crossing the southern incised valley (VI-0, VI-1, VI-2), meltwater drainage (I-3, I-4), CM feature and northern valley. Numerous additional individual paleochannels are also identified in profiles across the shelf; however lack of stratigraphic overlap makes it difficult to definitively correlate these units. Tentative correlations between these smaller channels and valleys are shown. There appears to be two paleochannel pathways emanating from the Utukok (Ut) and Kokolik (Ko)/Kukpowruk (Ku) Rivers on the northwest Alaskan margin. Note there are no channels present in the profiles between the Lisburne Peninsula and Herald Bank, suggesting the shelf paleochannels were not sourced from the Hope Valley region.

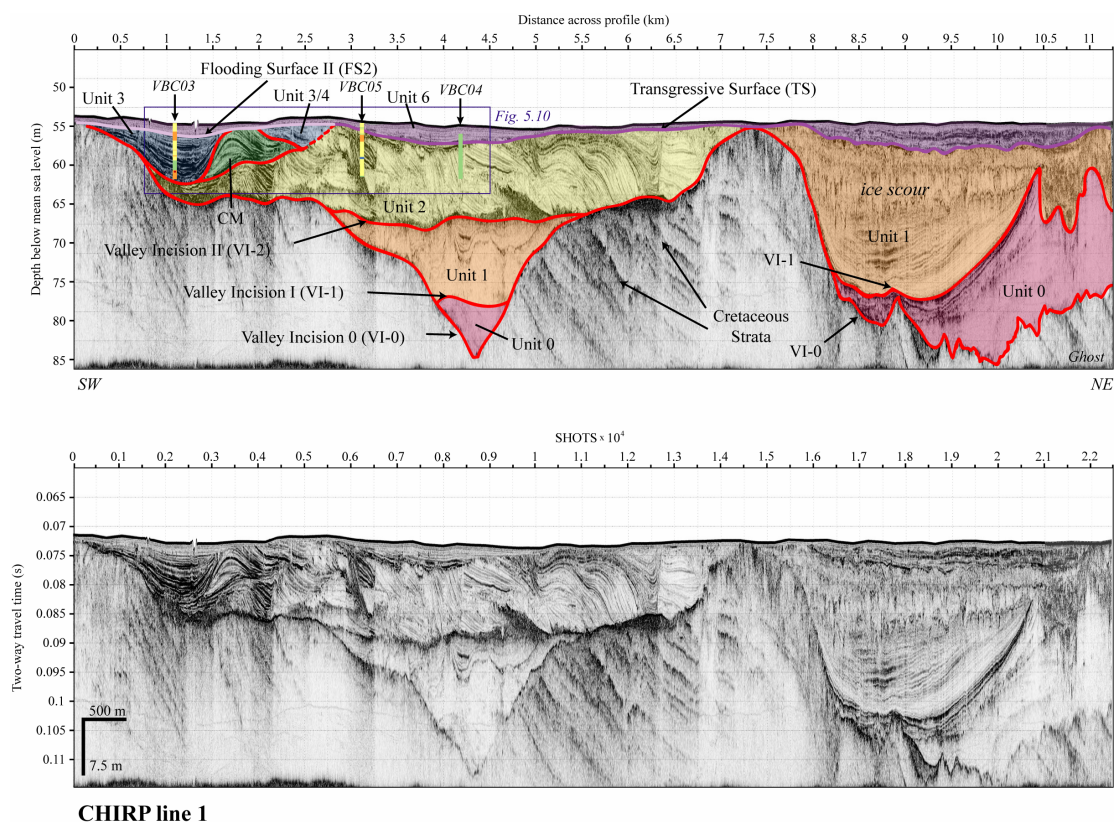


Figure 5.5 CHIRP subbottom profile across the incised valley (line 1). **Bottom:** Uninterpreted profile. **Top:** Interpreted profile with the reflectors color coded as follows: *Red* –Valley Incisions 0, 1, 2 (VI-0, VI-1, VI-2); *Dark Purple* –Most recent transgressive surface (TS); *Light purple* –Flooding surface (FS2). Sedimentary units are also labeled.

Figure 5.6 CHIRP subbottom profile across the incised valley (line 2). **Bottom:** Uninterpreted profile. **Top:** Interpreted profile with the reflectors color coded as follows : *Red* --Valley Incision I (VI-1), Valley Incision II (VI-2), Incision III (I-3) and Incision IV (I-4); *Light purple* --Flooding surfaces (FS1, FS2); *Dark Purple* --Most recent transgressive surface (TS); *Blue* --Most recent ice scour (IS), also the best estimate for TS in that area; *Green* --Post-depositional faulting. CM indicates a constructional mound feature. Sedimentary units are also labeled and core locations of JPC 08, 09, 10 are shown.

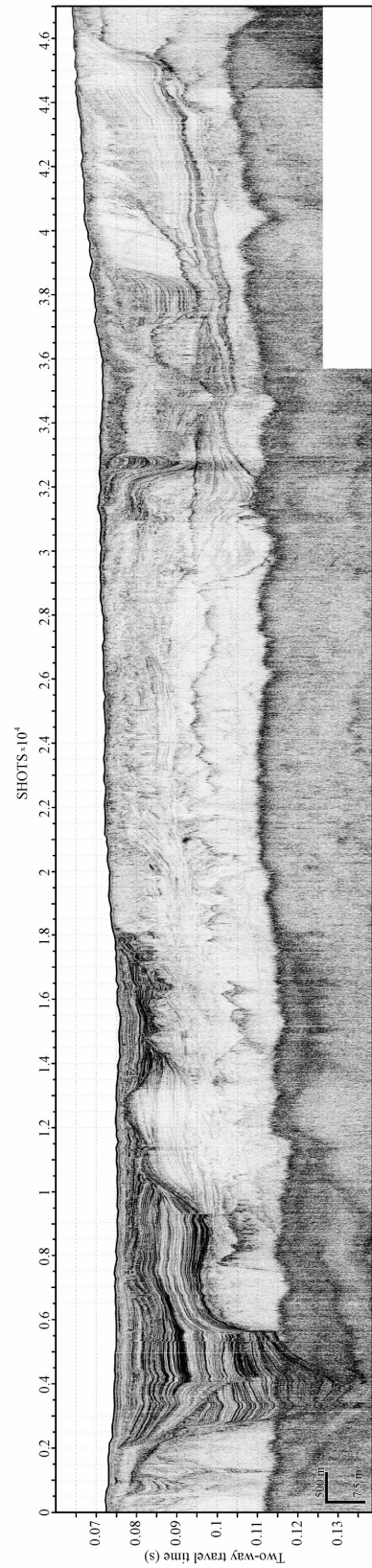
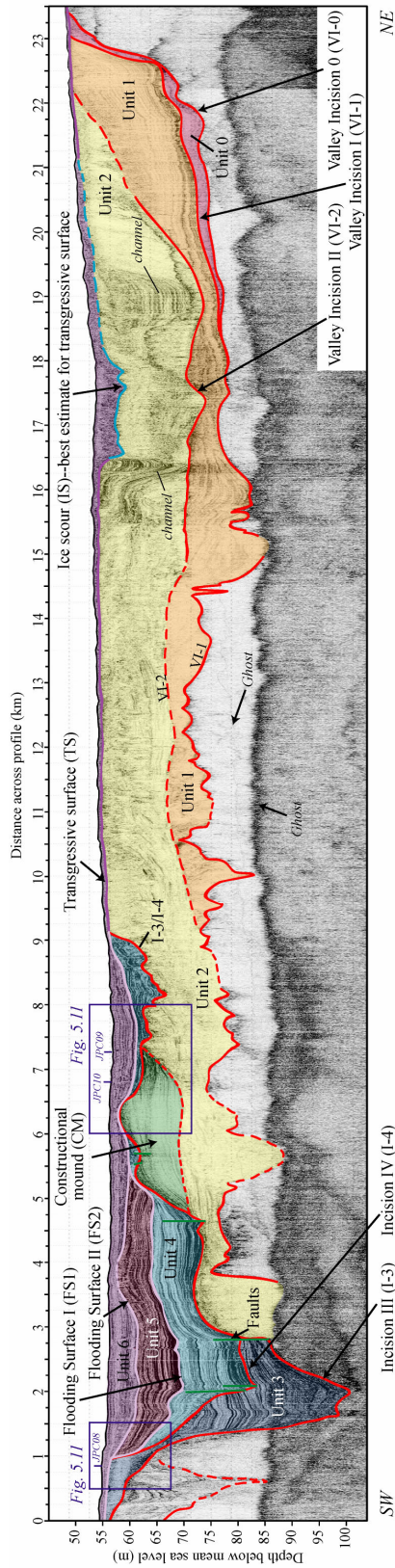


Figure 5.7 CHIRP subbottom profile across the incised valley (line 3). **Bottom:** Uninterpreted profile. **Top:** Interpreted profile with the reflectors color coded as follows : *Red* --Valley Incision I (VI-1), Valley Incision II (VI-2), Incision III (I-3) and Incision IV (I-4); *Light purple* --Flooding surface (FS); *Dark Purple* --Most recent transgressive surface (TS); *Blue* --Most recent ice scour (IS), also the best estimate for TS in that area. Gas in the shallow sediment results in acoustic wipeouts that obscure deeper reflectors.

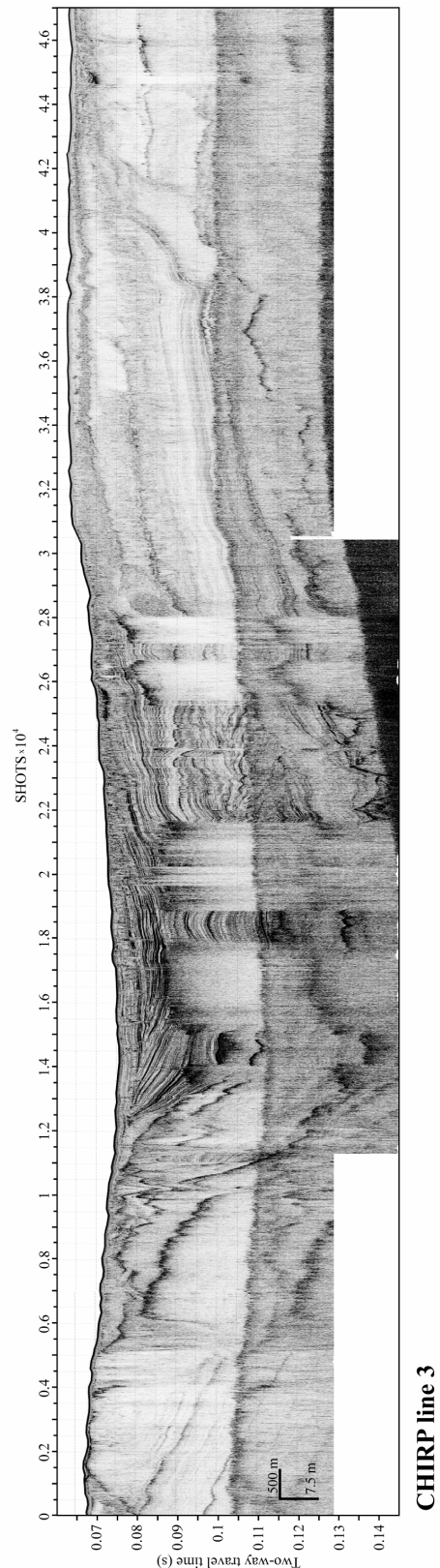
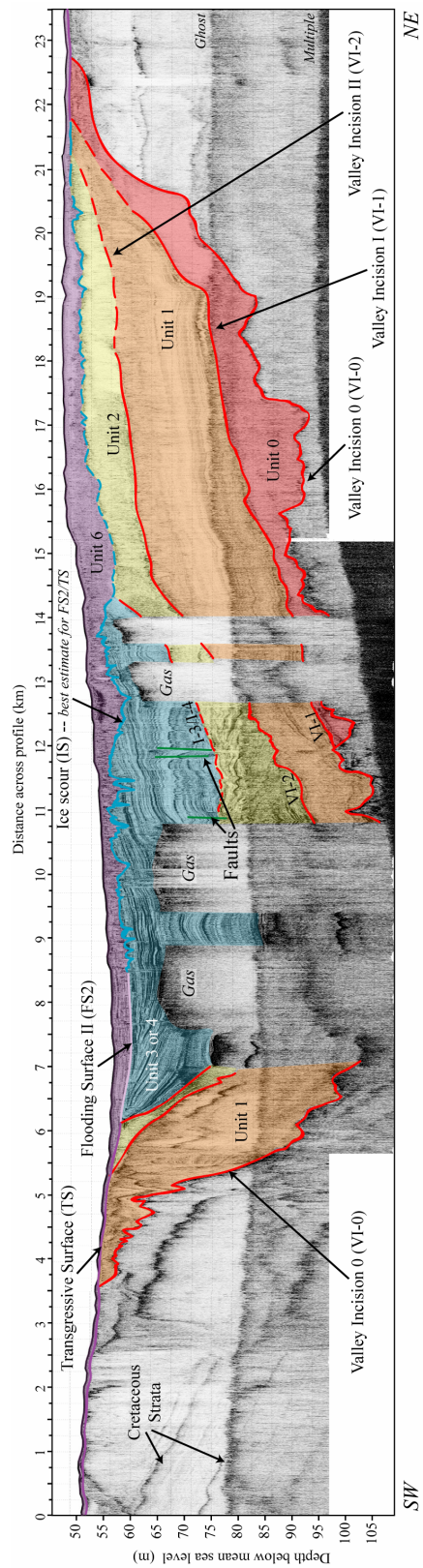
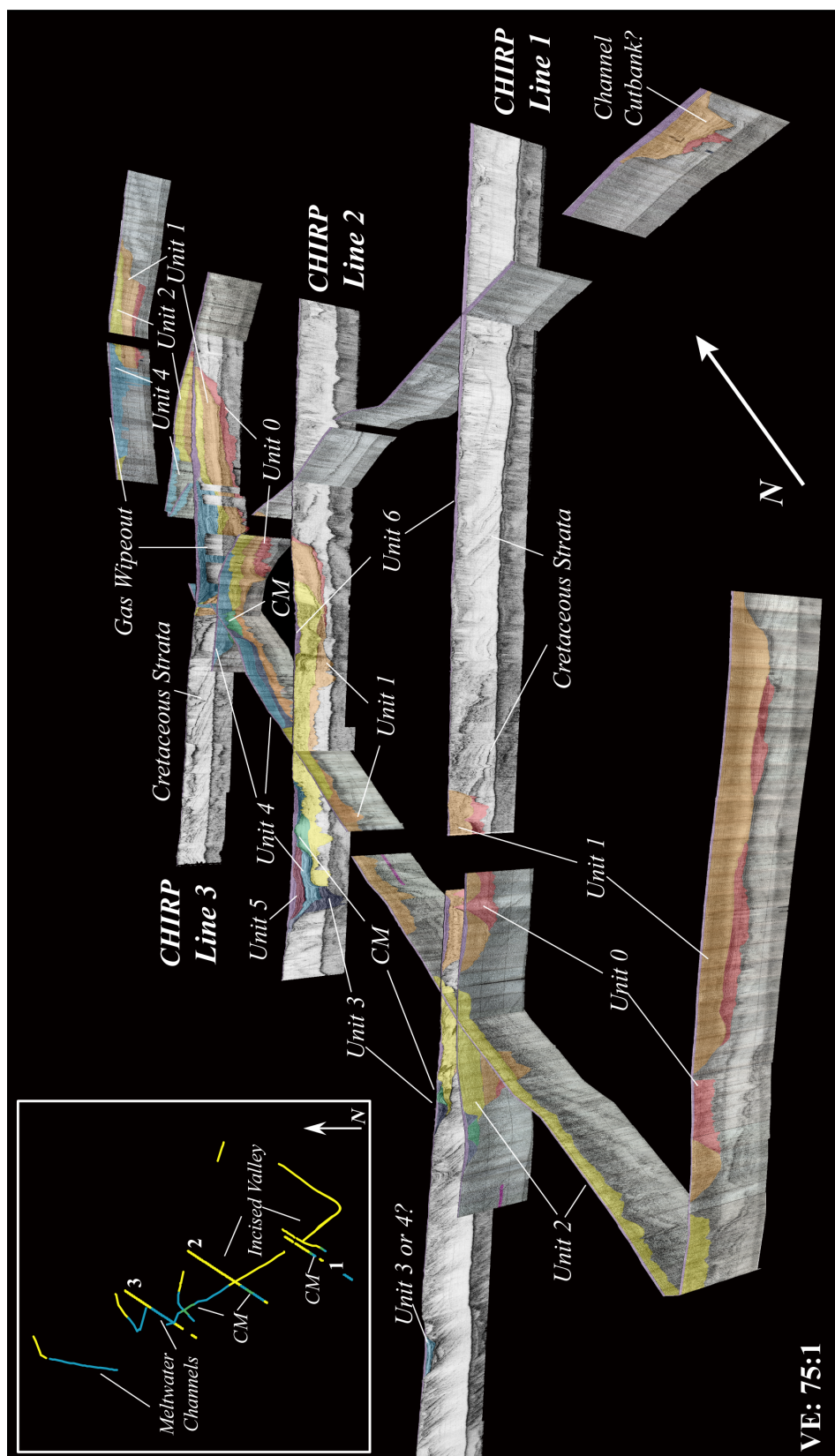


Figure 5.8 3-D perspective view of CHIRP and boomer subbottom profiles across the incised valley region, looking offshore. There is a strong correlation of units across the valley. The incised valley is continuous across 90 km on the shelf and is cut into steeply dipping, folded and faulted Cretaceous strata. **Inset:** Channel map, see Figure 3 for reference.



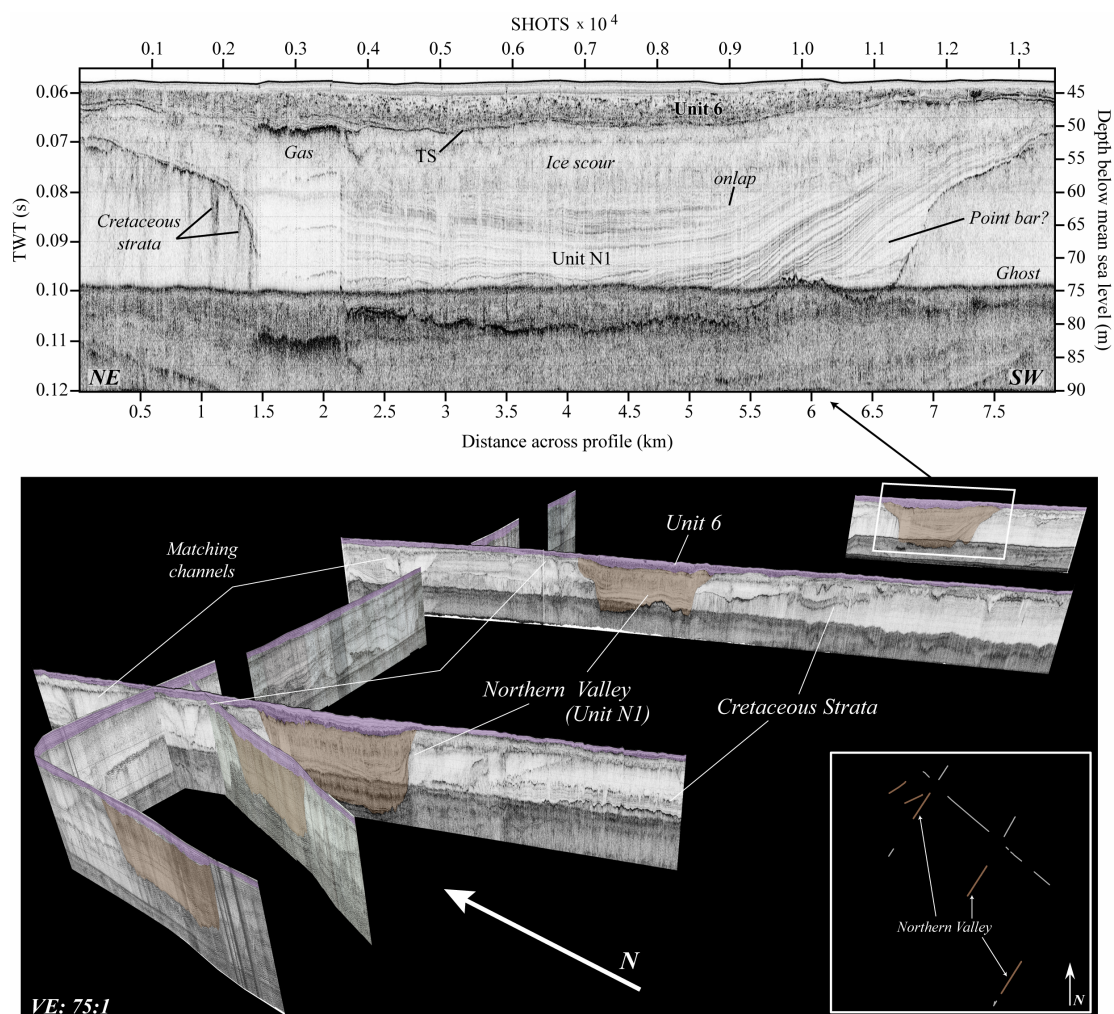


Figure 5.9 Bottom: 3-D perspective view of CHIRP and boomer subbottom profiles across the northern valley region, looking onshore. In addition to the large northern channel (shown in brown), several other channels can be correlated. **Inset:** Channel map, see Figure 5.3 for reference. **Top:** CHIRP subbottom profile across the northern valley. Possible fluvial fill in the base of the valley grades upward to marine sediment that onlaps the underlying topography. The valley is overlain by marine sediment of unit 6, observed across the shelf.

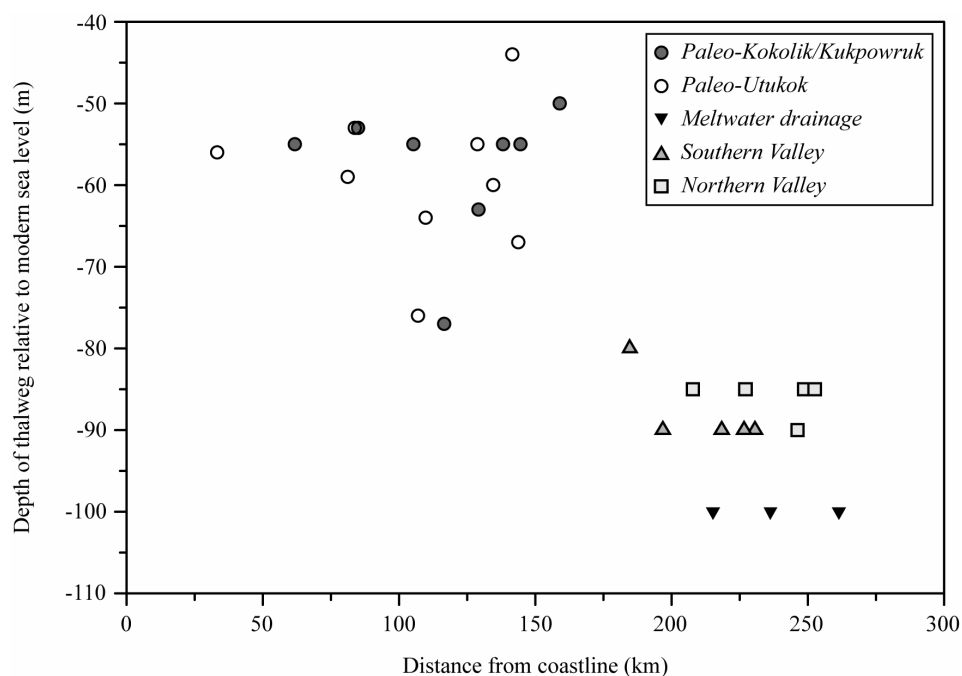


Figure 5.10 Plot showing the base of paleochannel (or valley) thalwegs relative to modern sea level versus distance from the coastline. Most of the drainage on the inner shelf has a channel base around ~55m below modern sea level, while the northern and southern incised valleys are much deeper, at ~85-100 m below modern sea level. This evidence suggests there may be a knickpoint on the midshelf such that the incised valleys were undergoing headward retrogressive erosion.

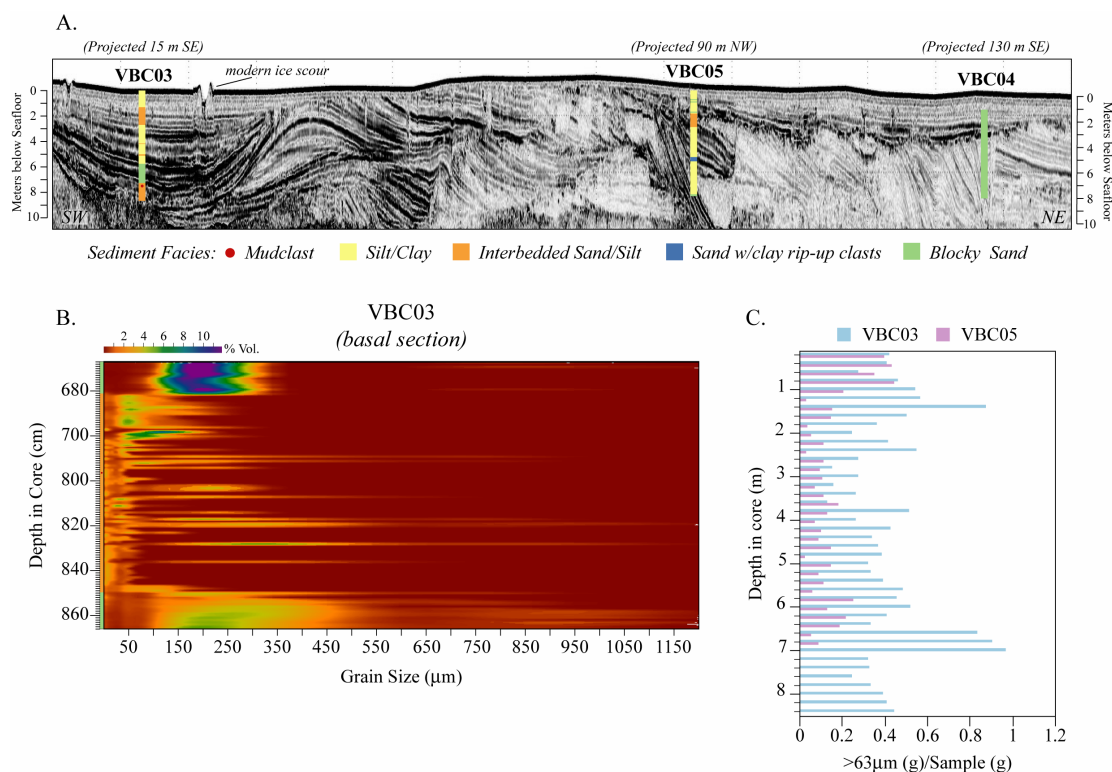
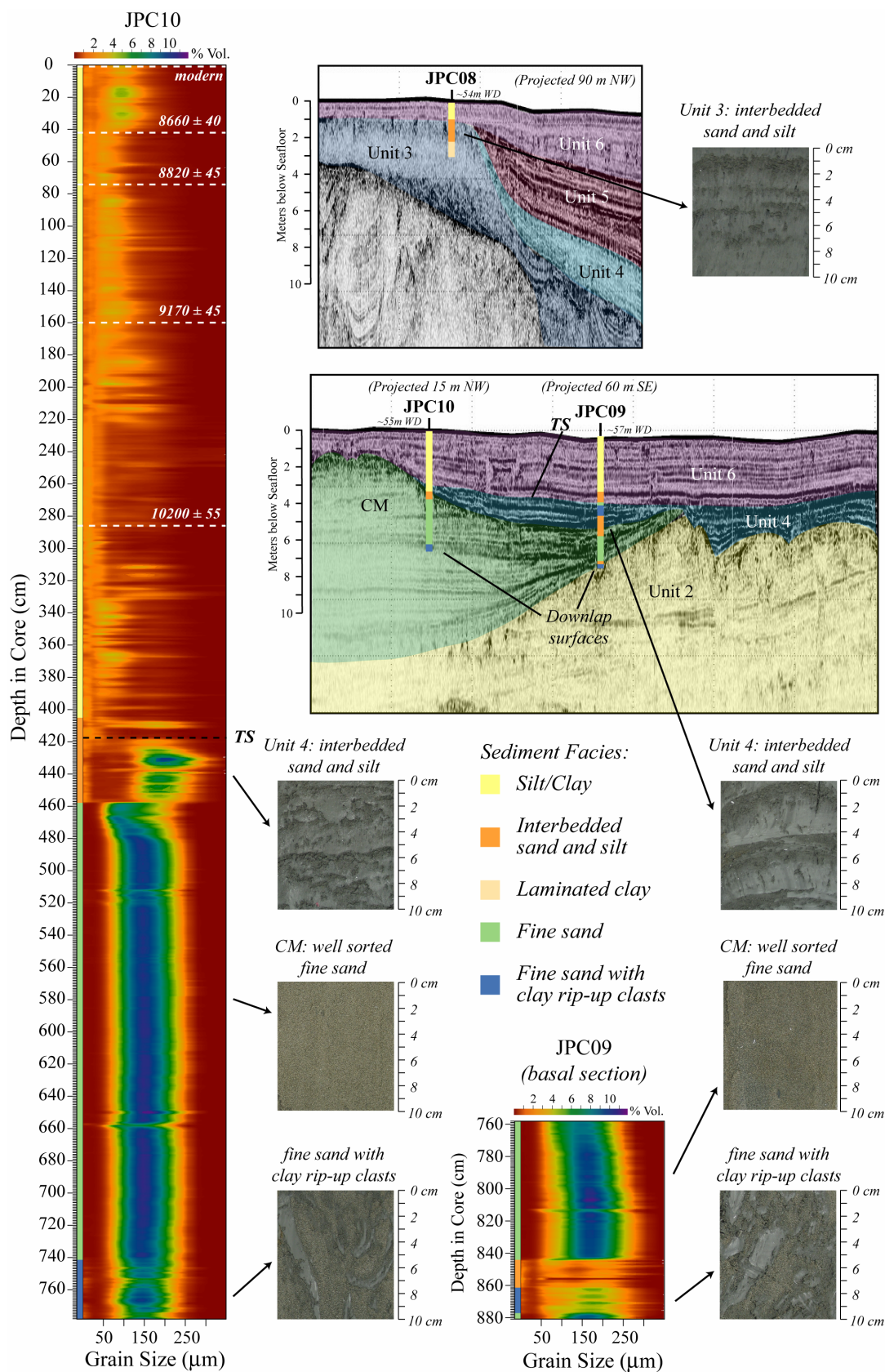


Figure 5.11 *a.* Sediment facies of vibracores in southern incised valley coregistered with CHIRP subbottom data. *Articulated bivalve mollusk ($12,300 \pm 65$ ^{14}C yrs. BP) was recovered from same depth (7.42 m) as the dropstone in VBC03. Note: The upper ~1 m of VBC04 is absent. *b.* Contour plot of grain size versus depth showing percent volume for 1 cm sampling of the basal section of VBC03. *c.* Comparison plot of $> 63 \mu\text{m}$ size fraction versus depth showing weight percent for 20 cm sampling of VBC03 and VBC05. Note the two cores show similar amounts of coarse fraction in the upper meter, where both cores collected Unit 6 sediment. Below this level, the grain size distributions diverge as VBC03 recovered Unit 3, while VBC05 recovered Unit 2

Figure 5.12 Sedimentary facies of piston cores in southern incised valley coregistered with CHIRP subbottom data. Contour plots of grain size versus depth showing percent volume for 1 cm sampling analysis are shown for JPC 10 and the basal section of JPC09. Radiocarbon dates from articulated bivalve mollusks in JPC10 are shown on the grain size plot. Both JPC09 and JPC10 have a similar stratigraphy of well sorted, fine sand with silty clay rip-up clasts in the base, grading upward into interbedded sand and silty clay, with marine clay at the top.



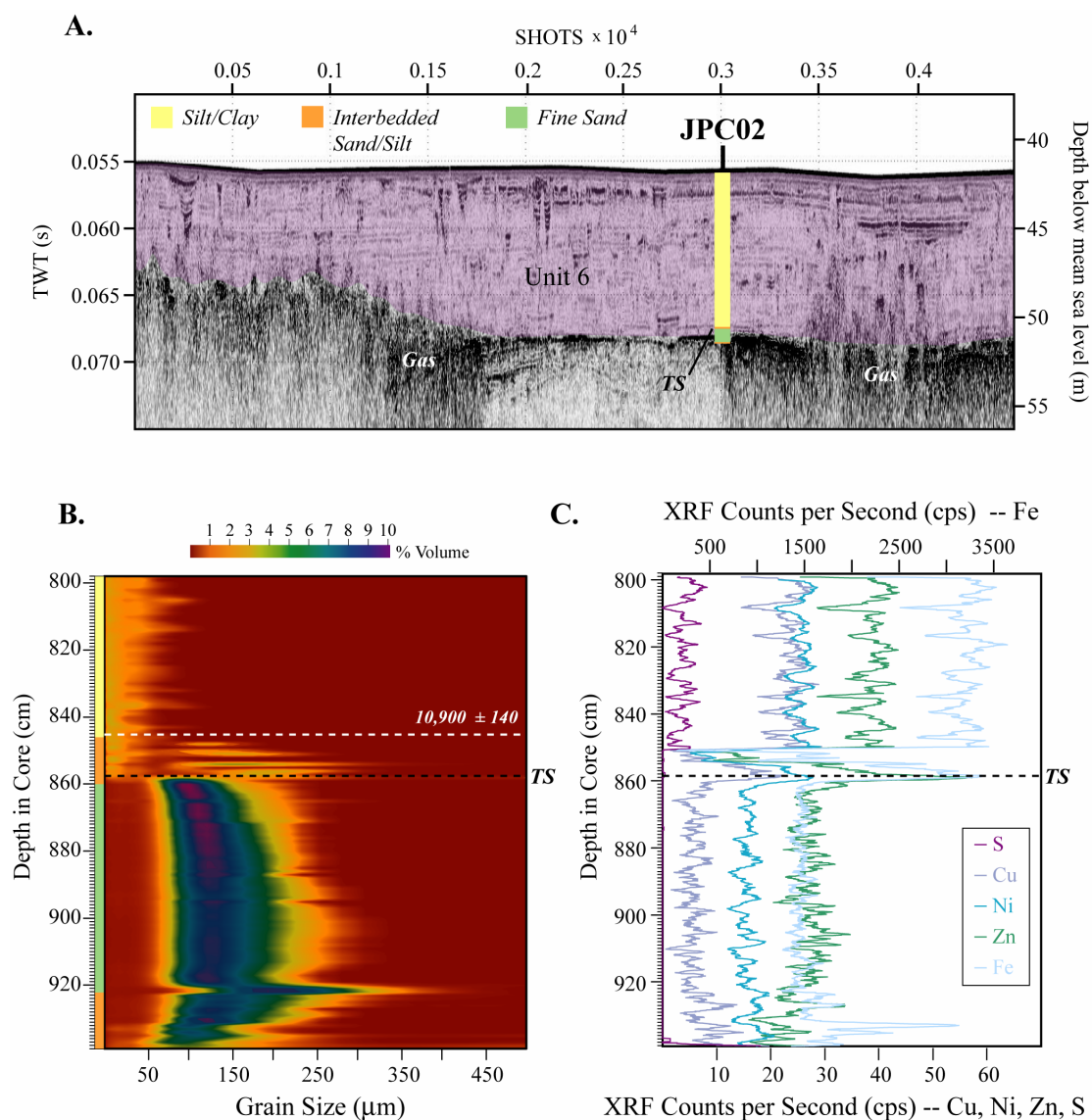


Figure 5.13 *a.* Sedimentary facies of piston core JPC02 in Hope Valley, coregistered with CHIRP subbottom data (line 10). *b.* Contour plot of grain size versus depth showing percent volume for 1 cm sampling analysis of basal section. *c.* X-ray fluorescence (XRF) analysis for basal section showing counts of Cu, Ni, Zn, S and Fe. Note the distinct change in both grain size and sediment composition at the transgressive surface (TS).

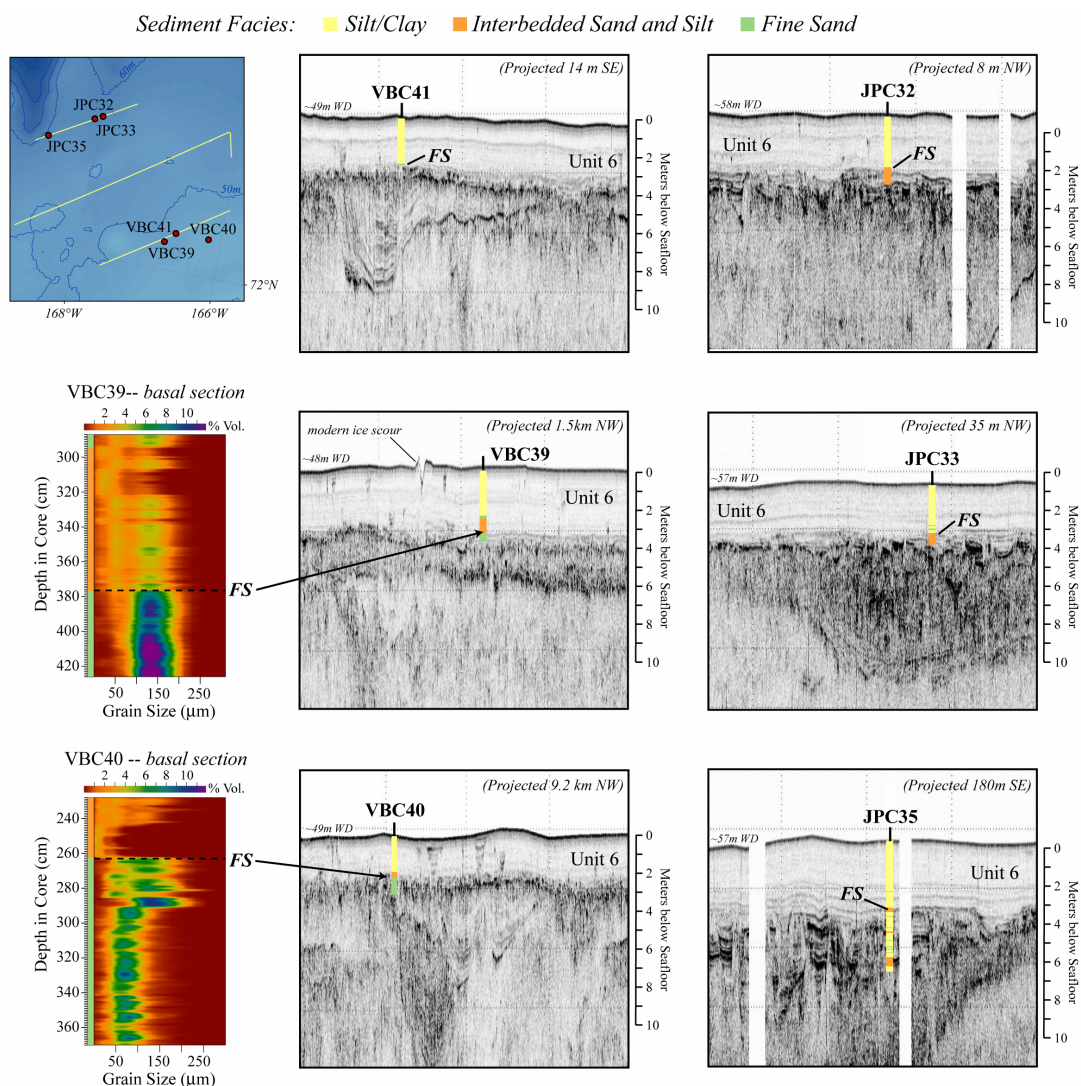


Figure 5.14 Sedimentary facies of mid/outer shelf vibracores. All of these cores exhibit a prominent flooding surface (FS) that is marked by a shift from sand or interbedded sand/silt to silt. Contour plots of grain size versus depth showing percent volume for 1 cm sampling analysis are shown for the basal sections of VBC39 and VBC40. Both cores show a distinct coarse-grained flooding surface that grades upward into marine clay. The core positions have been projected onto the profiles as noted.

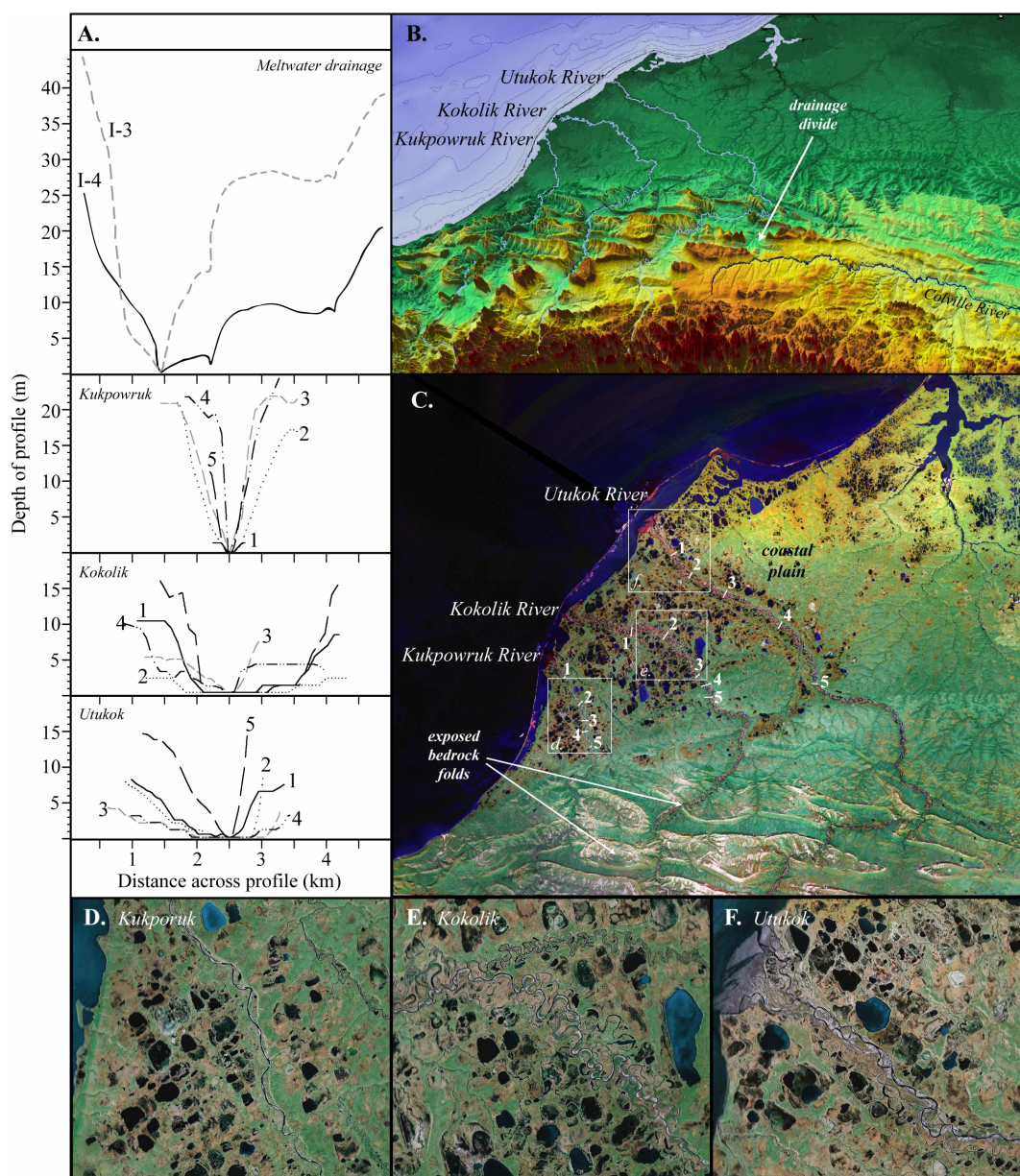
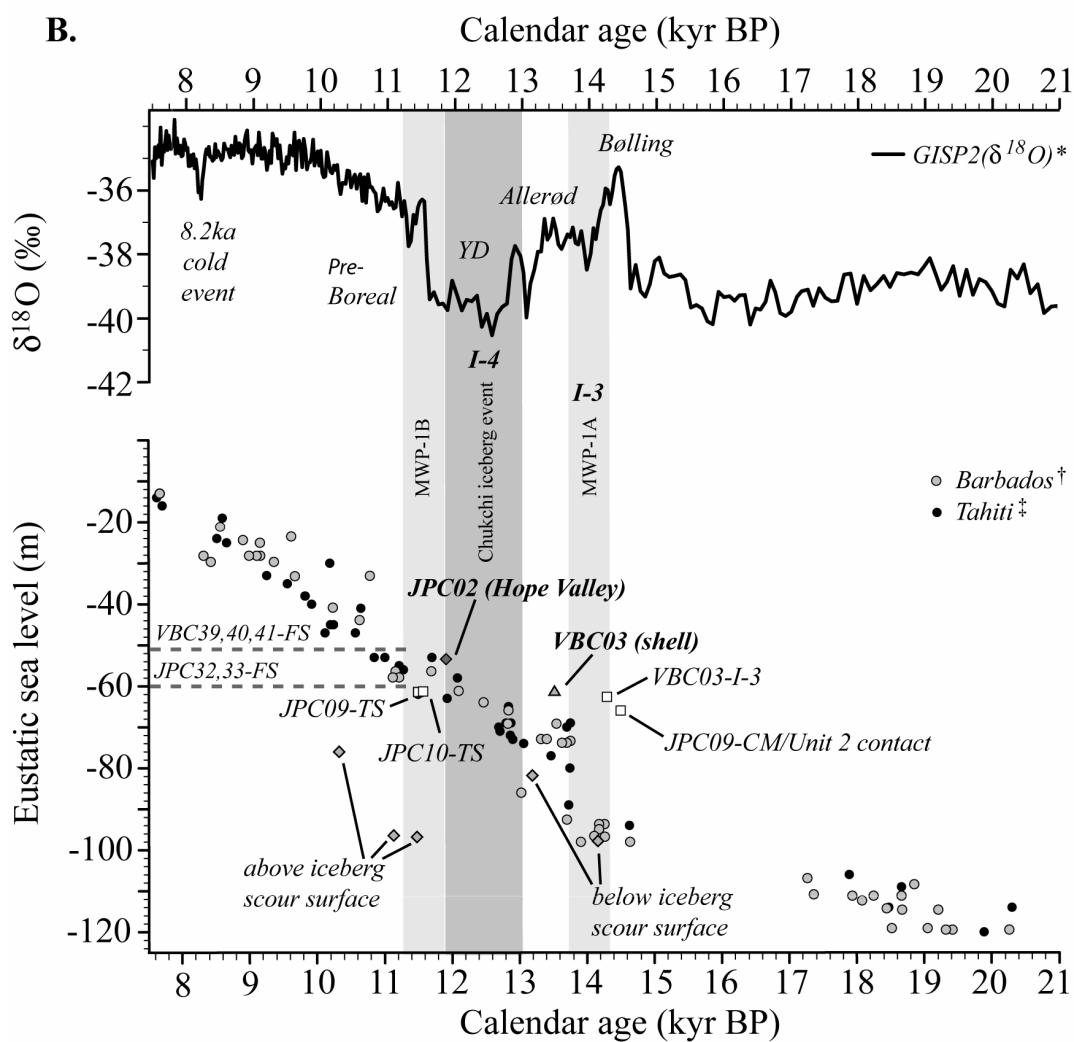
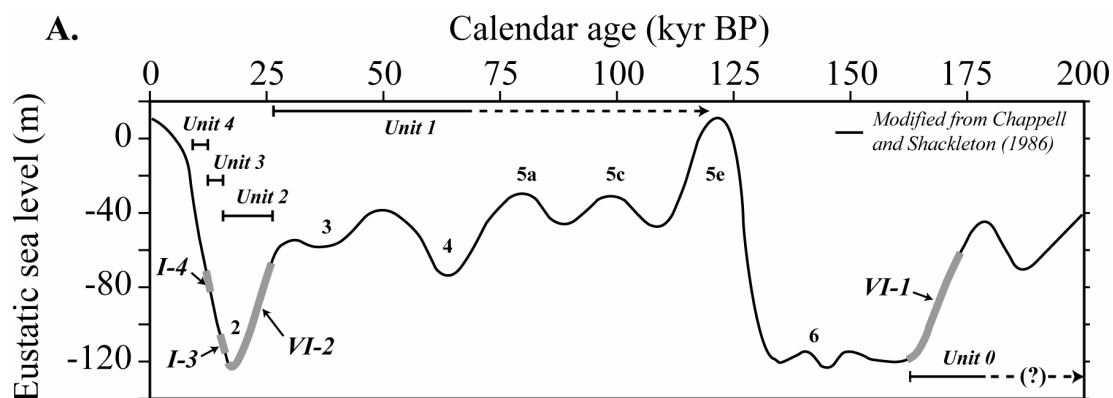


Figure 5.15 *a.* Profiles across the I-3 and I-4 reflectors compared with floodplain profiles across the three dominant northwestern Alaskan rivers inferred to connect with the midshelf valley. The river profiles were measured from a 100 m resolution DEM of northern Alaska (Manley, 2001). Note the meltwater channels/valleys are much wider and more deeply incised than the corresponding valleys onshore. *b.* 3-D perspective view of the topography in northwestern Alaska. The northward flowing trellis drainage incises the east-west trending fold belt of the Brooks Range foothills. *c.* Satellite imagery of northern Alaska showing river profile locations. *d.*, *e.*, *f.* Satellite imagery of the northwestern rivers on the coastal plain, showing meandering morphology and broad floodplains within the incised valleys.

Figure 5.16 *a.* Eustatic sea level curve and associated Marine Isotope Stages (MIS) modified from *Chappell and Shackleton* (1986). Suggested timing of the incised valley erosional surfaces and seismic facies are shown in relation to eustatic sea level. We interpret VI-2 and VI-1 to correlate with sea level lowering associated with MIS 2 and MIS 6, respectively, while VI-0 must be older. I-3 and I-4 appear to have been downcut during a period of sea level rise following the LGM. *b.* Climate and sea level records for the last 21 ka. Top: Greenland Ice Sheet Project (GISP) II oxygen isotope record (*Stuiver and Grootes*, 2000). More positive values indicate warmer temperatures; several climate periods are noted; YD—Younger Dryas. Bottom: Sea level history reconstructed from corals collected in Tahiti (*Bard, et al.*, 1996) and Barbados (*Fairbanks*, 1990) plotted along with new Chukchi data. Dates from JPC02 (Hope Valley FS) and VBC03 (shell), as well as the iceberg scour surface dates are calibrated ^{14}C -based ages. Points from JPC09, JPC10, and VBC03 are extrapolated from ^{14}C dates in JPC10, using the sedimentation rate of 1.5 m/kyr. Diamonds indicate radiocarbon dates from benthic foraminifera; triangles indicate radiocarbon dates from articulated bivalves; squares indicate dates extrapolated using the sedimentation rate from JPC10. Data presented here suggest incisions I-3 and I-4, which are interpreted to represent meltwater discharge, may correlate with Meltwater Pulse 1-A (MWP 1-A) and the Chukchi iceberg event, respectively. The iceberg scour surface on the outer Chukchi shelf is constrained to $\sim 11,000$ ^{14}C yrs BP ($\sim 12,080$ Cal. yrs. BP), following a warm period at the onset of the Younger Dryas (*Hill and Driscoll*, in prep). The regional transgressive surface (TS) appears to correlate with Meltwater Pulse 1-B.



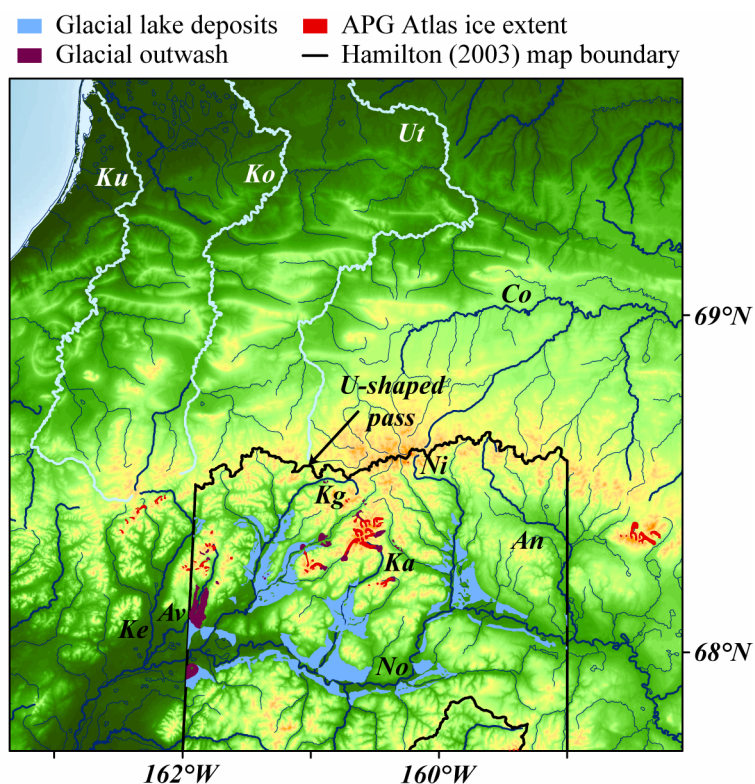


Figure 5.17 Map of western Brooks Range showing the mapped extent of Glacial Lake Noatak deposits from the LGM (*Hamilton, 2003*; the thick black line denotes the map boundaries). Also shown is the Alaska Paleoglacier Atlas LGM age ice extent for the region. The thick black line denotes the boundary of the *Hamilton (2003)* map. Note the close proximity of the Glacial Lake Noatak to the headwaters of the northwestern rivers. Abbreviations are as follows: Ku—Kukpowruk River, Ko—Kokolik River, Ut—Utukok River, Co—Colville River, Ke—Kelly River, Av—Avan River, Ka—Kaluktavik River, Ni—Nimiutuk River, An—Anisak River.

References

- Aagaard, K. and Carmack, E., 1989. The role of sea ice and other fresh water in the Arctic circulation. *Journal of Geophysical Research*, 94: 14,485-14,498.
- Barber, D. C., Dyke, A., Hillaire-Marcel, C., Jennings, A. E., Andrews, J. T., Kerwin, M. W., Bilodeau, G., McNeely, R., Southon, J., Morehead, M. D. and Gagnon, J.-M., 1999. Forcing of the cold event of 8,200 years ago by catastrophic drainage of Laurentide lakes. *Nature*, 400: 344-348.
- Barber, V. A. and Finney, B. P., 2000. Late Quaternary paleoclimatic reconstructions for interior Alaska based on paleolake-level data and hydrologic models. *Journal of Paleolimnology*, 24: 29-41.
- Bard, E., Hamelin, B., Arnold, M., Montaggioni, L., Cabioch, G., Faure, G. and Rougerie, F., 1996. Deglacial sea level record from Tahiti corals and the timing of global meltwater discharge. *Nature*, 382: 241-244.
- Bretz, J. H., 1969. The Lake Missoula floods and the Channeled Scabland. *Journal of Geology*, 77: 505-543.
- Brigham-Grette, J., 2001. New perspectives on Beringian Quaternary paleogeography, stratigraphy and glacial history. *Quaternary Science Reviews*, 20: 15-24.
- Brigham-Grette, J., Lozhkin, A. V., Anderson, P. M. and Glushkova, O. Y., 2004. Paleoenvironmental conditions in western Beringia before and during the Last Glacial Maximum, In: Madsen, D. B. (Ed.), *Entering America: Northeast Asia and Beringia before the Last Glacial Maximum*, Salt Lake City: University of Utah Press, pp. 29-61.
- Cassavant, R. R. and Miller, S. R., 2002. Tectonic geomorphic characterization of a transcurrent fault zone, western Brooks Range, Alaska. *AAPG Bulletin*, 86: 1139.
- Chappell, J. and Shackleton, N. J., 1986. Oxygen isotopes and sea level. *Nature*, 324: 137-140.
- Childers, J. M., Kernodle, D. R. and Loeffler, R. M., 1979. *Hydrologic reconnaissance of western Arctic Alaska, 1976 and 1977*. U.S. Geological Survey Open-File Report 79-699.
- Christie-Blick, N. and Driscoll, N. W., 1995. Sequence Stratigraphy. *Annual Review of Earth and Planetary Sciences*, 25: 451-478.

- Cohen, J. K. and Stockwell Jr., J. W., 1999. *CWP/SU: Seismic Unix Release 33: a free package for seismic research and processing*. Center for Wave Phenomena, Colorado School of Mines.
- Cook, M. S., Keigwin, L. D. and Sancetta, C. A., 2005. The deglacial history of surface and intermediate water of the Bering Sea. *Deep Sea Research II*, 52: 2163-2173.
- Dalrymple, R. W., Boyd, R. and Zaitlin, B. A., 1994. Incised-valley systems: Origin and sedimentary sequences. Society for Sedimentary Geology Special Publication 51, 391 p.
- Donnelly, J. P., Driscoll, N. W., Uchupi, E. A., Keigwin, L. D., Schwab, W. C., Thiel, E. R. and Swift, S. A., 2005. Catastrophic meltwater discharge down the Hudson Valley: A potential trigger for the Intra-Allerød cold period. *Geology*, 33: 89-92.
- Edwards, M. E., Mock, C. J., Finney, B. P., Barber, V. A. and Bartlein, P. J., 2001. Potential analogues for paleoclimatic variations in eastern interior Alaska during the past 14,000 yr: atmospheric-circulation controls of regional temperature and moisture response. *Quaternary Science Reviews*, 20: 189-202.
- Fairbanks, R. G., 1989. A 17,000-year glacio-eustatic sea level record; influence of glacial melting rates on the Younger Dryas event and deep-ocean circulation. *Nature*, 342: 637-642.
- Fairbanks, R. G., 1990. The age and origin of the "Younger Dryas climate event" in Greenland ice cores. *Paleoceanography*, 5: 937-948.
- Fairbanks, R. G., Mortlock, R. A., Tzu-Chien, C., Cao, L., Kaplan, A., Guilderson, T., Fairbanks, T. W. and Bloom, A. L., 2005. Marine Radiocarbon Calibration Curve Spanning 0 to 50,000 Years B.P. Based on Paired $^{230}\text{Th}/^{234}\text{U}/^{238}\text{U}$ and ^{14}C Dates on Pristine Corals. *Quaternary Science Reviews*, 24: 1781-1796.
- Grosswald, M. G. and Hughes, T. J., 2002. The Russian component of an Arctic ice sheet during the Last Glacial Maximum. *Quaternary Science Reviews*, 21: 121-146.
- Grosswald, M. G. and Hughes, T. J., 2004. Chlorine-36 and ^{14}C chronology support a limited last glacial maximum across central Chukotka, northeastern Siberia, and no Beringian ice sheet; discussion. *Quaternary Research*, 62: 223-226.

- Hamilton, T. D., 1982. A late Pleistocene glacial chronology for the southern Brooks Range: Stratigraphic record and regional significance. *GSA Bulletin*, 93: 700-716.
- Hamilton, T. D., 1986. Late Cenozoic glaciation of the central Brooks Range, In: Hamilton, T. D., K. M. Reed and R. M. Thorson (Eds.), *Glaciation in Alaska: The geologic record*, Alaska Geological Society, pp. 9-50.
- Hamilton, T. D., 2001. Quaternary, glacial, lacustrine, and fluvial interactions in the western Noatak Basin. *Quaternary Science Reviews*, 20: 371-391.
- Hamilton, T. D., 2003. *Surficial geologic map of parts of the Misheguk Mountain and Baird Mountain quadrangles, Noatak National Preserve, Alaska*. U.S. Geological Survey Open-File Report 03-367.
- Henkart, P., 2006. SIOSEIS. <http://sioseis.ucsd.edu>.
- Hill, J. C. and Driscoll, N. W., 2007. Evidence of iceberg armadas on the Chukchi Shelf during the Younger Dryas. *in prep*.
- Hill, J. C., Driscoll, N. W., Brigham-Grette, J., Donnelly, J. P., Gayes, P. T. and Keigwin, L. D., 2007. New evidence for high discharge to the Chukchi shelf during the Last Glacial Maximum. *Quaternary Research*, *in press*.
- Keigwin, L. D., Donnelly, J. P., Cook, M. S., Driscoll, N. W. and Brigham-Grette, J., 2006. Rapid sea-level rise and Holocene climate in the Chukchi Sea. *Geology*, 34: 861-864.
- Lamke, R. D., Brabets, T. P. and McIntire, J. A., 1995. *Hydrologic Unit Codes (HUC) for State of Alaska*. U.S. Geological Survey.
- Lundeen, Z., 2005. *Elemental and isotopic constraints on the late glacial-Holocene transgression and paleoceanography of the Chukchi Sea*. University of Massachusetts Amherst, M.S. Thesis.
- Manley, W. F., 2001. *Alaska North Slope 100 m Digital Elevation Model (DEM)*. National Snow and Ice Data Center, Boulder, CO. Digital media.
- Manley, W. F. and Kaufman, D. S., 2002. *Alaska PaleoGlacier Atlas, v. 1*. Institute of Arctic and Alpine Research (INSTAAR), University of Colorado http://instaar.colorado.edu/QGISL/ak_paleoglacier_atlas.
- McManus, D. A., Creager, J. S., Echols, R. J. and Holmes, M. L., 1983. The Holocene transgression of the flank of Beringia: Chukchi valley to Chukchi estuary to Chukchi Sea, In: Masters, P. M. and N. C. Flemming (Eds.),

Quaternary coastlines and marine archaeology: towards the prehistory of land bridges and continental shelves, London: Academic Press, pp. 365-388.

- Miley, J. M. and Barnes, P. W., 1986. *1985 Field Studies, Beaufort and Chukchi Seas, conducted from the NOAA Ship Discoverer*. U.S. Geological Survey Open-File Report 86-202.
- Mock, C. J. and Anderson, P. M., 1997. Some perspectives on the late Quaternary paleoclimate of Beringia. In: Isaacs, C. M. and V. L. Tharp (Eds.), *Proceedings of the thirteenth annual Pacific climate (PACLIM) workshop*.
- Moore, T. E., Dumitru, T. A., Adams, K. E., Witebsky, S. N. and Harris, A. G., 1994. Origin of the Lisburne Hills-Herald Arch structural belt: Stratigraphic, structural, and fission-track evidence from the Cape Lisburne area, northwestern Alaska, In: Miller, E. L., A. Grantz and S. L. Klemperer (Eds.), *Tectonic evolution of the Bering Shelf-Chukchi Sea-Arctic margin and adjacent landmasses*, Geological Society of America Special Paper 360, pp. 77-109.
- Moore, T. E., Wallace, W. K., Bird, K. J., Karl, S. M., Mull, C. G. and Dillon, J. T., 2002. Geology of northern Alaska, In: Pflaker, G. and H. C. Berg (Eds.), *The Geology of Alaska*, Boulder: Geological Society of America, pp. 49-140.
- Normark, W. R. and Reid, J. A., 1998. Extensive deposits on the Pacific plate from late Pleistocene North American glacial lake outbursts. *Journal of Geology*, 111: 617-637.
- Phillips, R. L., Pickthorn, L. G. and Rearic, D. M., 1987. Late Cretaceous sediments form the northeast Chukchi Sea, In: Galloway, J. P. and T. D. Hamilton (Eds.), *Geologic studies in Alaska by the U.S. Geological Survey during 1987*, U.S. Geological Survey Circular 1016, pp. 187-189.
- Phillips, R. L., Barnes, P., Huner, R. E., Reiss, T. E. and Rearic, D. M., 1988. *Geologic investigations in the Chukchi Sea, 1984, NOAA ship SURVEYOR cruise*. U.S. Geological Survey Open-File Report 88-25.
- Sable, E. G., Dutro, J. T., Mangus, M. D. and Morris, R. H., 1981. *Geology of the Kukpowruk-Nuka region, northwestern Alaska*. U.S. Geological Survey Open-File Report 81-1078.
- Schumm, S. A., Mosley, M. P. and Weaver, W. E., 1987. *Experimental fluvial geomorphology*, New York: Wiley, 413 p.

- Smith, L. M., Miller, G. H., Otto-Bliesner, B. and Shin, S.-I., 2003. Sensitivity of the Northern Hemisphere climate system to extreme changes in Holocene Arctic sea ice. *Quaternary Science Reviews*, 22: 645-658.
- Stanley, D. J. and Warne, A. G., 1994. Worldwide initiation of Holocene marine deltas by deceleration of sea-level rise. *Science*, 265: 228-231.
- Stuiver, M. and Grootes, P. M., 2000. GISP2 oxygen isotope ratios. *Quaternary Research*, 53: 277-284.
- Thurston, D. K. and Theiss, L. A., 1987. *Geologic report for the Chukchi Sea planning area, Alaska*. U.S. Department of the Interior Minerals Management Service OCS Report MMS 87-0046.
- Tolson, R. B., 1987. Structure and stratigraphy of the Hope Basin, southern Chukchi Sea, Alaska, In: Scholl, D. W., A. Grantz and J. G. Vedder (Eds.), *Geology and resource potential of the continental margin of western North America and adjacent ocean basins, Beaufort Sea to Baja California*, pp. 59-71.
- Uchupi, E., Driscoll, N., Ballard, R. D. and Bolmer, S. T., 2001. Drainage of late Wisconsin glacial lakes and the morphology and late quaternary stratigraphy of the New Jersey-southern New England continental shelf and slope. *Marine Geology*, 172: 117-145.
- Zweck, C. and Huybrechts, P., 2005. Modelling of the northern hemisphere ice sheets during the last glacial cycle and glaciological sensitivity. *Journal of Geophysical Research*, 110: doi:10.1029/2004JD005489.
- Van Wagoner, J. C., Mitchum, R. M., Campion, K. C. and Rahmanian, V. D., 1990. *Siliciclastic sequence stratigraphy in well logs, cores and outcrops: Concepts for high-resolution correlation of time and facies*, Tulsa: American Association of Petroleum Geologists, 55 p.
- Zaitlin, B. A., Dalrymple, R. W. and Boyd, R., 1994. The stratigraphic organization of incised-valley systems associated with relative sea-level changes, In: Dalrymple, R. W., R. Boyd and B. A. Zaitlin (Eds.), *Incised-valley systems: Origin and sedimentary sequences*, Tulsa: Society for Sedimentary Geology Special Publication 51, pp. 45-59.
- Zuffa, G. G., Normark, W. R., Serra, F. and Bruner, C. A., 2000. Turbidite Megabeds in an Oceanic Rift Valley Recording Jökulhaups of Late Pleistocene Glacial Lakes of the Western United States. *Journal of Geology*, 108: 253-274.

Vail, P. R., 1987. Seismic stratigraphy interpretation utilizing sequence stratigraphy, In: Bally, A. W. (Ed.), *Atlas of seismic stratigraphy*, Tulsa: American Association of Petroleum Geologists, pp. 1-10.

Chapter 6

Conclusions

This dissertation has presented two distinct case studies with a focus on examining the role of climatic and sea level influences on continental margin stratigraphy and morphology. In general, research discussed here presents examples of how sea level fluctuations and climate variability affect sediment distribution, erosion, slope stability, fluvial morphology, discharge patterns, and shelf responses to glacial cycles.

6.1 U.S. Atlantic margin: Slope stability

CHIRP subbottom and side-scan sonar mapping along the outer shelf of the U.S. Atlantic margin have allowed us to address the question of slope stability at different stages of progression along continental margins. Large-scale elongated gas blowouts observed on the shelf-edge are believed to represent an initial phase of shelf-slope destabilization and present an ideal opportunity to examine the potential for submarine failure prior to slumping. Evidence of gas charged doming at the head of the Albemarle-Currituck slide to the south also poses intriguing questions about the role of gas in this late Pleistocene failure and/or whether the region may be recharging such that it may represent a precursor for gas expulsion.

The principle results of this study are summarized as follows:

1. There is a strong spatial correlation between trapped gas and lowstand shelf-edge delta deposits.
2. Methane expulsion on outer shelf of U.S. Atlantic margin may play an important role in controlling slope stability.

3. Increased methane availability along the margin may be related to climate fluctuations.

Gas on the margin appears to have been trapped beneath a shelf-edge delta a few tens of meters thick exhibiting internal stratal deformation indicative of progressive downslope creep. Gravitational forces create tensional stress along the shelf edge, focusing fluid flow along zones of weakness. Sand layers within the deltaic strata may serve as conduits for fluid flow, allowing gas-charged fluids to migrate upsection and updip along bedding planes, while the interbedded clay facies act as an impediment to gas migration. Shoreward of the shelf-edge delta gas appears to be freely venting, which suggests the deltaic strata play a critical role in trapping gas along the margin. The blowouts presumably occurred when gas pressure below the delta ultimately exceeded the overburden. The expulsion features appear to be relatively recent (i.e. post-LGM) and may represent incipient slope failure.

This study highlights the interplay between sea level and climate in contributing to shelf/slope instability. Deposition of shelf-edge deltas occurs during sea level lowstand, while the presence of gas on the margin may be linked to climatic cycles. Numerous lowstand deltas are present on the outer shelf of the U.S. Atlantic, many of which occur at the head of significant submarine failures. This correlation is commonly attributed to rapid sedimentation, undercompaction and oversteepening; however we suggest it may also be related to the abundance of gas along the margin. We have introduced a two phase slumping model whereby gas hydrate melting as a result of climatic fluctuations can destabilize margins. In the proposed model,

introduction of warmer bottom waters during interglacial periods is expected to shift the top of the gas hydrate stability zone downward and dissociate any hydrates above the new threshold, releasing free gas into the sediment. The free gas should migrate upslope where it may be capped by lowstand delta deposits and build sufficient overpressure to create a blowout. Should the shelf-edge blowouts lead to slope failure in the upper few tens of meters, subsequent depressurization of gas hydrates on the lower slope may lead to further destabilization.

Modeling and experimental results increasingly suggest influx of warmer waters across the top of the hydrate occurrence zone can lead to significant dissociation and possible slope failure (*Kennett, et al.*, 2000; *Sultan, et al.*, 2004; *Mienert, et al.*, 2005), yet further work is needed to fully investigate the role that climate and hydrate dissociation may play in margin stability.

6.2 Chukchi margin of Alaska: Drainage and sedimentation history

The low gradient of the Chukchi shelf makes it very sensitive to changes in relative sea level such that small fluctuations can produce large shoreline migrations. During glacial periods, when sea level is substantially lower than the present (e.g., 125 m lower during the LGM), the broad expanse of shelf between Alaska and Russia is exposed. This creates an excellent natural laboratory for studying the effects of changing sea level and climate on drainage patterns, sedimentation, and onshore-offshore interactions.

The principle results of this study are summarized as follows:

1. Multiple sea level lowering events have resulted in an extensive system of incised channels and valleys on the Chukchi shelf.
2. The paleodrainage system offshore indicates a more complex drainage history onshore than previously recognized
3. Global climate signals and sea level variations (e.g., Younger Dryas, Meltwater Pulse 1A and 1B) are represented in the drainage and sedimentation history of the Chukchi margin.
4. The presence of meltwater drainage on the shelf, along with evidence for iceberg armadas on the shelf during the Younger Dryas, suggests more climatic variability and a greater extent of continental glaciation in northern Alaska during the LGM than previously recognized.
5. In glacially dominated landscapes, major incision events may not be related to a drop in base level (i.e., are out of phase with sea level change)

The Arctic basin and surrounding shelves are critically important to the global climate system in terms of freshwater balance, sea ice albedo and general circulation patterns. Evidence presented here suggest events such as the Younger Dryas cooling and periods of rapid eustatic rise (i.e. Meltwater Pulse 1A and 1B) are represented in the morphology, sedimentation and drainage history of the Chukchi shelf. The climate signals from the shelf coincide with records from the Hope Valley and Chukchi Borderland regions (e.g., *Keigwin, et al.*, 2006; *Polyak, et al.*, 2007), all of

which highlight the critical importance spatial and temporal variability that result from the complex interplay of changes in relative sea level and local climatic forcing.

Chirp subbottom data imaged a series of extensive drainage systems across the mid to outer Chukchi shelf comprised of both individual channels and larger incised valleys with compound fill that records multiple sea level cycles. Most sequence stratigraphic models predict downcutting and incision in response to base-level change; however, in some cases, particularly glaciated environments, there appears to be a phase lag between incision and maximum sea level fall. The southern incised valley displays two distinct types of incision events. The first three valley incisions represent in phase incision, i.e. fluvial downcutting, during a period of relative sea level fall, and the infill here displays characteristic fluvial stratigraphy (e.g., cut and fill structures, cutbanks and point bars). In contrast, the two most recent incisions appear to have been downcut during the period of rapid sea level rise following the LGM, subsequently filled with estuarine or marine sediment, such that they represent out of phase incision. These two different types of incision suggest timing that is inconsistent with a simple sequence stratigraphic model based on relative sea level changes and highlight the importance of discharge and ice sheet dynamics in controlling shelf morphology in glaciated environments.

Sedimentation patterns on the shelf also appear somewhat out of phase with sea level cycles. Sequence stratigraphic models commonly predict decreased shelf sedimentation during sea level as more sediment is sequestered in nearshore environments due to backstepping shorelines, gradually increasing as the rate of sea level rise begins to slow and river deltas equilibrate and build out. Evidence from the

midshelf as well as the Hope Valley, however, suggests relatively high sedimentation rates during the rapid sea level rise following the most recent deglaciation, dropping off dramatically $\sim 7\text{ka}$. While this trend is the reverse of the model predictions, it is consistent with additional sediment inputs from glacial melting.

Drainage across the shelf appears structurally controlled as a result of uplift along two thrust fronts, the northern verging Brooks onshore and the northeast verging Herald offshore. Trending northwest along the axis of the Herald Arch, the southern valley appears strongly controlled by underlying topography and the tectonic framework of the Herald thrust belt. The southern valley exhibits a series of nested incisions that suggest flow was repeatedly directed along this preferential drainage pathway over multiple sea level cycles. Onshore, the Colville River flows axial parallel through the foreland basin of the Brooks Range, capturing most of the northern foothill drainage before discharging into the Beaufort Sea. The few small rivers that drain northwest to the Chukchi shelf from the Brooks Range flow parallel to the onshore extension of the Herald thrust front.

The research presented here concerning the offshore drainage history and iceberg discharge across the Chukchi shelf draws into question existing knowledge of the late Cenozoic history of the western Arctic Coastal Plain as well as the glacial history of the northwestern Brooks Range.

References

- Keigwin, L. D., Donnelly, J. P., Cook, M. S., Driscoll, N. W. and Brigham-Grette, J., 2006. Rapid sea-level rise and Holocene climate in the Chukchi Sea. *Geology*, 34: 861-864.
- Kennett, J. P., Cannariato, K. G., Hendy, I. L. and Behl, R. J., 2000. Carbon isotopic evidence for methane hydrate instability during Quaternary interstadials. *Science*, 288: 128-133.
- Mienert, J., Vanneste, M., Bünz, S., Andreassen, K., Haflidason, H. and Sejrup, H. P., 2005. Ocean warming and gas hydrate stability on the mid-Norwegian margin at the Storegga slide. *Marine and Petroleum Geology*, 22: 233-244.
- Polyak, L., Darby, D. A., Bischof, J. F. and Jakobsson, M., 2007. Stratigraphic constraints on late Pleistocene glacial erosion and deglaciation of the Chukchi margin, Arctic Ocean. *Quaternary Research*, 67: 234-245.
- Sultan, N., Cochonat, P., Foucher, J.-P. and Mienert, J., 2004. Effect of gas hydrates melting on seafloor slope instability. *Marine Geology*, 213: 279-401.

Appendix

**Active methane venting observed
at giant seafloor pockmarks along the
mid-Atlantic shelf break with the
Autonomous Underwater Vehicle SeaBED**

A.1 Abstract

Detailed near-bottom investigation of a series of giant, kilometer scale, elongate pockmarks on the edge of the mid-Atlantic continental shelf confirms that methane is actively venting at the site. Dissolved methane concentrations, measured with a METS methane sensor mounted on an autonomous underwater vehicle (AUV), are as high as 100 nM, values well above expected background levels for the open ocean. Sediment pore water geochemistry gives further evidence of methane advection through the seafloor. Isotopically light carbon in the dissolved methane samples indicates a biogenic source. The spatial distribution of the near-bottom methane anomalies, combined with water column salinity and temperature vertical profiles, indicate that methane-rich water is horizontally restricted, suggesting focused venting along the top of the pockmarks' walls with some advection and dispersion due to local currents. Focused methane venting is observed at a circular, smaller pockmark at the southern end of the study area. This observation is compatible with a scenario where the larger, elongate pockmarks are the result of coalescing smaller pockmarks.

A.2 Introduction

It is estimated that 6.6-19.5 Tg of methane per year are released from the marine environment into atmosphere, making natural gas seeps an important part of the global methane cycle (*Judd, et al., 2002*). Methane seeps can occur in a most marine environments (*Judd, 2003*) with seep characteristics ranging from diffuse seafloor venting to more focused escape (*Lonke, et al., 2004*). In addition to the

environmental significance, gas in marine sediments might hold possible geohazard and resource significance (e.g., *Sills and Wheeler*, 1992).

Pockmarks associated with the venting of gasses and fluids have become widely observed seafloor features since their first discovery by King and McLean (1970) offshore Nova Scotia (*Hovland and Judd*, 1988). The cross-sectional shape of these features varies from U-shaped and V-shaped seafloor depressions to truncated cones with steep, low angled or asymmetric walls; some are circular in plan view while others are elongate (*Dimitrov and Woodside*, 2002; *Hovland, et al.*, 2002). While most agree that pockmarks are the result of focused fluid flow (*Hovland, et al.*, 2002), the exact nature of venting remains poorly understood (*Paull, et al.*, 2002). Kelley, et al. (1994) suggest two models for pockmark formation: 1) organic matter deposited above an erosional surface decomposes, releasing gas that excavates the pockmark; once the excavation extends to the erosional surface, the pockmark spreads out laterally along the erosional surface, and 2) a catastrophic event such as an earthquake or tsunami reduces the confining pressure in the area, allowing gas and fluids to suddenly escape. The first model can explain why U-shaped, V-shaped and flat-floored pockmarks are observed and the later model why pockmark formation and increased methane venting have been documented to occur in response to earthquakes (*Hovland, et al.*, 2002; *Christodoulou, et al.*, 2003).

Using newly released gridded bathymetry from NOAA, several large, elongate, en echelon pockmarks were discovered at the edge of the Virginia/North Carolina continental shelf (Fig. 1) (*Driscoll, et al.*, 2000). While the usual scale of pockmarks ranges from a few meters to ~300 m in diameter and up to 25 m in relief

(*Christodoulou et al.*, 2003, *Çifçi, et al.*, 2003, *Dimitrov, et al.*, 2002), these shelf-edge features are several kilometers long, up to a kilometer across and 50 m in relief. Until these pockmarks were discovered, pockmarks that are 350 m in diameter and 35 m in relief were classified as “giant” (*Kelly, et al.*, 1994). These shelf-edge features were initially interpreted as small-offset normal faults diagnostic of some incipient slope failure (*Driscoll et al.*, 2000). However, further investigation in 2000 using sidescan sonar and high-resolution subbottom profiling (chirp) showed that these features are produced by gas seepage because abundant gas is imaged in the sedimentary section housing the giant pockmarks (Fig. 2) (*Hill et al.*, 2004). The authors propose a mechanism for formation of the pockmarks in which methane migrates upslope beneath the impermeable shelf edge delta, creating an overpressure that, combined with downslope creep, eventually leads to failure during which gas is expelled; Hill, et al. (2004) thus describe them as “gas blowouts.” This scenario implies a pockmark age younger than the last glacial maximum when the shelf edge delta presumably formed.

Based on these existing data, it is not clear whether gas continues to vent at this site since the development of the pockmarks and whether the gas is thermogenic or biogenic in origin. For example, pockmark fields recently mapped in Belfast Bay, ME and off shore Big Sur, CA show no sign of active venting (*Ussler, et al.*, 2003; *Paull, et al.*, 2002). The grid of chirp profiles collected during the 2000 study clearly document gas within the shallow sediment at the walls of the pockmarks (Fig. 2) (*Hill, et al.*, 2004). However, unlike what has been reported in some other regions (e.g., *Christodoulou, et al.*, 2003), gas bubble plumes have not been acoustically

imaged in the water column. No sampling was performed during the 2000 survey that would verify if gas venting is occurring.

In July 2004, we carried out a detailed survey of the giant pockmarks with the R/V Cape Hatteras to determine if methane is actively venting at these sites, and if so, to constrain the source of the gas and its fate in the water column. We collected cores, pore fluid, and water column samples for geochemical analysis to document the presence and nature of the gas discharge. We made in situ measurements of dissolved methane concentration in the pockmarks and surrounding areas using two emerging technologies, an Autonomous Underwater Vehicle (AUV) and a vehicle mounted underway METS methane sensor.

A.3 Data Acquisition

A.3.1 SeaBED AUV Missions

AUVs are now sophisticated enough that they can perform accurately geo-referenced, detailed, near-bottom surveys that were considered too expensive using remotely operated vehicles (ROVs) or manned submersibles (*Whitcomb, et al.*, 2000; *Singh, et al.*, 2004a). The AUV SeaBED (Fig. 3) was designed at the Woods Hole Oceanographic Institution for easy transport to remote locations as well as to be deployable from small ships of opportunity, both of which reduce operational costs and ease survey logistics (*Singh, et al.*, 2004a, b).

The SeaBED AUV completed 16 successful dives (out of 18 deployments) across the pockmarks during which the vehicle followed a pre-programmed track at a speed of approximately 0.5 m/s over ground while maintaining an altitude of 3 m \pm

0.1 m above the seafloor. The AUV made continuous, in situ measurements of the water properties in the pockmarks. A METS methane sensor, designed by Capsum Monitoring Technologies to measure in situ dissolved methane concentration, and a Seabird Fastcat CTD were mounted on the AUV. Water was simultaneously pumped into both instruments so that each was measuring the same water sample. Microbathymetric data and color photographs of the seafloor were also acquired continuously along track. Water property measurements were made approximately every second and photographs taken every 3 seconds. The interval between photographs was selected to ensure some overlap between frames so that continuous photomosaics could be constructed.

The shipboard Acoustic Doppler Current Profiler (ADCP) was used to determine the overall trend and strength of currents in the area, as needed for planning the AUV dives. Underway AUV navigation was based on compass readings on the vehicle and a vehicle mounted ADCP. Track navigation was adjusted after the completion of each dive using sonar ranging from the ship to the vehicle in conjunction with shipboard differential GPS. Further re-navigation, comparing AUV measured seafloor depth with the shipboard, GPS-navigated multibeam bathymetry, was needed because the vehicle's bottom-track velocity measurements included a component of the strong SSW shelf-edge current (*Eustice, et al., 2005*). This current is detected in the ADCP data (Fig. 4) and corresponds to the motion of the current that flows down the US east coast shelf edge (*Bumpus, 1973*).

A.3.2 Water and Sediment Sampling Program

Hydrocasts were deployed to collect water column samples. The Conductivity, Temperature and Depth (CTD) profiles during each descent of the hydrocast were used to identify optimal water sample collection depths during ascent. Collected water samples were immediately stored in nitrogen-purged 125 ml serum bottles, poisoned with mercuric chloride to halt any methane production and oxidation, and were later analyzed for dissolved hydrocarbon concentrations and methane $\delta^{13}\text{C}$. Methane concentrations were performed with a gas chromatograph equipped with a flame ionization detector (GC 8A, Shimadzu Corp.) and the $\delta^{13}\text{C}$ - CH_4 isotopic analyses were performed on a Finnigan MAT252 mass spectrometer with a GC1 interface at the University of Hawaii following the technique of Popp et al. (2005). The average percent precision of the methane concentration and $\delta^{13}\text{C}$ - CH_4 analyses are <3% and +/- 0.6‰, respectively. Other water column aliquots were analyzed shipboard for salinity and alkalinity and the rest preserved for shore-based analyses.

Sediment cores were collected throughout the survey site (Fig. 1). Approximately half of the cores were saved for sedimentology and stratigraphy. Selected cores were subsampled under anaerobic conditions and the pore water was extracted onboard using titanium squeezers. All pore water samples were filtered through 0.45 μm Gelman polysulfone filters to remove the remaining suspended silt and were immediately sub-sampled under anaerobic conditions for various shore-based analyses. Aliquots for major and minor element analyses were stored in acid-cleaned polypropylene centrifuge tubes and acidified with Optima nitric acid.

Dissolved inorganic carbon (DIC) samples were poisoned with a saturated mercuric chloride solution and stored in vacutainers. Sample aliquots for sulfate analyses were added to acid-cleaned polypropylene centrifuge tubes containing a 50% CdNO_3 solution to precipitate out the sulfide, thus leaving only sulfate in solution. Alkalinity and pH were immediately measured shipboard by Gran titration, and chloride concentrations were determined by titration with AgNO_3 . Sulfate concentrations were determined via ion chromatography (% precision $<0.6\%$), and $\delta^{13}\text{C}$ -DIC was measured on a ThermoFinnigan Delta XP Plus stable isotope ratio mass spectrometer with an average percent precision $<1.8\%$. Sediment sub-samples for pore water methane concentration and $\delta^{13}\text{C}$ isotope ratios were immediately taken after core recovery, stored in nitrogen-purged serum bottles, and preserved with a saturated mercuric chloride solution. Methane concentrations and carbon isotopic ratios were determined using the same techniques as described for the water column samples.

A.3.3 Multibeam Bathymetric Survey

In addition to the sampling program and the AUV missions, we acquired new, high-resolution swath bathymetry data (Figs. 1, 7). The area was previously mapped in 1990 by NOAA (www.ngdc.noaa.gov/mgg/bathymetry/hydro.html) using a 36 kHz Hydrochart II multibeam bathymetric system which provided a horizontal resolution of about 90 m. GPS navigation at that time was discontinuous, and the resulting bathymetric map displayed some navigation artifact. Precise navigation of the AUV required maps of greater accuracy, so a pole-mounted SeaBeam/ELAC multibeam system was leased to produce a new, higher resolution map of the pockmarks. The

multibeam system operates at 180 kHz with a swath width of 153° and 126 beams per ping. Velocity profiles used for processing the multibeam data were calculated from daily casts of expendable bathythermographs (XBTs).

A.4 Results

A.4.1 New Multibeam Bathymetric Map

The new bathymetric map (Figs. 1, 7) is of higher resolution than the existing NOAA map and also filled in small data gaps. The higher sonar frequency and the dense across track spatial sampling allowed us to produce a map with a grid spacing of 8 m. Although the giant pockmarks were well imaged with the less dense grid spacing, the higher resolution map yields more accurate information in steeper terrain. In particular, it highlights the striking linearity of the landward pockmark walls.

A.4.2 AUV Along Track Data

The METS sensor, mounted on the SeaBED AUV, routinely detected methane concentration anomalies. Furthermore, along track time series exhibit a systematic negative correlation between dissolved methane concentration and temperature and salinity (Fig. 5). However, a significant time lag exists in the METS sensor response. At places where strong gradients in salinity and temperature occur, indicating a change in water masses, dissolved methane concentrations grow or decay over a ~15 minute period and plateau until a similar strong salinity and temperature gradient is encountered. This pattern suggests that the methane concentration values are affected

by some measurement artifacts and we have devised a method to correct for the instrument response (see Appendix). After correction, the resulting dissolved methane concentration data mirror that of salinity and temperature, increasing when salinity and temperature decrease (Figs. 5, 6). Additionally, we observe a correlation between methane concentrations and bathymetry where methane anomalies are all located at depths shallower than 130 m, which correspond to the upper walls of the pockmarks and the adjacent shelf edge (Figs. 6, 7).

Dissolved methane concentrations also vary temporally. The data from the first three AUV dives show generally high methane concentrations throughout the deployments. Two storms occurred during the early part of the cruise, before dive 4 and before dive 9. Immediately after the second storm, methane concentrations dropped to very low levels for the next three dives. During the remainder of the AUV dives the average background methane concentration increased slowly with time after the storms. This is demonstrated by crossover errors in relative methane concentration between the data collected recently after the storm and those collected near the end of the survey (Fig. 6b).

Inspection of the 44,000 photos collected by the AUV do not show the faunal or bacterial communities typical of cold seeps (e.g., *Hovland and Judd, 1988; Sibuet and Olu, 1998*). Instead, seafloor sediment texture varies from mud to gravel, and the commonly observed fauna include fish (such as skate and chain dogfish), starfish and anemones. Hence, if cold seeps were present within the study area, their lateral extent must be less than the average spacing of the AUV tracks (50 meters to a few hundred meters).

A.4.3 Spatial Distribution of Methane Anomalies

Instead of interpreting the temporally varying absolute methane concentrations, we grouped methane anomalies into three categories: background concentration, high concentration and intermediate concentration (Fig. 6). Background concentration is defined as the average low concentration for each dive (usually <10 nM). High concentration areas display distinct methane anomalies well above background (>50 nM) and are characterized by a steep along-track gradient at either end. Areas identified as intermediate concentration have dissolved methane concentrations that are higher than background, but are either lower than areas identified as high concentration, are slowly increasing or decreasing along-track, or are fluctuating.

Figure 7 displays the spatial distribution of methane anomalies according to the above categories. It includes 13 SeaBED dives that we evaluated to be the most consistent and reliable of the successful deployments on the basis of cross-over errors at track intersections. The northern part of the survey area (Fig. 7a) shows high methane on the landward walls of the pockmarks and on the shelf landward of the pockmarks with no methane on the floors of the pockmarks. The southern pockmarks (Fig. 7c) show a similar pattern, but the smallest, circular pockmark appears to have little or no methane to the north and west of it and a streak of elevated methane concentration extending from its southern wall toward the southeast. The middle section of the survey (Fig. 7b) is the most complex and the most densely sampled. High methane is observed along the western walls of the pockmarks and continues along the shelf to the west. Elevated methane is observed at the bathymetric highs

along the eastern edges of the pockmarks. All dives, except dive 4, show little to no methane venting at the floors of the pockmarks. Dive 4, one of the earliest dives, is anomalous and displays high methane throughout most of the deployments, even along the floor of the pockmark; low methane concentration is only observed down the continental slope, outside of the pockmark at depths greater than 160 m. Dives 5 and 8 were not plotted because the corrected methane concentrations appear too internally inconsistent within the deployments: methane concentrations change only when the vehicle begins to travel down slope suggesting that other factors, such as the vehicle's response to the changing bathymetry may also affect measurements. Dive 1 displays higher dissolved methane concentrations compared to all the other dives and was omitted due to inability to separate the data into the three previously mentioned classifications and because the dissolved methane concentration, salinity and temperature correlation is less robust. This pattern might be due to initial calibration issues.

A.4.4 Dissolved Hydrocarbons in Water Column Samples

We measured dissolved methane concentrations as high as ~43 nM in water column samples collected with the hydrocasts (Table 1). The measured concentrations are significantly higher than those in average seawater (open-ocean values 1-4 nM; *Holmes, et al.*, 2000; *Sansone, et al.*, 2001; *Reeburgh*, 2007). In all the hydrocast profiles, low methane occurs near the floors of the pockmarks and higher concentrations occur at depths corresponding to the top of the pockmark walls (100-130 m), consistent with the remote measurements made from the AUV. In most

profiles, the correlation between salinity, temperature and methane concentration, observed for near-bottom AUV measurements (Fig. 6), breaks down with altitude above the seafloor (Fig. 8 & 9). In addition to the elevated methane concentrations, trace amounts of higher molecular weight hydrocarbons, mainly ethane and propane, were measured in the water column.

Isotopic analysis of the dissolved methane in the hydrocast samples shows the methane $\delta^{13}\text{C}$ values are ranging from -65 to -45‰ , with most measurements less than -60‰ . This suggests the methane is primarily biogenic in origin and the -50 to -45‰ values suggest aerobic methane oxidation in the water column (*Valentine, et al.*, 2001) and/or some admixed thermogenic methane (*Ussler, et al.*, 2003; *Whiticar, et al.*, 1986).

A.4.5 Pore Water Geochemistry

Dissolved Inorganic Carbon (DIC) $\delta^{13}\text{C}$ values and sulfate concentration profiles in sediment pore water yield information about the nature of the microbiological reactions, on organic matter diagenesis, methane flux, and anaerobic methane oxidation (AMO). Sulfate profiles have been obtained for pore water squeezed from piston cores 10P, 23P, 25P, 30P and 31P and DIC $\delta^{13}\text{C}$ profiles from 10P, 23P and 25P (Table 2). Sulfate is reduced with depth below the seafloor, reaching zero concentration at depths as shallow as 50-65 cm below the seafloor in core 25P and 30P. DIC $\delta^{13}\text{C}$ also decreases with depth, reaching a minimum of -34.4‰ at 115-138 cm below the seafloor in core 10P. The shallowness of the sulfate

reduction zone and isotopically light DIC $\delta^{13}\text{C}$ suggest active methane advection and AMO at these pockmarks (*Browski, et al., 1999*).

A.5 Discussion

A.5.1 Temporal Variations in Methane Venting

During this survey we observed temporal variations in methane concentration with background methane concentrations near the seafloor dropping to insignificant levels after two storms and then gradually increasing. Examination of XBT and CTD profiles collected throughout the cruise show that the structure of the water column also changed in response to the two storms. Thus, it seems likely that the storms either shifted the water masses in the area, clearing the methane-rich water that had accumulated in the pockmarks or induced water column mixing so that methane concentrations were greatly reduced near the seafloor. In effect, these storms seem to have reset the system, and provided an unexpected opportunity to track the build up of the methane anomalies.

Changes in seepage rates that coincide with tidal variations are commonly observed (e.g., *Boles, et al., 2001; Forrest, et al., 2005; Mikolaj and Ampaya, 1973; Orange, et al., 1997; Torres, et al., 2002*). *Christodoulou, et al. (2003)* observe both seasonal changes in methane concentration after sampling water above pockmarks on a monthly basis as well as increased methane concentrations following an earthquake. *Boles, et al. (2001)* document tidal forcing resulting in 4-7% variations about the mean in methane concentrations measured in situ by tent-shaped traps placed on the seafloor. Within the study area, the tidal effect at the seafloor is apparent in the

shifting current directions (Fig. 4). However, because our measurements were not taken in a stationary position over a tidal cycle, the magnitude of the tidal forcing on these pockmarks cannot be quantified. Nonetheless, based on reported variations in methane concentration in other nearshore settings and cross-over errors between subsequent AUV dives, we estimate that tidal forcing results in less than a 20% variation in methane concentration about the mean local value.

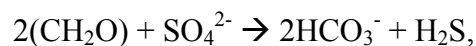
A.5.2 Methane Source

The $\delta^{13}\text{C}$ of the methane is sufficiently light to indicate a primarily biogenic source for some of the vented methane. Methane $\delta^{13}\text{C}$ lower than -60‰ is generally attributed to biogenic methane while methane $\delta^{13}\text{C}$ heavier than -45‰ is considered thermogenic in origin (Ussler *et al.*, 2003; Whiticar, *et al.*, 1986). Since most of the water column methane $\delta^{13}\text{C}$ is less than -60‰ , the vented methane must have a primarily biogenic signature. . The presence of higher hydrocarbons indicates that there is also a minor thermogenic component in the vented fluids. While microbes can produce some of the ethane, Bernard, *et al.* (1976) attribute ethane concentrations comprising 0.14% or more of measured hydrocarbons as a signal of a thermogenic component. At some depths in the water column, we sampled ethane percentages orders of magnitude larger than this accompanied by trace concentrations of propane and butane.

A.5.3 Methane Venting at the Pockmarks

The observed methane anomaly concentrations of 50-150 nM and ~30 nM observed in the METS sensor data and in the hydrocast samples, respectively, are significantly higher than average seawater dissolved methane concentrations (1-4 nM), confirming that methane is actively venting in the pockmarks. While these values are lower than the 200-1500 nM concentration measured at some other pockmarks (*Bohrmann et al.*, 2002; *Christodoulou, et al.*, 2003), they are much higher than 1-3 nM concentrations observed in other pockmarks with no evidence of venting (*Paull, et al.*, 2002).

The shallowness of the sulfate methane interface (SMI) and the isotopic signature of the DIC also supports methane advection and AMO (Table 2). Two processes contribute to sulfate reduction (*Claypool and Kaplan*, 1974; *Borowski, et al.*, 1999): Organic Matter Oxidation (OMO)



and Anaerobic Methane Oxidation (AMO)



OMO is the more common of the two reactions and occurs in all sulfate-reducing environments when organic matter is present. In the presence of only OMO, the minimum $\delta^{13}\text{C}$ of the resulting DIC is equal to that of the organic carbon involved in the reaction. Conversely, the $\delta^{13}\text{C}$ -DIC value resulting from AMO can be less than that of organic carbon because methane is isotopically lighter. Organic carbon has a typical $\delta^{13}\text{C}$ range of -20‰ to -22‰ for marine carbon and -26‰ to -32‰ for terrigenous carbon (*Hedges*, 1992). The minimum $\delta^{13}\text{C}$ of the DIC in the pore water

ranges from -30.9‰ to -34.4‰ . The $\delta^{13}\text{C}$ -DIC suggest that AMO is the dominant sulfate reducing process in the surficial sediment and is consistent with the other independent evidence for high methane flux through the sediment column. Even if it is assumed that the source of the $\delta^{13}\text{C}$ -DIC is entirely the extremely light terrigenous material with $\delta^{13}\text{C}$ of $\sim -32\text{‰}$, the measured $\delta^{13}\text{C}$ -DIC of -34.4‰ would still suggest some AMO in the sediment column requiring a significant flux of methane.

A.5.4 Diffuse vs. focused venting

The spatial distribution of the elevated methane concentrations (Fig. 7) and the CTD profiles (Fig. 8) show that methane rich fluids are not present along the floors of the pockmarks. This is consistent with previous observations based on high-resolution (CHIRP) seismic profiling (*Hill, et al., 2004*), where gas-charged sediments are seismically imaged along the walls of the pockmarks, but in most cases are not seismically imaged beneath the floors of the pockmarks (e.g., Fig. 2).

The pattern of methane venting illustrated by the AUV data itself is not sufficient to determine the overall venting pattern in the area. Since the AUV maintained an altitude of 3 m above seafloor during the dives, its depth below the sea surface constantly changed. Thus, the observed variations in methane concentration might be due to horizontal stratification, such as those observed by *Berner, et al. (2003)*, rather than to focused venting of methane-rich fluids. To determine if a horizontally extensive methane-rich layer exists, the near-systematic correlation between salinity, temperature and dissolved methane concentration was exploited by examining CTD profiles acquired by the AUV during its descent to and ascent from

the seafloor. The observed near seafloor relationship between dissolved methane concentration, salinity and temperature tends to break down in the water column (Fig. 8), likely due to mixing occurring in a water column with existing vertical structure. Vertical profiling may still be useful to evaluate the horizontal extent of a well defined methane-rich layer. Near the seafloor, methane anomalies occur in areas where the salinity and temperature are lower than the surrounding water, suggesting that the vented methane-rich fluid is less saline and cooler than the bottom water. These observed salinity and temperature gradients are not due to the interfingering of shelf and slope water resulting from the summer weakening of the shelf/slope front as described by Flagg, et al. (1994), Burrage and Garvine (1982) and Gordon and Aikman (1981). Structure related to that feature is visible farther up in the water column, at water depths shallower than 80 m. The overall trend in the 100-150 m water depths of the study area is that temperature and salinity increase with depth (Figs. 8, 9). Therefore, as altitude increases, the affect on temperature and salinity due to mixing will become less pronounced as the physical characteristics of the water approach those of the vented fluids. This water column structure enables us to locate the base of the methane-rich layer by a sharp gradient in temperature and salinity, but above that step-like variation in physical properties, the previously observed correlation between dissolved methane concentration, salinity and temperature will become less robust and the top of the methane-rich layer may not be sharply defined in the temperature and salinity data.

We observe evidence of a methane-rich layer in most of the CTD profiles generated during the AUV descents and ascents that extend deep enough to record the

transition from deep methane-poor water to the layer of methane-rich water. This is expected as most of the vehicle launches and retrievals were specifically sited near the landward (west) walls of the pockmarks. However, profiles collected during the ascents of dives 9 and 18 (Fig. 8) do not show steps in salinity and temperature, suggesting that the observed methane-rich mass is not horizontally continuous. These two profiles are far enough away from the pockmark walls that advection due to tidal forcing (Fig. 4) would not have carried the methane-rich fluids to the profile location.

Based on these observations, we hypothesize that the pattern in the spatial distribution of the methane anomaly mostly reflects an area of venting along the walls of the pockmarks with some transport by local currents contributing to the observed distribution of the methane (Fig. 9). We have considered other venting scenarios, including localized venting at specific sites, either along the pockmarks' walls or through the floor of the pockmarks, or a methane-rich water mass transported from elsewhere. However, these are unlikely because they require the presence of a laterally extensive methane-rich water layer that is not supported by the data.

A.5.5 Evolution of Elongate Pockmarks

Most of the pockmarks in our survey area are kilometer-scale, elongate features, but a smaller, round pockmark is present at the southernmost part of the survey area (Fig. 1). This pockmark is only ~300 m in diameter and has slightly less relief (<40 m) than the other pockmarks in the area. The largest methane anomaly was recorded along the southwestern wall of this pockmark during AUV dive 12, possibly indicating that venting is more vigorous in this pockmark. Pockmark fields

with no evidence of gas or fluid venting have been identified (e.g., *Paull, et al.*, 2002). Judd and Holvand (2007) suggest that features like these might be relict, indicating earlier gas or fluid venting. We further hypothesize that as the pockmarks age and the reservoir of vent material becomes depleted, it may result in reduced venting rates. Thus, based on the measured methane concentration, the southernmost pockmark might be the youngest. Our data are spatially limited, so it is possible that high methane concentrations exist in other parts of the survey area and were not sampled. However, if the smallest pockmarks are indeed the youngest, it would support the Kelly, et al. (1994) model of pockmark formation in which the pockmarks are gradually excavated due to gas or fluid escape.

Hill, et al. (2004) attribute the elongate nature of the pockmarks to stress changes resulting from downslope creep within the shelf edge delta. Çifçi, et al. (2003) hypothesized that elongate pockmarks on the Turkish shelf of the Black Sea formed by the merging of smaller pockmarks. There, the round pockmarks were 1/4-1/2 the size of the larger, elongate pockmarks. A combination of these mechanisms might be responsible for the formation of the pockmarks in our study area. The smaller pockmarks could be younger and thus have not yet had sufficient time to grow and merge with adjacent pockmarks. The irregularly shaped pockmark that cores 10P, 23P and 25P were collected from (Fig. 7b) might get its shape from the coalescing of three or more smaller pockmarks (the thin northward extension and the easternmost section of the pockmark could each have been separate features before joining with what is now the central portion of the pockmark). Downslope creep also likely contributes to the shape of the features by influencing where the pockmarks

form and by causing them to preferentially spread parallel to the shelf break. The inner walls of the pockmarks are very linear, systematically oriented parallel to the continental slope, and are arranged in an en-echelon, left stepping pattern, all of which suggest their formation is partially controlled by local stress at the shelf edge. Hence, the tensional regime at the shelf edge controls the locations of the pockmarks, likely resulting in linear array of pockmarks that eventually coalesce into en echelon, elongate features.

A.6 Conclusions

Near seafloor dissolved methane concentration measurements from the SeaBED AUV, combined with CTD profiles illustrate the distribution of active venting. Methane venting is concentrated along the upper parts of the pockmark walls and adjacent shelf area, and is not occurring through the floors of the pockmarks. A correlation is observed, both in the AUV and the lower section of hydrocast data, between methane concentration and the salinity and temperature. This correlation allows the use of CTD casts to determine that the methane-rich water mass is not laterally extensive across the pockmarks. The formation and linear arrangement of these pockmarks is likely related to linearly trending tension due to downslope creep at the shelf break. The elongate shape may be related to the merging of smaller pockmarks as evidenced by differences in venting intensity with pockmark size.

A.7 Acknowledgements

We thank the captain and crew of the *R/V Cape Hatteras* for their cooperation and Kevin Tomanka of Seafloor System, Inc. for his assistance in acquiring the multibeam bathymetric data. We thank Robert Houghton and Douglas Martinson for helpful conversations. This work was supported by NSF grants OCE-0242426, OCE-0242804 and OCDE-0242449.

A.8 Chapter acknowledgment

The appendix, in full, is the material as submitted to Earth and Planetary Science Letters: Newman, K.R., Cormier, M., Weissel, J.K., Driscoll, N.W., Kastner, M., Solomon, E.A., Robinson, G., Hill, J.C., Singh, H., Camilli, R., and Eustice, R., 2007. Active methane venting observed at giant seafloor pockmarks along the mid-Atlantic shelf break with the Autonomous Underwater Vehicle SeaBED. *EPSL*, submitted.

A.9 Appendix: Response and Correction of the METS Sensor

The METS sensor allows for near real time measurement of dissolved methane concentration from a moving platform. Most users report that the METS sensor reacts as expected with the ability to detect subtle changes in methane concentration (Bussel, et al., 1999). However, other studies (Lamontagne, et al., 2001; Paull, et al., 2002) show a time lag in its response and a delay in returning to “normal” values after reading high methane concentrations. Occasionally, concentrations measured by the METS sensor are significantly lower than those

measured analytically. Conventional methods for determining dissolved methane concentration involve retrieving water samples from depth for later analysis (e.g., Christodoulou, et al., 2003; Clarke, et al., 2000). The METS sensor employs a semiconductor whose resistance varies with the amount of methane present in the detection chamber. As methane molecules in the water diffuse across a silicon membrane into the chamber, they participate in an electron exchange with oxygen and modify the resistance across the semiconductor. The resulting change in the measured voltage is directly related to dissolved methane concentration (http://www.capsun.com/capsun_online/mets.html).

Visual inspection of the raw dissolved methane concentration, salinity and temperature time series data (Fig. 5) shows a correlation between the three constituents: elevated dissolved methane concentrations are observed in areas of decreased salinity and temperature. However, it appears the variations in dissolved methane concentration lag the corresponding salinity and temperature variations. When a square-shaped signal is observed in the salinity and temperature data, the dissolved methane concentration, recorded by the METS sensor, begins to increase at the start of the excursion and continues to increase until the end of the salinity/temperature anomaly, at which time it decays back to background levels. This is the expected response for diffusion across a membrane (Fukasawa et al., 2006; Newman, et al., 2005). The theoretical response of this process is that concentrations should increase as a function of $1 - e^{-t/\tau}$, and decay as a function of $e^{-t/\tau}$, where τ is the time constant of the system. Fukasawa, et al. (2006) give τ as the function $VL/RTAP_T$ where V is the volume of the detector room, L is the membrane thickness,

R is the gas constant, T is the water temperature, A is membrane permeation area and P_T is boundary layer resistance. The response of the sensor can be expressed as the finite difference function

$$y(t_n) = y(t_{n-1}) + [x(t_{n-1}) - y(t_{n-1})](1 - e^{-\Delta t/\tau}),$$

where $x(t)$ is the input function and $y(t)$ is the output. The actual signal can then be retrieved as

$$x(t_n) = y(t_n) + \frac{y(t_{n+1}) - y(t_n)}{1 - e^{-\Delta t/\tau}},$$

All dive data were corrected using the above algorithm (Fig. 5) with the time constant for the system of approximately 11 minutes giving the best visual fit to the data. Although a low signal to noise ratio exists in the data recorded by the METS sensor, the data had to be low pass filtered prior to applying the correction because the algorithm amplifies high frequency noise. The noise was removed through empirical orthogonal function analysis. Each time series was analyzed separately. In all cases the first principle component was used as the filtered form of the data because it represented over 93%, and in most cases, over 97% of the variance in the data.

Corrected methane concentrations are significantly larger than those measured in the hydrocast samples. This may be accounted for by the hydrocast samples being taken at a greater altitude above the seafloor than the AUV measurements. This is also consistent with the results of Chirstodoulou, et al. (2003) where they observe an order of magnitude difference between near seafloor and upper water column measurements.

This instrumental response can also explain the differences in METS measured and analytically measured methane concentrations by Lamontagne, et al. (2001). Since the amount of time spent in some methane-rich areas is considerably shorter than the time constant of the instrument, the concentration measured by the instrument would not have had enough time to ramp up to the true value.

Table A.1 Hydrocarbon concentrations in hydrocast samples.

CTD #	Depth (mbsl)	Methane (nM)	Ethane (nM)	Propane (nM)	Butane (nM)
CH I	136	5.05	0	0	0
	130	5.637	0	0	0
	120	14.1	0	0	0
	110	13.217	0	0	0
	100	--	--	--	--
	85	36.655	0	0	0
CH II	127	10.485	0	0	0
	122	11.728	0	0	0
	117	11.864	0	0	0
	107	20.831	0	0	0
	97	35.751	0	0	0
	87	22.883	0	0	0
CH III	132*	21.228	0	0	0
	127*	--	--	--	--
	122*	29.186	0	0	0
	117*	25.465	0	0	0
	107*	22.350	0	0	0
	97*	20.487	0	0	0
CH IV	130	18.840	0	0	0
	126	22.515	0	0	0
	121*	29.721	0	0	0
	109	36.089	0	0	0
	100	29.134	0	0	0.740
	91	27.540	2.583	3.050	0.959
CH V	140	15.047	0	0	0.829
	130	30.945	0	0	0
	125	25.931	0	0	0
	120	21.122	0	0	0.758
	115	23.713	0	0	0
	105	22.440	0	0	0.755
CH VI	139	22.418	0	3.123	0.998
	130	21.390	0	0	0.775
	122	33.400	0	3.555	0.806
	115	33.248	0	0	0.731
	106	24.628	0	0	0
	98	23.957	0	0	0
	88	26.604	0	0	0
	68	42.743	0	0	0
	59	23.724	0	3.007	0.780
	50	2.544	0	0	0.787
	30	10.375	2.619	0	0
	16	5.227	0	0	0
CH VII	134	24.429	2.579	3.233	1.203
	129	24.541	0	0	0.734
	124	29.695	0	0	0
	119	21.593	0	3.412	0.769
	109	24.925	0	0	0.856
	99	27.796	0	3.189	0.802

*Sample contained ~1 ml of headspace upon arrival from the cruise, most likely introduced when poisoned with mercuric chloride. This would amount to a maximum of 1/15 increase in concentration due to air contamination.

Table A.2 Pore water geochemistry data.

Number	SMI Depth (cm)	Min. $\delta^{13}\text{C}$ DIC (‰)
10P	115-138	-34.4
23P	125-145	-32.1
25P	50-65	-30.9
30P	50-65	
31P	125-147	

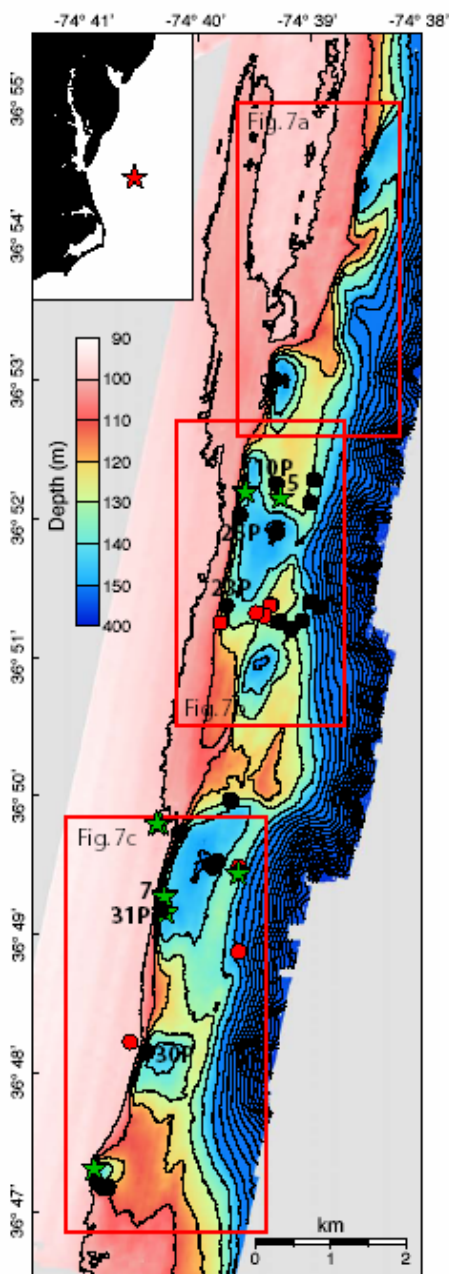


Figure A.1 Bathymetric map of the survey area produced with the ELAC-1180 multibeam sonar during the July 2004 survey. Core locations are plotted as circles, black for cores squeezed for pore water geochemistry, red for those saved for stratigraphy. Green stars show the locations of hydrocast sampling. Cores 10P, 23P, 25P, 30P and 31P and hydrocasts 5 and 7 are identified. Red boxes show the areas displayed in Figure A.7. Inset is an overview map of the area with the red star showing the location of the survey area. Visible coastlines in the inset map are, from north to south, the southern tip of New Jersey, the Delmarva Peninsula, and the barrier islands offshore North Carolina.

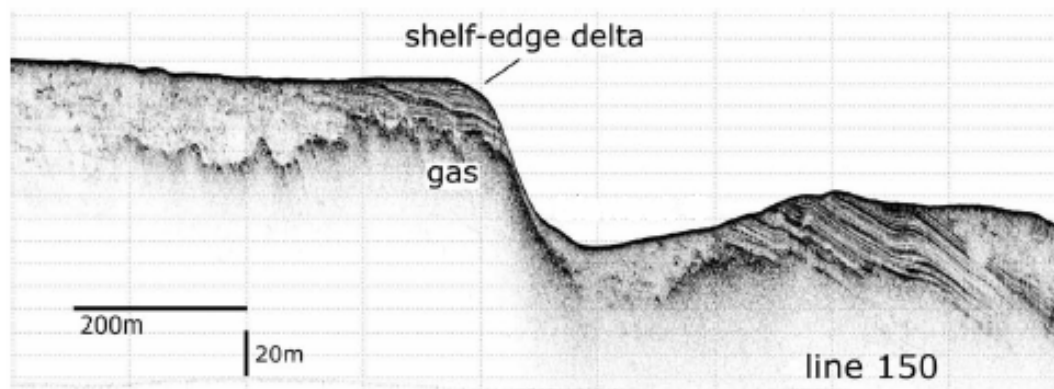


Figure A.2 Chirp seismic profile across a shelf edge pockmark, modified from Hill, et al. (2004). Gas-charged sediments are visible along the inner wall of the pockmark, extending westward under the shelf. Gas-charged sediments are identified as a high amplitude reflector that obscures underlying reflectors.



Figure A.3 The SeaBED AUV.

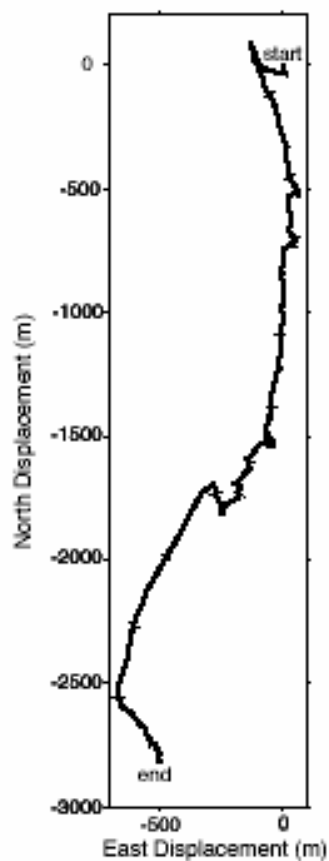


Figure A.4 Near bottom currents measured by the ship's ADCP in the survey area. The plot shows total displacement of a parcel of water over a 12 hour period with ticks every hour. A southerly current of 0.2 km/h dominates, which is consistent with the previously observed shelf-edge current (e.g., *Bumpus*, 1973). Tidal effects are expressed as east/west excursions.

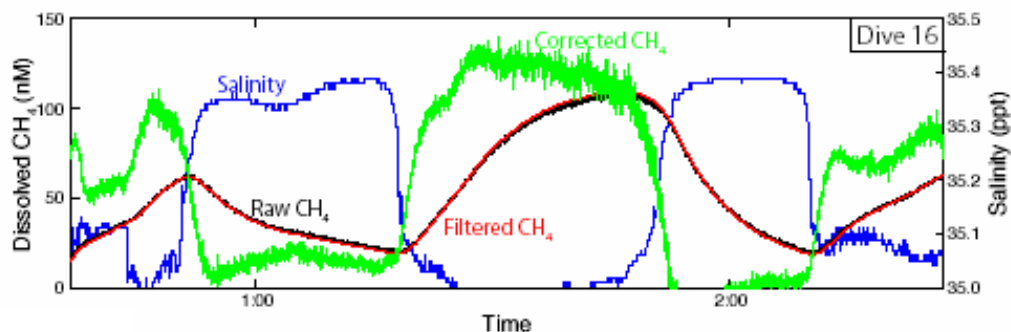


Figure A.5 Near-bottom water properties collected by the SeaBED AUV during dive 16 (located in Figure A.7a). The black line is the raw dissolved methane data generated by the METS sensor. The red line is the data filtered using the first principle component from empirical orthogonal function analysis (see Section A.9). The green line is the corrected dissolved methane. The blue line is salinity, measured by the AUV mounted SeaBird CTD. Temperature data are not plotted, but they follow a similar pattern as the salinity data and are shown in Figure A.6

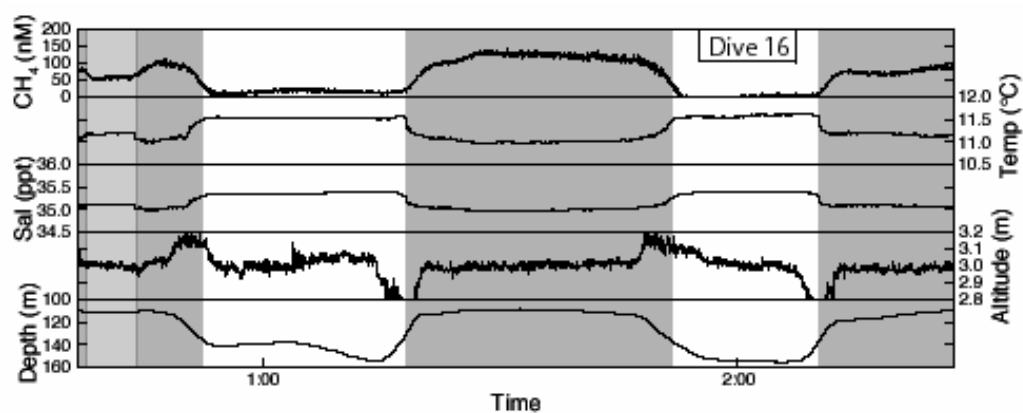


Figure A.6 Along track data from dive 16 (located in Figure A.7a) displaying the categorization of the methane anomaly. White areas are background concentration, darkly shaded high methane concentration and lightly shaded intermediate methane concentration. A correlation is typically observed in all dives between salinity, temperature and dissolved methane concentration.

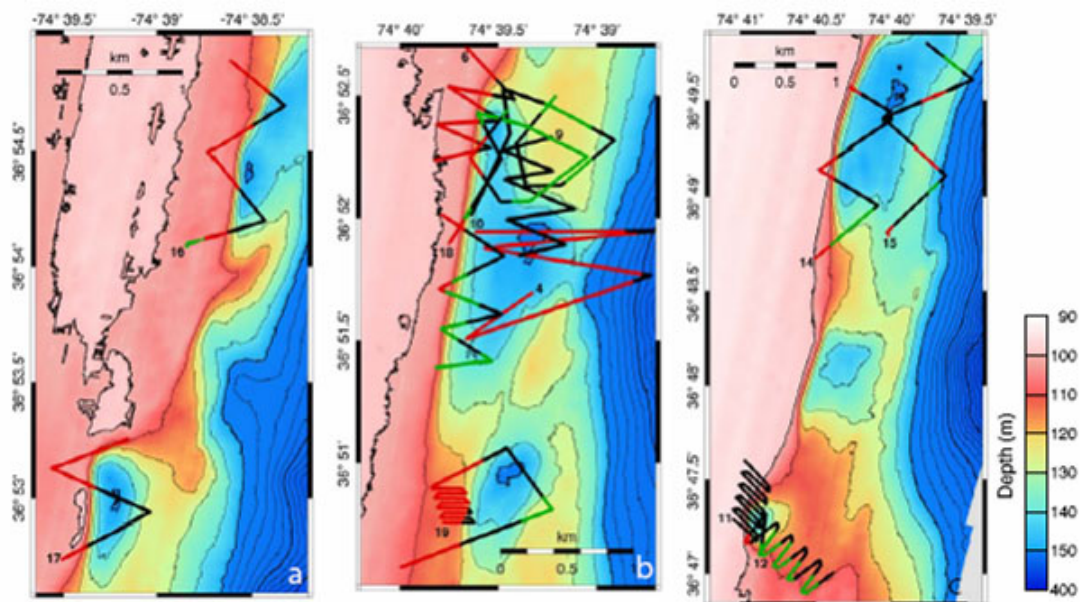


Figure A.7 Bathymetry maps of the pockmarks showing the spatial distribution of the methane anomaly. Black is background methane concentration, red is high methane concentration and green is intermediate methane concentration. AUV dive numbers are given at the beginning of the dive track.

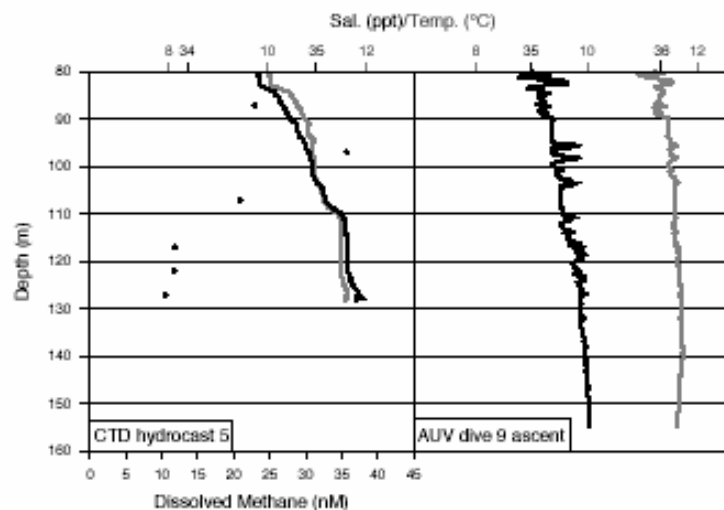


Figure A.8 Left panel: CTD and dissolved methane concentration profile from hydrocast 5 (located in Figure A.1). Salinity is plotted in black, temperature in gray and the laboratory measured dissolved methane concentration as points. Some correlation between dissolved methane concentration, salinity and temperature is seen in the lower part of the profile, but it begins to break down at depths shallower than the peak methane concentration. A step is visible in salinity and temperature at 110 m, the depth at which methane begins to increase in the profile. Right panel: CTD profile from AUV dive 9 ascent. No steps, except for noisy excursions, are visible in this profile. This shows that the methane-rich water mass that is slightly colder and fresher than the bottom water is not present at this location.

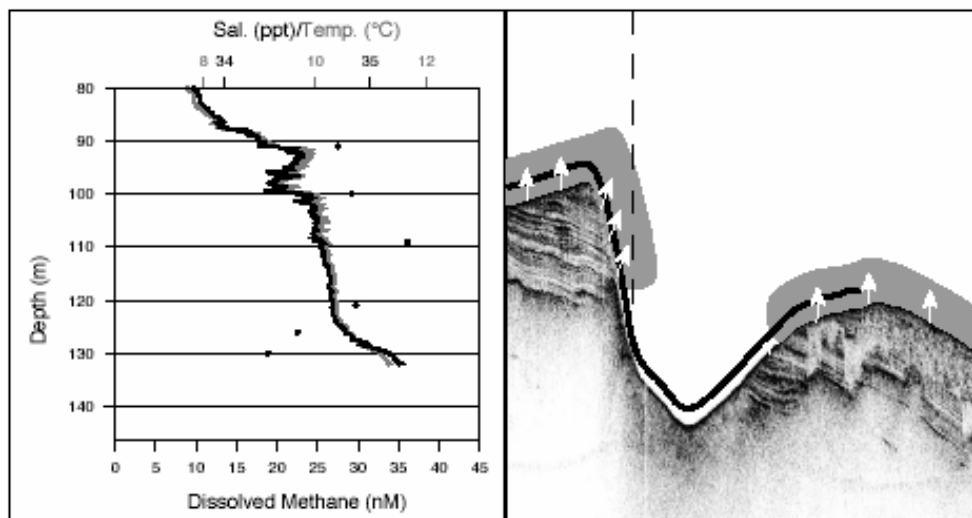


Figure A.9 Proposed methane venting scenario. The right panel shows a chirp seismic line from the Hill, et al. (2004) survey. The shaded area represents the area where methane-rich water is found as it spreads due to diffusion and advection due to currents. White arrows denote the location of methane venting. The bold line represents the AUV track across the pockmark and the dashed line represents the location of the hydrocast data presented in the left panel. Left panel data are from hydrocast 7 and plotting conventions are the same as in Figure A.8

References

- Bernard, B. B., Brooks, J. M. and Sacket, W. M., 1976. Natural gas seepage in the Gulf of Mexico. *Earth and Planetary Science Letters*, 31: 48-54.
- Berner, U., Poggenburg, J., Faber, E., Quadfasel, E. and Frische, A., 2003. Methane in the ocean waters of the Bay of Bengal: its sources and exchange with the atmosphere. *Deep-Sea Research II*, 50: 925-9250.
- Bohrmann, G., Heeschen, K., Jung, C., Weinrebe, W., Baranov, B., Cailleau, B., Heath, R., Hühnerbach, V., Hort, M., Masson, D. and Trummer, I., 2002. Widespread fluid expulsion along the seafloor of the Costa Rica convergent margin. *Terra Nova*, 14: 69-79.
- Boles, J. R., Clark, J. F., Leifer, I. and Washburn, L., 2001. Temporal variation in natural methane seep rate due to tides, Coal Oil Point area, California. *Journal of Geophysical Research*, 106: 27077-27086.
- Borowski, W. S., Paull, C. K. and W.Ussler, 1999. Global and local variations of interstitial sulfate gradients in deep-water, continental margin sediments: Sensitivity to underlying methane and gas hydrates. *Marine Geology*, 159: 131-154.
- Bumpus, D. F., 1973. A description of the circulation on the continental shelf of the east coast of the United States, *Progress in Oceanography*, Pergamon Press, pp. 111-157.
- Burrage, D. M. and Garvine, R. W., 1982. Summertime Hydrography at the shelfbreak front in the Middle Atlantic Bight. *Journal of Physical Oceanography*, 18: 1309-1319.
- Bussell, J., Klinkhammer, G., Collier, R., Linke, P., Appel, F., Heeschen, K., Suess, E., Angelis, M. A. d., Masson, M. and Marx, S., 1999. Applications of the METS methane sensor to the in-situ detection of methane over a range of time scales and environments, *Fall AGU Meeting*, San Francisco, CA.
- Christodoulou, D., Papatheodorou, G., Ferentinos, G. and Masson, M., 2003. Active seepage in two contrasting pockmark fields in the Patras and Corinth gulfs, Greece. *Geo-Marine Letters*, 23: 194-199.
- Clarke, J. F., Washburn, L., Hornafus, J. S. and Luyendyk, B. P., 2000. Dissolved hydrocarbon flux from natural marine seeps to the southern California Bight. *Journal of Geophysical Research*, 105: 11509-11522.

- Çifçi, G., Dondurur, D. and Ergün, M., 2003. Deep and shallow structures of large pockmarks in the Turkish shelf, Eastern Black Sea. *Geo-Marine Letters*, 23: 311-322.
- Dimitrov, L. and Woodside, J., 2002. Deep sea pockmark environments in the eastern Mediterranean. *Marine Geology*, 195: 263-276.
- Driscoll, N. W., Weissel, J. K. and Goff, J. A., 2000. Potential for large-scale slope failure and tsunami generation along the U.S. mid-Atlantic coast. *Geology*, 28: 407-410.
- Eustice, R., Camilli, R. and Singh, H., 2005. Bathymetry-Aided Doppler R- Navigation for AUVs, *Proceedings of IEEE OCEANS*.
- Flagg, C. N., Houghton, R. W. and Pietrafesa, L. J., 1994. Summertime thermocline salinity maximum intrusions in the Mid-Atlantic Bight. *Deep-Sea Research II*, 41: 325-340.
- Forrest, M. J., Ledesma-Vásquez, J., Ussler, W., Kulongoski, J. T., Hilton, D. R. and Greene, H. G., 2005. Gas geochemistry of a shallow submarine hydrothermal vent associated with the El Requesón fault zone, Bahía Concepción, Baja California Sur, México. *Chemical Geology*, 224: 82-95.
- Fukasawa, T., Hozumi, S., Morita, M., Oketani, T. and Masson, M., 2006. Dissolved Methane Sensor for Methane Leakage Monitoring in Methane Hydrate Production, *Proceedings of IEEE OCEANS*.
- Gordon, A. L. and III, F. A., 1981. Salinity maximum in the pycnocline of the Middle Atlantic Bight. *Limnology and Oceanography*, 26: 123-130.
- Hedges, J. I., 1992. Global biogeochemical cycles: progress and problems. *Marine Chemistry*, 39: 67-93.
- Hill, J. C., Driscoll, N. W., Weissel, J. K. and Goff, J. A., 2004. Large-scale elongate gas blowouts along the U.S. Atlantic margin. *Journal of Geophysical Research*, 109: doi:10.1029/2004JB002969.
- Holmes, M. E., Sansone, F. J., Rust, T. M. and Popp, B. N., 2000. Methane production, consumption, and air-sea exchange in the open ocean: An evaluation based on carbon isotopic ratios. *Global Biogeochemical Cycles*, 14: 1-10.
- Hovland, M. and Judd, A. G., 1988. *Seabed pockmarks and seepages*, London: Graham and Trotman, 293 p.

- Hovland, M., Gardner, J. V. and Judd, A. G., 2002. The significance of pockmarks to understanding fluid flow processes and geohazards. *Geofluids*, 2: 127-136.
- Judd, A. G., Hovland, M., Dimitrov, L. I., Gil, S. C. and Jukes, V., 2002. The geological methane budget at Continental Margins and its influence on climate change. *Geofluids*, 2: 109-126.
- Judd, A. G., 2003. The global importance and context of methane escape from the seabed. *Geo-Marine Letters*, 23: 147-154.
- Judd, A. G. and Hovland, M., 2007. *Seabed Fluid Flow: The Impact on Geology, Biology and the Marine Environment*, New York: Cambridge University Press.
- Kelley, J. T., Dickson, S. M., Belknap, D. F., Barnhardt, W. A. and Henderson, M., 1994. Giant sea-bed pockmarks: Evidence for gas escape from Belfast Bay, Maine. *Geology*, 22: 59-62.
- King, L. H. and McLean, B., 1970. Pockmarks on the Scotian Shelf. *GSA Bulletin*, 81: 3141-3148.
- Lamontagne, R. A., Rose-Pehrsson, S. L., Grabowski, K. E. and Knies, D. L., 2001. Response of METS Sensor to Methane Concentrations found on the Texas-Louisiana Shelf in the Gulf of Mexico. Naval Research Laboratory Interim Report 6110-01-8584.
- Lonke, L., Mascle, J. and Parties, F. S., 2004. Mud volcanoes, gas chimneys, pockmarks and mounds in the Nile deep-sea fan (Eastern Mediterranean): geophysical evidences. *Marine and Petroleum Geology*, 21: 669-689.
- Mikolaj, P. G. and Ampaya, J. P., 1973. Tidal effects on the activity of natural submarine oil seeps. *Marine Technology Society Journal*, 7: 25-28.
- Newman, K., Cormier, M., Driscoll, N., Hill, J., Kastner, M., Singh, H. and Weissel, J., 2005. Geophysical and Geochemical Evidence for Methane Venting at Large Gas Blowouts Along the US Mid-Atlantic Shelf Edge. *Eos Trans. AGU*, 86 (52), Fall Meet. Suppl., Abstract OS32A-05.,
- Orange, D. L., Saffer, D. and Maher, N., 1997. Tidally Mediated Fluid Expulsion at a Cold Seep,. *Eos Trans. AGU*, 78 (52), Fall Meet. Suppl. Abstract T31E-11.
- Paull, C. K., Ussler, W. and Maher, N., 2002. Pockmarks off Big Sur, California. *Marine Geology*, 181: 323-355.

- Popp, B. N., Sansone, F. J., Rust, T. M. and Merritt, D. A., 1995. Determination of concentration and carbon isotopic composition of dissolved methane in sediments and nearshore waters. *Analytical Chemistry*, 67: 405-411.
- Reeburgh, W. S., 2007. Oceanic methane biogeochemistry. *Chemistry Reviews*, 107: 486-513.
- Sansone, F. J., Popp, B. N., Gasc, A., Graham, A. W. and Rust, T. M., 2001. Highly elevated methane in the eastern tropical North Pacific and associated isotopically enriched fluxes to the atmosphere. *Geophysical Research Letters*, 28: 4567-4570.
- Sibuet, M. and Olu, K., 1998. Biogeography, biodiversity and fluid dependence of deep-sea cold-seep communities at active and passive margins. *Deep-Sea Research II*, 45: 517-567.
- Sills, G. C. and Wheeler, S. J., 1992. The significance of gas for offshore operations. *Continental Shelf Research*, 12: 1239-1250.
- Singh, H., Armstrong, R., Gilbes, F., Eustice, R., Roman, C., Pizarro, O. and Torres, J., 2004a. Imaging Coral I: Imaging Coral Habitats with The SeaBED AUV. *The Journal for Subsurface Sensing Technologies and Applications*, 5: 498-514.
- Singh, H., Can, A., Eustice, R., Lerner, S., McPhee, N., Pizzaro, O. and Roman, C., 2004b. SeaBED AUV Provides New Platform for High Resolution Imaging. *Eos Trans., AGU*, 85: 289, 294-295.
- Torres, M. E., McManus, J., Hammond, D., Angelis, M., Heeschen, K. U., Colbert, S. L., Tryon, M. D., Brown, K. M. and Suess, E., 2002. Fluid and chemical fluxes in and out of sediments hosting methane hydrate deposits on Hydrate Ridge, OR, I. Hydrological provinces. *Earth and Planetary Science Letters*, 201: 525-540.
- Ussler, W., Paull, C. K. and Boucher, J., 2003. Submarine pockmarks: a case study from Belfast Bay, Maine. *Marine Geology*, 202: 175-192.
- Valentine, D. L., Blanton, D. C., Reeburgh, W. S. and Kastner, M., 2001. Water column methane oxidation adjacent to an area of active hydrate dissociation, Eel River Basin. *Geochimica et Cosmochimica Acta*, 65: 2633-2640.
- Whitcomb, L., Yoerger, D., Singh, H. and Howland, J., 2000. Advances in Underwater Robot Vehicles for Deep Ocean Exploration: Navigation, Control and Survey Operations, Robotics Research - The Ninth International Symposium, London: Springer-Verlag Publications, pp. 439-448.

Whiticar, M. J., Faber, E. and Schoell, M., 1986. Biogenic methane formation in marine and freshwater environments: CO₂ reduction vs. acetate fermentation - Isotope evidence. *Geochimica et Cosmochimica Acta*, 50: 693-709.